การจำลองและการสร้างภาพนามธรรมของความสัมพันธ์เชิงปริมาณและความสัมพันธ์แบบอัลโลเมตริก

ของส่วนต่าง ๆ ของข้าวด้วยโครงข่ายประสาทแบบบูรณาการ
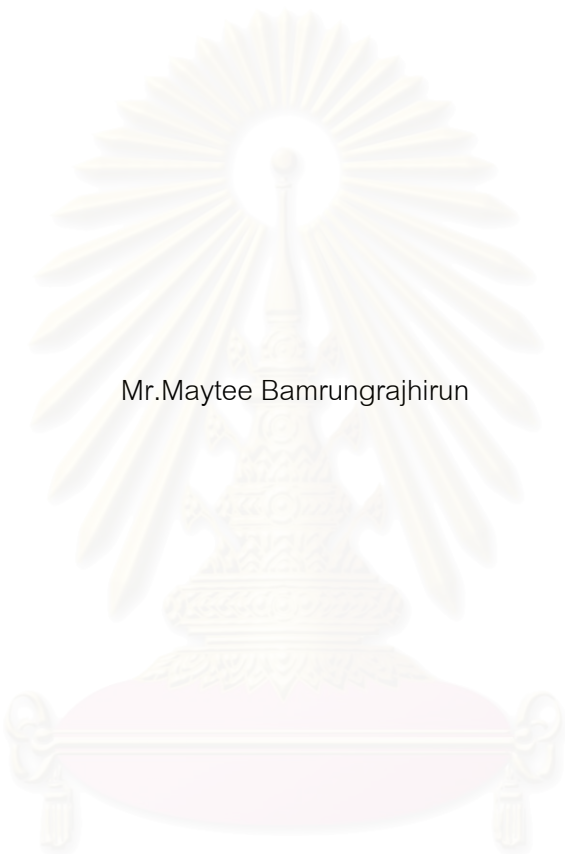
นายเมธี บำรุงราชหิรัณย์

MODELING AND VISUALIZING THE QUANTITATIVE AND ALLOMETRIC RELATIONSHIP

OF INDIVIDUAL PARTS OF RICE BY AN INTEGRATED NEURAL NETWORK

Mr.Maytee Bamrungrajhirun

A Dissertation Submitted in Partial Fulfillment of the Requirements

for the Degree of Doctor of Philosophy Program in Computer Science

Department of Mathematics

Faculty of Science

Chulalongkorn University

Academic year 2007

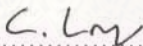|	
Thesis Title	MODELING AND VISUALIZING THE QUANTITATIVE AND ALLOMETRIC RELATIONSHIP OF INDIVIDUAL PARTS OF RICE BY AN INTEGRATED NEURAL NETWORK
By	Mr. Maytee Bamrungrajhirun
Field of Study	Computer Science
Thesis Advisor	Professor Chidchanok Lursinsap. Ph.D.
Thesis Co-advisor	Associate Professor Suchada Siripant

Accepted by the Faculty of Science, Chulalongkorn University in Partial Fulfillment of the Requirements for the Doctoral Degree

.... Dean of the Faculty of Science
(Professor Supot Hannongbua, Ph.D.)

THESIS COMMITTEE

.... Chairman
(Associate Professor Peraphon Sophatsathit, Ph.D.)

.... Thesis Advisor
(Professor Chidchanok Lursinsap, Ph.D.)

.... Thesis Co-advisor
(Associate Professor Suchada Siripant)

.... External Member
(Assistant Professor Poonpipope Kasemsap, Ph.D.)

.... External Member
(Khamron Sunat, Ph.D.)

.... Member
(Assistant Professor Supachitra Chadchawan, Ph.D.)

เมธี บำรุงราชหิรัณย์ : การจำลองและการสร้างภาพนามธรรมของความสัมพันธ์เชิงปริมาณและความสัมพันธ์แบบอัลโลเมตริกของส่วนต่าง ๆ ของข้าวด้วยโครงข่ายประสาทแบบบูรณาการ. (MODELING AND VISUALIZING THE QUANTITATIVE AND ALLOMETRIC RELATIONSHIP OF INDIVIDUAL PARTS OF RICE BY AN INTEGRATED NEURAL NETWORK) อ.ที่ปรึกษา : ศ.ดร. ชิดชนก เหลือสินทรัพย์, อ.ที่ปรึกษาร่วม : รศ. สุชาดา ศิริพันธุ์, 120 หน้า.

วิทยานิพนธ์ฉบับนี้เสนอขั้นตอนและวิธีการประยุกต์ใช้แบบจำลองโครงข่ายประสาทเทียมในการสร้างความสัมพันธ์เชิงปริมาณและความสัมพันธ์แบบอัลโลเมตริกระหว่างส่วนต่างๆ ของข้าวได้แก่ ลำต้น ราก ใบ และรวงข้าว รวมทั้งการสร้างแบบจำลองการคำนวณปริมาณแสงที่ใบข้าวได้รับตลอดช่วงการเจริญเติบโตเพื่อนำผลไปวิเคราะห์หาความสัมพันธ์ของปริมาณผลผลิตต่อต้น แนวทางที่ใช้คือการคำนวณปริมาณแสงที่ใบข้าวได้รับคำนวณได้จากแบบจำลองซึ่งผลที่ได้สามารถนำใช้เสนอการคำนวณหาปริมาณแสงวิธีใหม่ด้วยการสร้างแบบจำลองโครงสร้างสามมิติด้วยระบบแอลผสมผสานกับเทคนิคการคำนวณปริมาณแสงแบบเรดิโอซิตี้ ซึ่งจะนำไปเป็นตัวแปรหนึ่งร่วมกับตัวแปรสิ่งแวดล้อมอื่นสำหรับกระบวนการโครงข่ายประสาทเทียมเพื่อการทำนายมวลชีวภาพของต้นข้าว

ภาควิชา	คณิตศาสตร์	ลายมือชื่อนิสิต
สาขาวิชา	วิทยาการคอมพิวเตอร์	ลายมือชื่ออาจารย์ที่ปรึกษา
ปีการศึกษา	2550	ลายมือชื่ออาจารย์ที่ปรึกษาร่วม

4673845723   : MAJOR COMPUTER SCIENCE

KEY WORD: Rice Growth Modeling / *Oryza sativa* L. / Neural Networks / Light Interception / Radiosity

MAYTEE BAMRUNGRAJHIRUN : MODELING AND VISUALIZING THE QUANTITATIVE AND ALLOMETRIC RELATIONSHIP OF INDIVIDUAL PARTS OF RICE BY AN INTEGRATED NEURAL NETWORK. THESIS ADVISOR : PROF. CHIDCHANOK LURSINSAP, Ph.D., THESIS COADVISOR : ASSOC.PROF. SUCHADA SIRIPANT, 120 pp.

This dissertation proposes an artificial neural network (ANN) to establish quantitative relation and allometric relation of individual parts of rice, namely, stems, roots, leaf, and panicles. A novel quantitative model for calculating the amount of light incident to the leaves is also introduced. The amount of light incident to the leaves can be calculated by applying radiosity rendering technique to a three dimensional architectural model of rice which is constructed by L-system. Computations of light incidence will be used as one of the environment parameters in the artificial neural network process for predicting rice biomass.

Department	Mathematics	Student's signature	
Field of study	Computer Science	Advisor's signature	
Academic year	2007	Co-advisor's signature	

Acknowledgements

This is perhaps the easiest and hardest part that I have to write. There are lots of people I would like to thank. It will be simple to name all the people that helped get this work done, but it will be tough to thank them enough. I will nonetheless try.

My deepest gratitude is to my advisors, Prof. Dr. Chidchanok Lursinsap and Assoc. Prof. Suchada Siripant for guiding me through finishing this dissertation with untiring help. They gave me the freedom to explore on my own, and at the same time the guidance to recover when my steps faltered. Their patience and support helped me overcome many crisis situations and finish this dissertation. I also express my special thanks to the committee, Assoc. Prof. Dr. Peraphon Sophatsathit, Asst. Prof. Dr. Poonpipope Kasemsap, Asst. Prof. Dr. Supachitra Chadchawan, and Dr. Khamron Sunat for correcting the manuscripts and sharing their critical comments and suggestions, which helped make further improvements. I am also thankful to Dr. Sirapat Chiewchanwattana for her suggestion concerning to the interpolation technique and software. Sincere thanks to Prof. Dr. Frank C. Lin for the extensive knowledge, vision, and creative thinking in forecasting world.

I am also indebted to the members of the Advanced Virtual and Intelligent Computing (AVIC) Center with whom I have interacted during the course of my graduate studies. Particularly, I would like to acknowledge Mr. Somporn Chuai-aree for the many valuable discussions that helped me understand my research area better.

I wish to dedicate this dissertation to the memory of my lovely aunt, Miss Rachaneekorn Bamrungrajhirun, for her love and supports. Most importantly, none of this would have been possible without the love and patience of my family, Mr. Cham, Mrs. Siriporn, Mr. Sarayut, Mrs. Supkarn, and Mr. Jumpon. I wish to thank my aunt, Mrs. Panida Kosanunt for all of her help and supports. Especially, I would like to give my special thanks to Miss Rouirush Worakijthamrongchai whose patient love enabled me to complete this work. This dissertation is indeed a realization of their dream.

Table of Contents

Chapter | Page

List of Tables

List of Figures

Figure   Page

Figure   Page

List of Abbreviations

A_l	Area of leaf
α	Angle in the horizontal plane measured from north eastward
β	Elevation angle measured from plane
B_i	The radiosity of patch i
D_i	The desired output of output node i^{th} in the BPNN
D_y	Day of year: January 1st is 1 and December 31st is 365
E_i	emitted energy
F_{ij}	The fraction valued of the radiation leaving i and hitting patch j
H	Relative Humidity (%, RH)
k	Elastic modulus parameter depends on plant species
L_l	Length of leaf segment
L_p	Length of panicle branch
L_r	Length of root segment
L_s	Length of stem segment
M_l	Mass of leaf part
M_p	Mass of panicle part
M_r	Mass of root part
M_s	Mass of stem part
N_g	Number of rice grain
N_p	Number of rice panicle branch
N_r	Number of rice root branch
O_i	The ith output from output layer in the BPNN
Par	Photosynthetically Active Radiation (PAR, Mole quantum /m^2/day)
P_i	Penetration light through other leaf impact to the ith element
R_i	Reflectivity of the patch (energy which arrives from other patches)
R_n	Rain-fall (mm/day)
$Solar$	Solar Radiation (Energy flux, MJ/m^2/day)
T	Air Temperature ($^{\circ}C$)
W_d	Wind Speed (km/day)
W_l	Width of leaf
W_s	Width of stem
θ	Zenith angle measured from vertical

ADEL	Architectural model of development based on L-systems
ANN	Artificial Neural Network
BPNN	Back-Propagation Neural Network
DiPAR	Direct Photosynthetically Active Radiation (μmol quantum /m^2/s)
DfPAR	Diffused Photosynthetically Active Radiation (μmol quantum /m^2/s)
DpPAR	Penetrated Photosynthetically Active Radiation (μmol quantum /m^2/s)
DPAR	Diffused PAR (μmol quantum /m^2/s)
DSHP	Dividing Sky Hemisphere with Projection
DW	Dry Weight (g, mg)
DVI	Developmental Index
ETM+	Landsat Enhanced Thematic Mapper Plus (Satellite's name)
IR64	Rice variety number 64 (The International Rice Research Institute)
IRRI	The International Rice Research Institute
KDML105	Thai Jasmine Rice or Khao Dok Mali 105
LAI	Leaf Area Index
LM	Levenberg-Marquardt
MSE	Mean Squared Error, MSE = $\sum_{i=1}^{n}(D_i - O_i)^2$
NN	Neural Network
PAR	Photosynthetically Active Radiation (μmol quantum /m^2/s)
PPFD	Photosynthetic Photon Flux Density (μmol quantum /m^2/s)
PTT1	Thai Patumthani 1 Rice
SLA	Specific Leaf Area
SR	broadband simple ratio vegetation index
SRL	Specific Root Length

CHAPTER I

INTRODUCTION

Gaining a high productivity of rice in the actual rice field under some controlled condition is very costly and time consuming. To overcome these problems, prior to the actual growing process, a mathematical simulation of rice growth under various pre-specified parameters must be developed.

Virtual plants and the computational model of plants are increasingly seen as a useful tool for comprehending complex relationships between plant architecture, gene function, plant physiology, plant development, and plant productions [1]. Morphogenesis of the aerial parts of a plant has been successful in simulation. On the other hand, in agronomic applications where growers hope to control environmental conditions to seek for the highest possible yields, growers can use the virtual plant model to simulate plant growth under different cropping conditions so that they can optimize the best possible production yield.

1.1 Problem Review and Motivation

The allometric relationship which is the relation between a physical or physiological attributes and plant size has been found in a broad variety of plant modeling research. They are often used for estimating unmeasured plant traits based on some easily measurable traits such as length or diameter. Examples of allometric relationship discussed in the literature include relationships between height and stem mass, height and stem diameter, fruit and seed mass, developmental rates of different organs, and growth rate and cell biomass. However, no unified allometric relation of the whole plant was previously reported. Each part of plant must be combined together with consistent growth. In addition, morphological and architectural model of plant should be considered and developed consequently.

In rice research, there are many rice growth models proposed by researchers and organizations [2, 3, 4, 5]. The rice growth models focus on studying the impact of climate that changes rice growth, including rice yields, and exploring adaptive management options (fertilizer, cultivar type, irrigation strategy, sowing date, etc.) [3, 4, 5, 6, 7, 8]. Most models are proposed in forms of one-by-one function or simple

function with a small number of parameters as the input parameter of model. A more complex function is needed for finding more realistic relation of plant growth, but there is very hard to solve those complex functions. The mathematical techniques such as neural network, which mimic the biological human learning process, are excellent tools to solve many complex problems. The neural networks have the potential for solving problems in which some inputs and corresponding output values are known, but the relationship between the inputs and outputs is very complex. So, can we use this intelligent method to help simulate rice growth by mimicking its relationship between individual parts?

Light is usually the most important factor influencing the growth and development of plants while nutrients and water are not limited [9, 10]. To gain more understanding and take advantage from plant, many light interception models were developed and investigated in plant science research. Both 2D and 3D computer graphics was used as a tool for calculating amount of light that can be absorbed by the plant leaves or canopy. Leaf area estimation for light interception model could be estimated by satellite image [11, 12], and the rough calculation of light transmission through a plant canopy could be measured by processing the fish-eye hemispherical images [13, 14]. Many techniques for estimating light interception on 3D plant canopy were proposed [15, 16, 17, 18]. A more complex model of light calculation was also investigated. Indirect light such as diffuse and penetrated light was considered [9, 19], but did not integrate with the direct light interception model yet. Thus, a complex and realistic modeling technique of light calculation is also required.

This dissertation proposed a system of rice growth which integrated the neural networks for describing the relationship of rice parts. A new technique for calculating amount of light incident to leaves is also proposed. Research objectives are illustrated in the second section. The scope and limitations of this work will be shown in the third section. Section four summarizes the research contributions. Research methodology is described in section five. The last section expresses the organization of the dissertation.

1.2 Research Objectives

The objectives of this research are listed as follows:

1. To find the quantitative relation and allometric relation of four individual parts of rice; stem, leaves, root, and panicle, by using a neural network.

2. To propose a new methodology in simulating crop growth of rice by integrating the neural network which describes the growing behavior of individual rice parts.

3. To construct the virtual rice, a three dimension architectural model of rice.

4. To develop a novel technique for calculating amount of light incident to the leaves by applying radiosity rendering technique to the virtual rice.

1.3 Scope and Limitations

In this dissertation, the scope of work is constrained as follows:

1. Two types of rice; Khao Dawk Mali 105 (KDML105) rice and Pathumthani 1 (PTT1) rice were investigated.

2. In the light interception model, only area of leaf blade was considered. The light incident to other parts was ignored.

3. For modeling of rice growth, we considered and investigated in the vegetative stage of rice.

4. Biological knowledge such as germination behavior, direction of root part, and the sequencing in seedling phase were considered in constructing three-dimension model but were ignored in rice growth system.

5. Weather information and nutrients were considered in the rice growth system, but did not vary.

6. The back-propagation neural network was used for describing the quantitative and allometric relationship among rice parts.

1.4 Research Methodology

1. Review and study the research papers that are related to the rice crop system, rice structure, rice growth model and simulation, light interception model of plant, and three-dimension architectural model of rice.

2. Design and set up the field experiment.

3. Collect and analyze data.

4. Develop a three-dimension architectural model of rice based on the L-system and rice growth data.

5. Find the quantitative relation and allometric relation between four individual parts of rice; stem, leaves, root, and panicle, by using an artificial neural network (ANN).

6. Develop a light interception model for rice leaves.

7. Develop a new rice growth system by integrating neural network of four rice parts together.

8. Evaluate the proposed light interception model by comparing the amount of light which calculate from model to the measured value.

9. Evaluate the proposed rice growth model with the actual growing data.

10. Analyze the results and summarize the outcome of study.

1.5 Organization of the Dissertation

The dissertation is organized into six chapters. Chapter 2 expresses the theoretical background of rice architecture, rice growth stage, neural network, quantitative and allometry relationship, L-systems, and radiosity rendering technique. The reviews of the publications related to the architectural model of rice, rice growth modeling, famous rice crop modeling, usage of neural network in agricultural researches, and light interception model in plants are also revised in this chapter. Chapter 3 illustrates the growing conditions in the field experiment, including data

acquisition, and experimental design. Chapter 4 describes steps of three-dimension rice architectural model construction, a new technique for calculating amount of light incident to rice leaves, and the proposed rice crop system which combines a growing three-dimension architectural model of rice with the neural network. The results of constructing the three-dimension model of rice, calculation methodology of light incident to leaves, and use of neural network in rice growth simulation are shown in chapter 5. Chapter 6 concludes the research work and presents some directions for future work.

CHAPTER II
BACKGROUND AND LITERATURE REVIEW

In this chapter, the theoretical background on rice structure, rice growth stage, back propagation neural network, quantitative and allometric relationship, the L-system, and radiosity rendering technique are described. Literatures related to rice architectural modeling, rice growth modeling, light interception model of plant, rice crop modeling, and usage of neural network in agriculture are also reviewed.

2.1 Theoretical Background

2.1.1 Rice (*Oryza sativa* L.) Details and Nomenclature of Rice Components

Rice, *Oryza sativa* L., is a staple for a large part of the world's human population, especially in East, South and Southeast Asia, making it the second-most consumed cereal grain [20]. Rice provides approximately more than one-fifth of the calories consumed by humans [21].

Rice cultivation is suite to countries and regions with low labor costs and high rainfall, as it is very labor-intensive to cultivate and requires plenty of water for cultivation. Rice can be grown practically anywhere, even on a steep hill or mountain. Although its species are native to South Asia and certain parts of Africa, centuries of trade and exportation have made it commonplace in many cultures. Rice can grow to 1–1.8 m. tall, occasionally more depending on the variety and soil fertility. The edible seed is a grain 5–12 mm. long and 2–3 mm. thick.

The traditional method for cultivating rice is flooding the fields with or after setting the young seedlings. This simple method requires sound planning and servicing of the water damming and channeling, but reduces the growth of lesser robust weed and pest plants and reduces vermin that has no submerged growth state. However, with rice growing and cultivation the flooding is not mandatory, whereas all other methods of irrigation require higher effort in weed and pest control during growth periods and a different approach for fertilizing the soil.

This dissertation intends to construct the architecture of rice shoot as a first objective, so that major components of rice structure are intensified. Nomenclature of rice components are described below:

Nomenclature of rice components
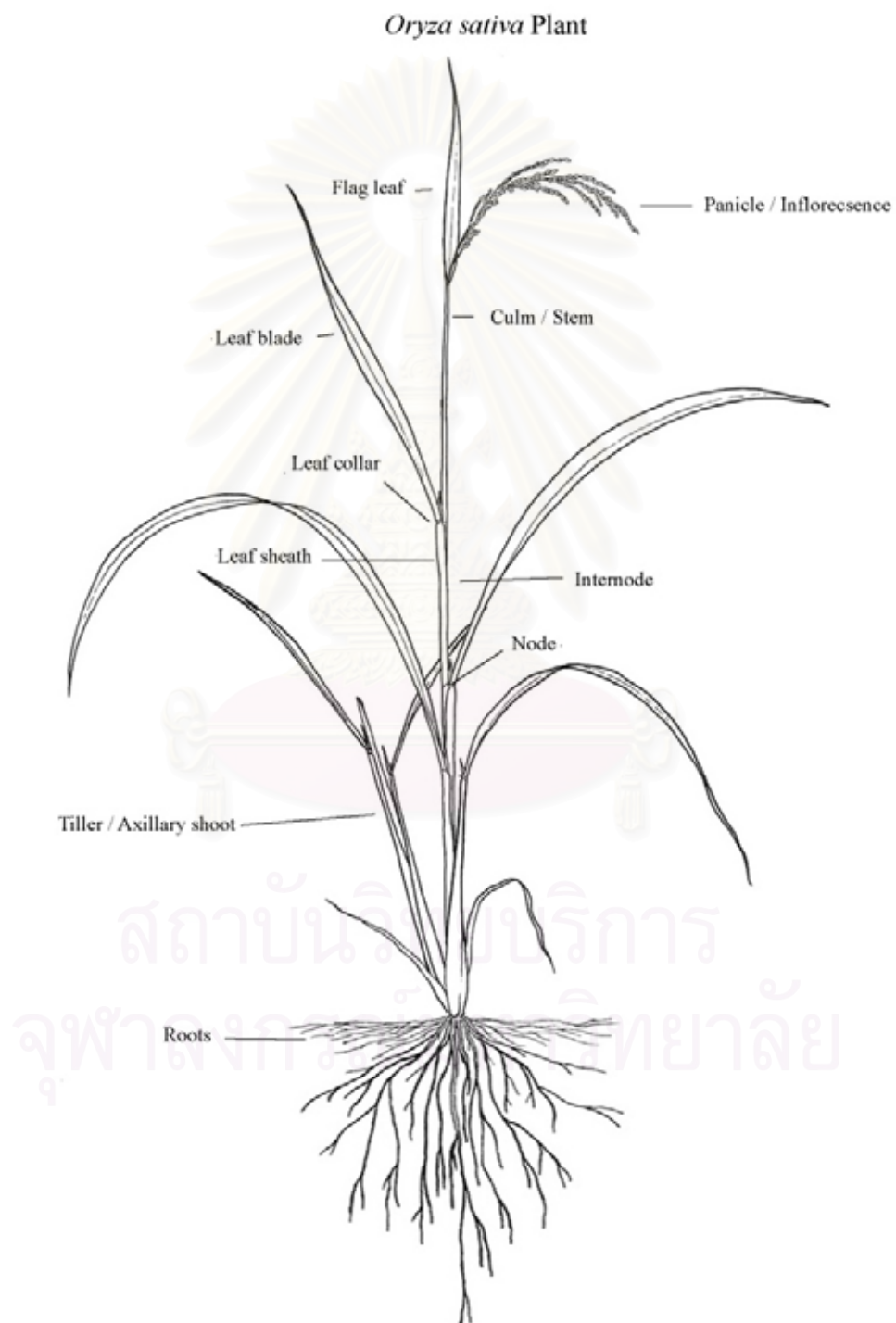
Figure 2.1: Structure and nomenclature of rice components (IRRI).

The parts of rice are the following

Tiller - The shoot developing from the axillary bud meristem.

Root - An axial system which is usually underground and more or less positively geotropic.

Stem - An axial system which is usually above ground and more or less negatively geotropic.

Node - The level (transverse plane) of a stem at which one or more leaves and associated auxiliary bud(s) arise.

Internode - The portion of a stem between the level of insertion of two successive leaves, i.e. between two nodes.

Leaf - Commonly thought of as one of the three basic parts of the seed plant body, a structure usually of determinate growth, without secondary thickening, and of superficial origin, often flattened and photosynthetic in part, and in the axil of which is found a bud.

Leaf blade - The blade of a leaf, usually flattened, and expanded.

Leaf sheath - Any tubular portion of the leaf surrounding the stem, as in the Poaceae.

Leaf collar - A thin band of intercalary meristematic tissue at the junction of the leaf blade (lamina) and the leaf sheath found in grasses.

Panicle - The grouping or arrangement in which flowers are borne on a plant.

Flag leaf - The last mature leaf before the inflorescence in a cereal crop plant.

2.1.2 Rice Growth Stages System

This section discusses the growth stages of the rice plant. The information presented is based on the data and characteristics of IR64 variety, but applies generally to other rice varieties [2].

The growth of the rice plant is divided into three phases:

1. Vegetative (germination to panicle initiation),

2. Reproductive (panicle initiation to flowering), and

3. Ripening (flowering to mature grain).

These 3 growth phases consist of a series of 10 distinct stages. These stages are numbered and described as follows:

Stage 0: germination to emergence. Seeds are usually pregerminated by soaking for 24 hours and incubating for another 24 hours. After pregermination, the radicle and coleoptile protrude through the hull. By the second or third day after seeding in the seedbed, the first leaf breaks through the coleoptile.

(IRRI, 2005)
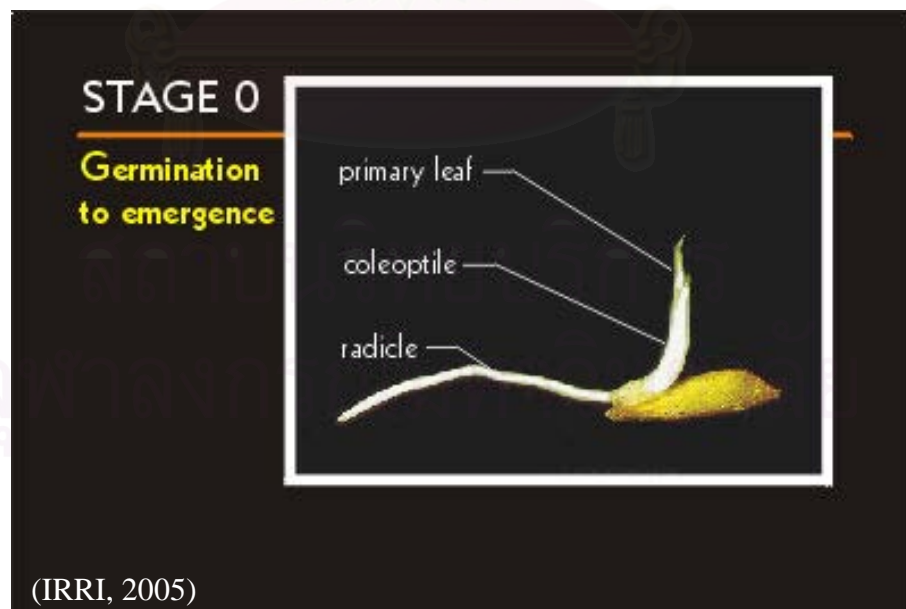
Figure 2.2: Germination to emergence stage shows the emerged primary leaf still curled and an elongated radicle.

Stage 1: seedling. The seedling stage starts right after emergence and lasts until just before the first tiller appears. During this stage, seminal roots and five leaves (including primary leaf) are developed.
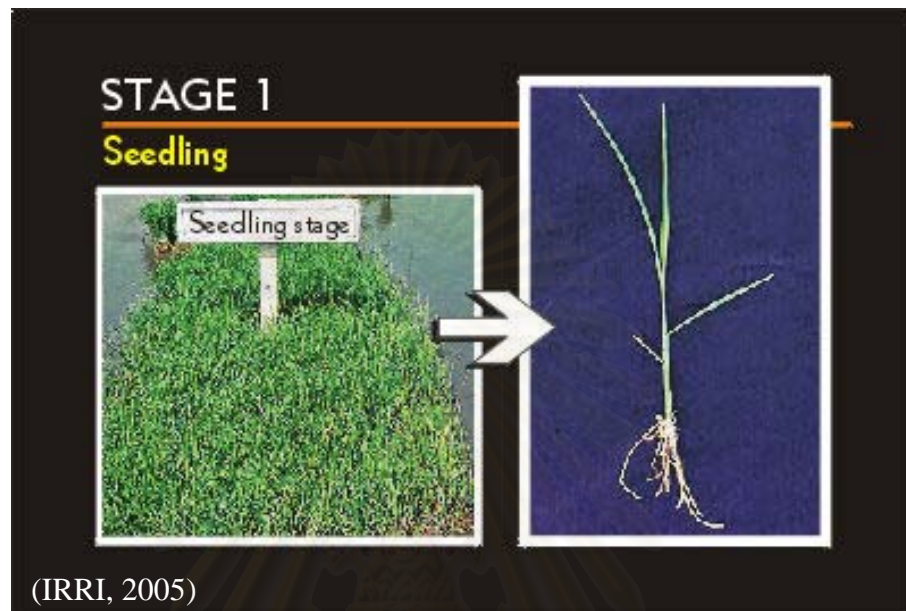
Figure 2.3: Stage 1, five leaves (including primary leaf) and root system are appeared.

As the seedling continues to grow, two more leaves develop. Leaves continue to develop at the rate of 1 every 3-4 days during the early stage. Secondary adventitious roots that form the permanent fibrous root system rapidly replace the temporary radicle and seminal roots.

Stage 2: tillering. This stage extends from the appearance of the first tiller until the maximum tiller number is reached. Tillers emerge from the axiliary buds of the nodes and displace the leaf as they grow and develop. After emerging, the primary tillers give rise to secondary tillers. This occurs about 30 days after transplanting. The plant is now increasing in length and tillering very actively. Here is a field with plants at the early tillering stage. Note the tiller size and canopy development due to increased leafing and tiller development. Besides numerous primary and secondary tillers, new tertiary tillers arise from the secondary tillers as the plant grows longer and larger.

By this stage, the tillers have multiplied to the point that it is difficult to pick out the main stem. Tillers continuously develop as the plant enters the next stage which is stem elongation.

(IRRI, 2005)
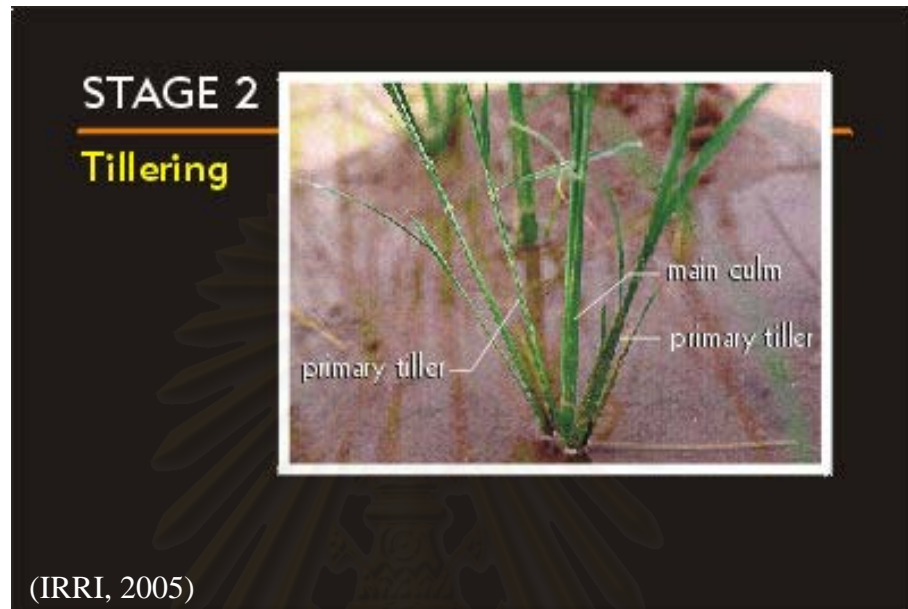
Figure 2.4: The seedling shows the position of the two primary tillers with respect to the main culm and its leaves.

Stage 3: stem elongation. This stage may begin before panicle initiation or it may occur during the latter part of the tillering stage. Thus, there may be an overlap of stages 2 and 3. The tillers continue to increase in number and height, with no appreciable senescence of leaves noticeable. Ground cover and canopy formation by the growing plants have advanced. Growth duration is significantly related to stem elongation. Stem elongation is more in varieties with longer growth duration. In this respect, rice varieties can be categorized into two groups: the short-duration varieties which mature in 105-120 days and the long-duration varieties which mature in 150 days.
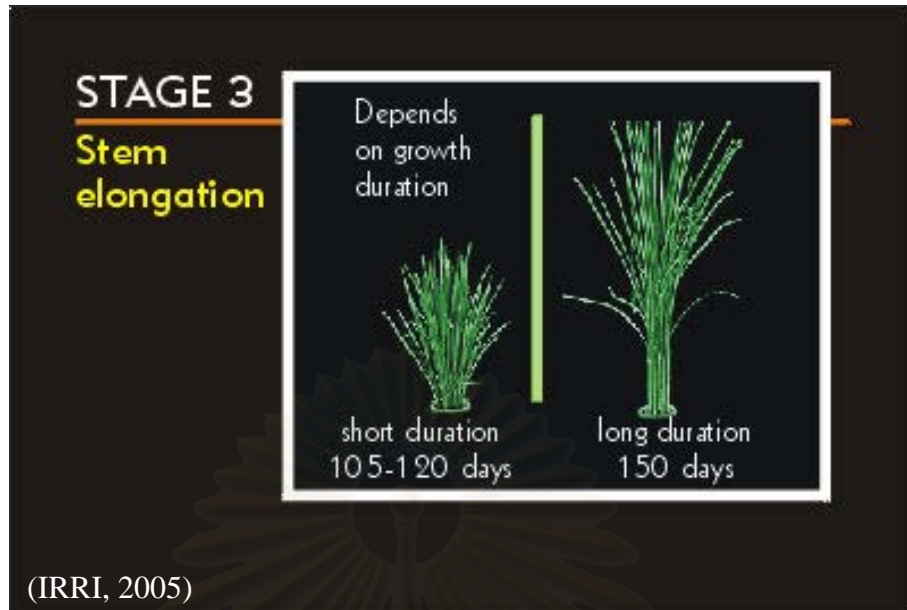
Figure 2.5: In early-maturing semi-dwarfs like IR64, the fourth internode of the stem, below the point where the panicle emerges, elongates only from 2 to 4 cm before panicle initiation becomes visible.
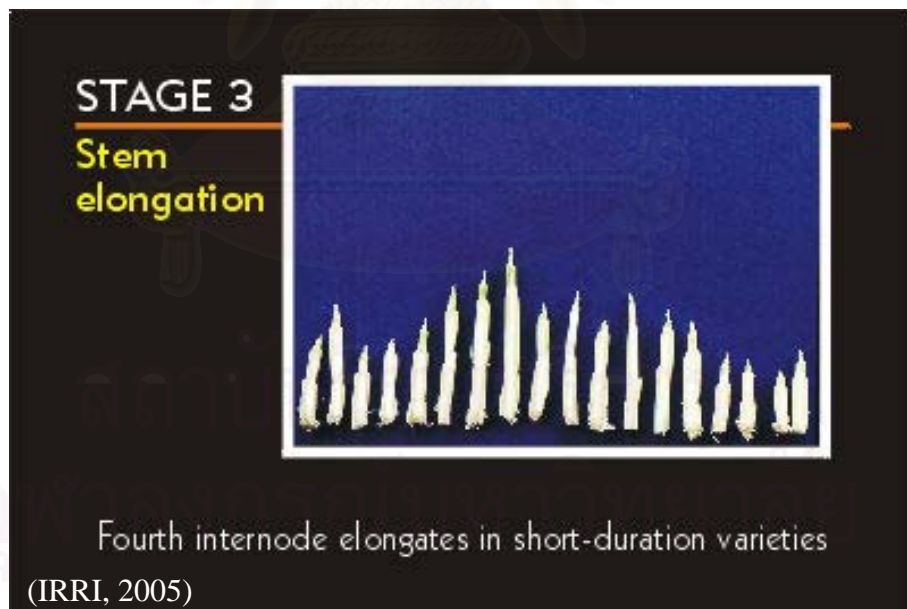
Figure 2.6: Stems which have been dissected to show the length of the fourth internode at the panicle initiation stage.

Maximum tillering, stem elongation, and panicle initiation occur almost simultaneously in short-duration varieties (105-120 days). In long-duration varieties (150 days), there is a so-called lag vegetative period during which maximum tillering occurs. This is followed by stem or internode elongation, and finally by panicle initiation.

These first four stages make up the vegetative phase, the first phase of rice plant growth.

Stage 4: panicle initiation to booting. The initiation of the panicle primordium at the tip of the growing shoot marks the start of the reproductive phase. The panicle primordium becomes visible to the naked eye about 10 days after initiation. At this stage, 3 leaves will still emerge before the panicle finally emerges.
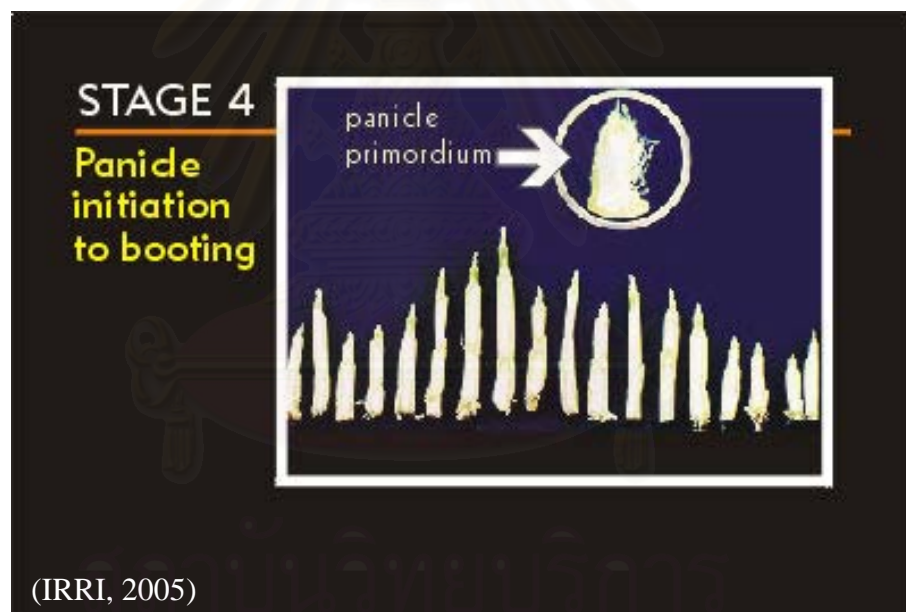
Figure 2.7: In short-duration varieties, the panicle becomes visible as a white feathery cone 1.0-1.5 mm long. It occurs first in the main culm and then in tillers where it emerges in uneven pattern. It can be seen by dissecting the stem.

As the panicle continues to develop, the spikelets become distinguishable.

(IRRI, 2005)
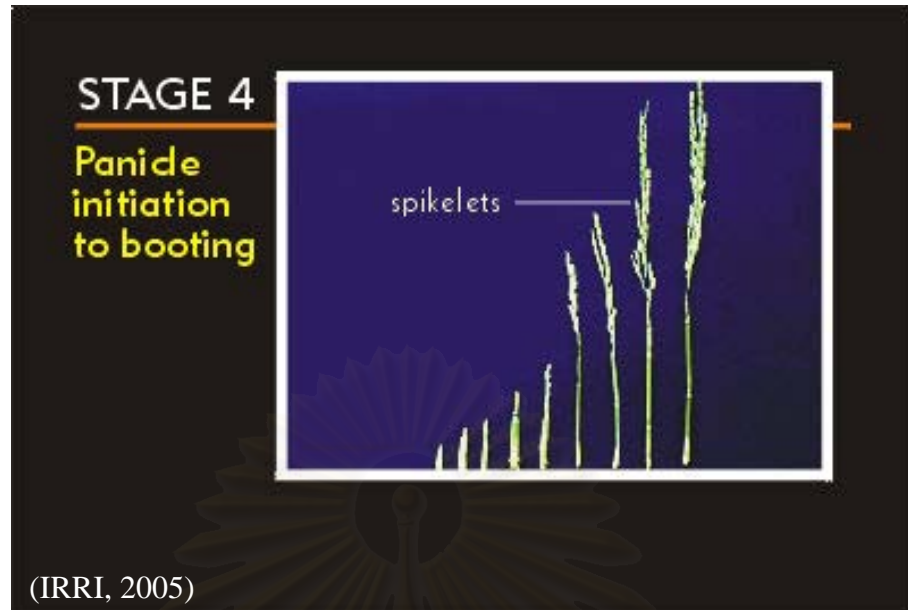
Figure 2.8: The young panicle increases in size and its upward extension inside the flag leaf sheath causes the leaf sheath t bulge. This bulging of the flag leaf sheath is called booting. Booting is most likely to occur first in the main culm.

(IRRI, 2005)

Figure 2.9: At booting, senescence (aging and dying) of leaves and nonbearing tillers are noticeable at the base of the plant.

Stage 5: heading or panicle exsertion. Heading is marked by the emergence of the panicle tip from the flag leaf sheath. The panicle continues to emerge until it partially or completely protrudes from the sheath.

Figure 2.10: Heading stage, panicle protrudes from flag leaf sheath.

Stage 6: flowering. It begins when anthers protrude from the spikelet and, then, fertilization takes place.
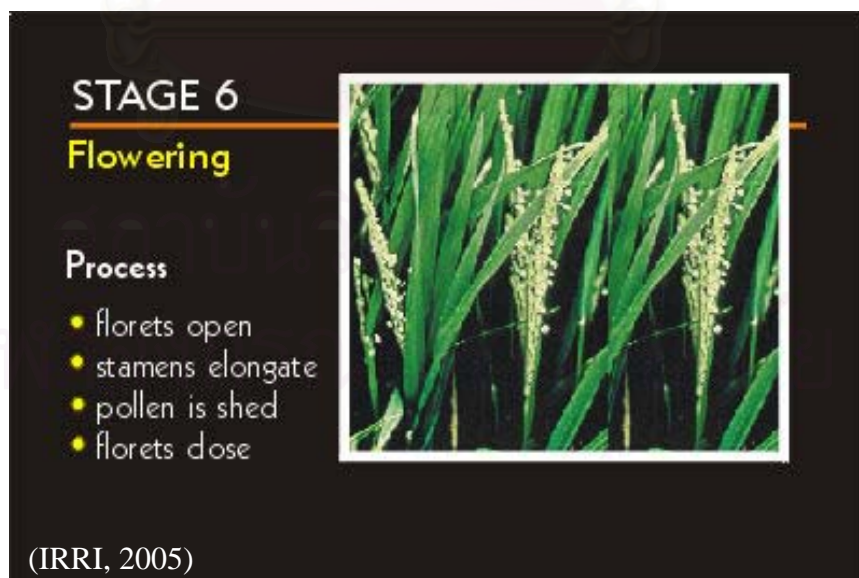
Figure 2.11: At flowering, the florets open, the anthers protrude from the flower glumes because of stamen elongation, and the pollen is shed. The florets then close.

The pollen falls on the pistil, thereby fertilizing the egg. The pistil is the feathery structure through which the pollen tube of the germinating pollen (round, dark structures in this illustration) will extend into the ovary.

Generally, the florets open in the morning. It takes about 7 days for all spikelets in a panicle to open. At flowering, 3-5 leaves are still active.

(IRRI, 2005)

Figure 2.12: The flowering process continues until most of the spikelets in the panicle are in bloom.

Stage 4, 5, and 6 constitute the reproductive phase, the second phase of rice growth. The last 3 stages of growth, stages 7, 8, and 9 comprise the ripening phase.

Stage 7: milk grain stage. In this stage, the grain has begun to fill with a milky material. The grain starts to fill with a white, milky liquid, which can be squeezed out by pressing the grain between the fingers.

(IRRI, 2005)
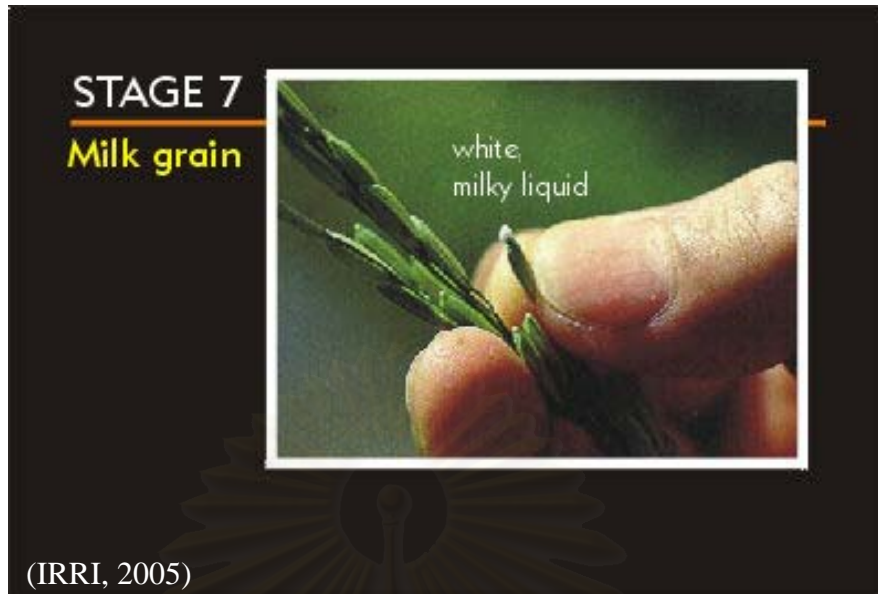
Figure 2.13: The panicle looks green and starts to bend. Senescence at the base of the tillers is progressing. The flag leaves and two lower leaves are green.

Stage 8: dough grain stage. During this stage, the milky portion of the grain first turns into soft dough and later into a hard dough. The grains in the panicle begin to change from green to yellow. Senescence of tillers and leaves is noticeable.

(IRRI, 2005)
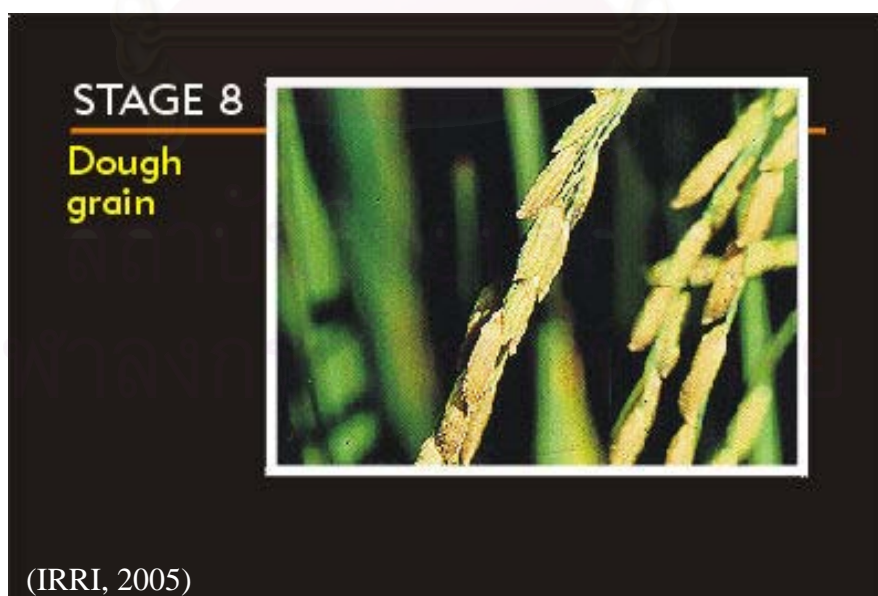
Figure 2.14: The field starts to look yellowish. As the panicle turns yellow, the last two remaining leaves of each tiller begin to dry at the tips.

Stage 9: mature grain stage. The individual grain is mature, fully developed, hard, and has turned yellow. The upper leaves are now drying rapidly although the leaves of some varieties remain green. A considerable amount of dead leaves accumulate at the base of the plant.

Figure 2.15: Rice plants at the mature grain stage. Most of the filled grains have turned yellow and hard.
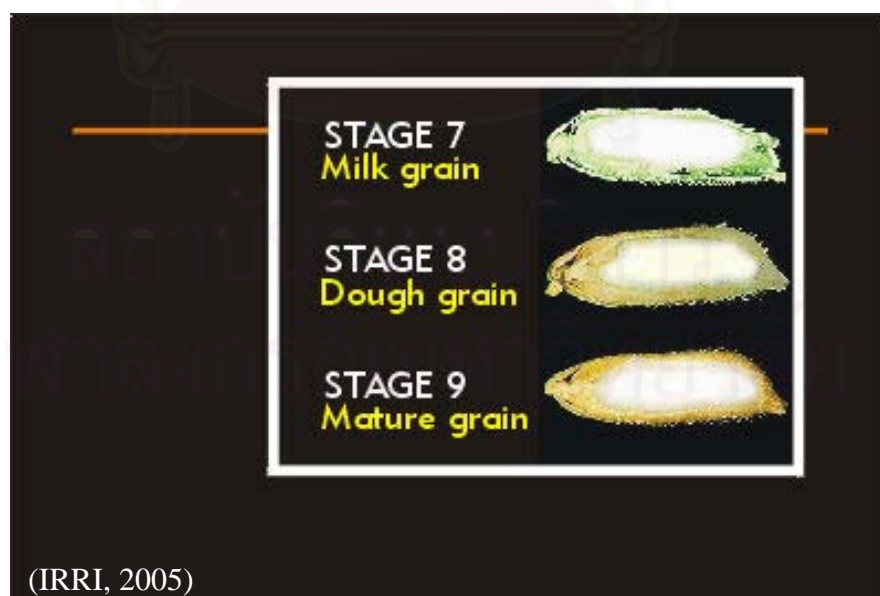
Figure 2.16: Stages 7 through 9, produce the milk grain, dough grain, and mature grain correspond to the ripening phase, the last phase in the development of rice plant.

2.1.3 Artificial Neural Network (ANN)

Biological Neural Network

An artificial neural network (ANN), often just called a "neural network" (NN), is a mathematical model or computational model based on biological neural networks. Figure 2.17 shows the biological neural network which has two parts very important called the synapse and the dendrite. The dendrites are extensions of a neuron which connect to other neurons to form a neural network, while synapses are a gateway which connects to dendrites that come from other neurons. A biological neuron may thus be connected to other neurons as well as accepting connections from other neurons, and so we have the basis of a network.

Through those connections electrical pulses are transmitted, and information is carried in the timing and the frequency with which these pulses are emitted. So, our neuron receives information from other neurons, processes it and then relays this information to other neurons. The neuron must generate some kind of output based on the cumulative input. We still don't know the exact answer to the question as to what happens in a biological neuron. However, we do know that our neuron integrates the pulses that arrive and when this integration exceeds a certain limit, our neuron in turn emits a pulse. Finally, one more thing that you should know is that dendrites modify the amplitude of the pulses travelling through them. This modification varies with time, as the network `learns'.
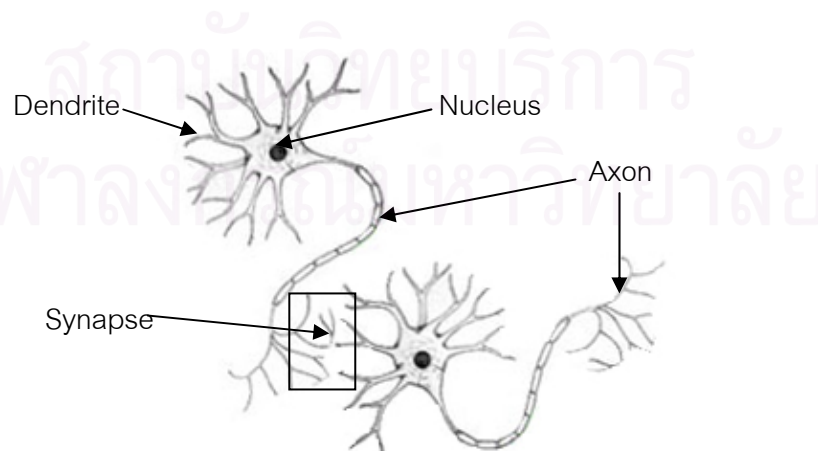
Figure 2.17: A biological neural network.

Mathematical Representation of a Neuron

In order to represent the mathematical representation, a neural network can be represented as shown in Figure 2.18. We called one node of neuron as a perceptron. Incoming connections are represented by input lines with an associated weight. The neuron itself only performs accumulation and thresholding for incoming pulses from its inputs.
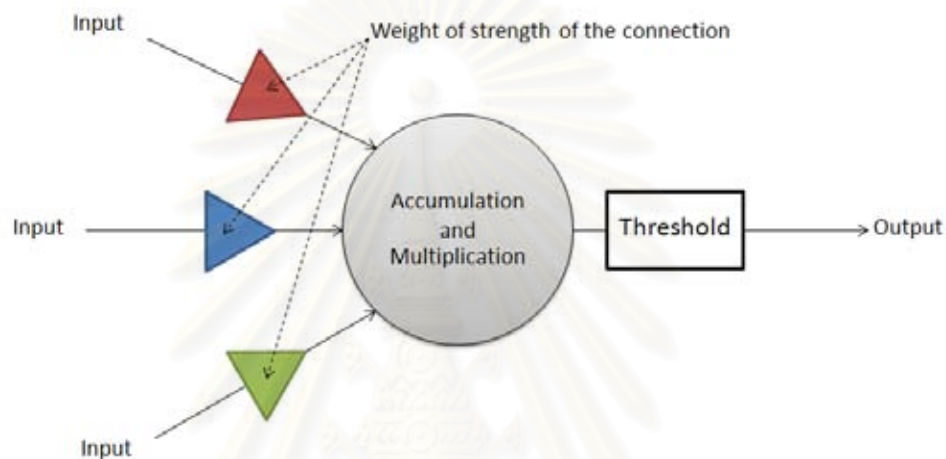
Figure 2.18: Mathematical representation of a neuron.

When a pulse comes from a connection, it is first multiplied by a number called the "weight" of the connection which assigns a certain importance to the connection (identical to the largeness of a biological dendrite). Then, the neuron accumulates the overall result, and passing the value through a threshold which emits a pulse when a certain value is reached. The output of the threshold stage is in turn connected to the inputs to several other neurons, which forms a complete network.

Neural network consists of an interconnected group of artificial neurons and processes information using a connectionist approach to computation (see Figure 2.19). In most cases an ANN is an adaptive system that changes its structure based on external or internal information that flows through the network during the learning phase. In more practical terms neural networks are non-linear statistical data modeling tools. They can be used to model complex relationships between inputs and outputs or to find patterns in data.
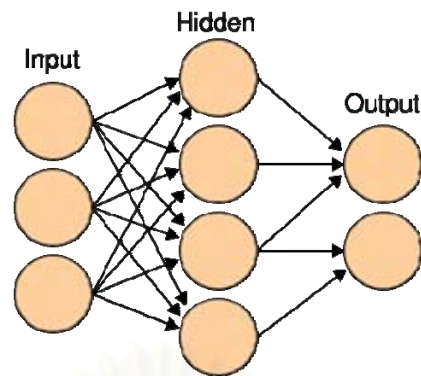
Figure 2.19: A biological neural network is an interconnected group of nodes, mimicking the network of neurons in the human brain.

Unfortunately, we can apply this simple mathematical model to practical computing and signal processing applications, since the signals transmitted through biological neurons are in the form of pulses. Instead, we adopt a further simplification by assuming that a set of real numbers are fed in, and a single real number is generated at the output. More sophisticated neural networks which continue to learn as they are being used may retain memory of the previous run. One may also employ feedback. So, we can use real input and output numbers to model the transactions between the different neurons. Instead of a biological threshold function, we use a mathematical function such as the sigmoid function, arctangent, arcsine, etc. These functions should be smooth and continuous (i.e. you should not use a piecewise linear or step function) and have an absolute upper and lower limit. They should also be differentiable.

The sigmoid function is one of the most widely used node transfer functions, and is illustrated in Figure 2.20:
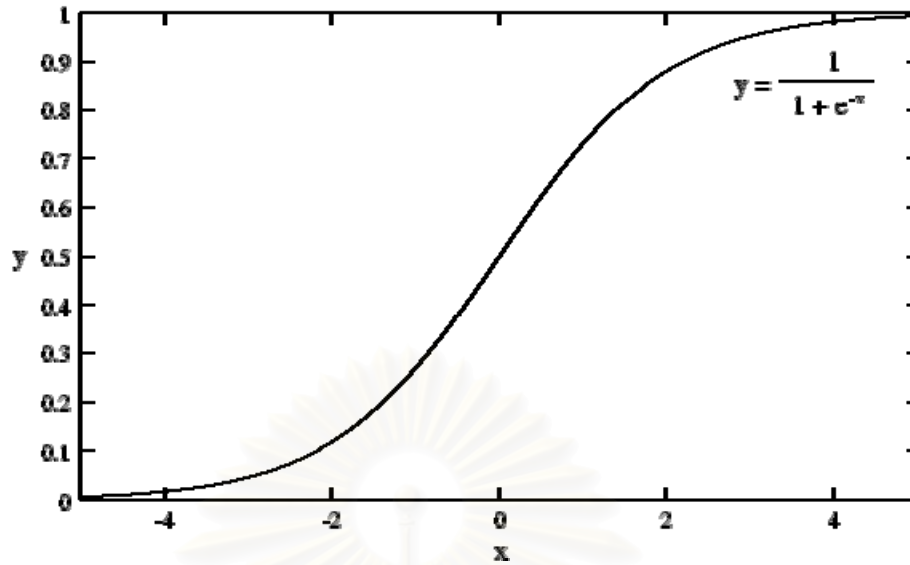
Figure 2.20: Sigmoid function

Multilayer Perceptron

The principal importance of a neural network is not only the way a neuron is implemented but also how their interconnections (more commonly called topology) are made. The topology of a human brain is too complicated to be used as a model because a brain is made of hundreds of billions of connections which can't be effectively described using such a low-level or highly simplified model.

A simple topology designed for easy implementation on a digital computer. One of the easiest forms of this topology at the moment is made of three layers :

- One input layer (the inputs of the network)

- One hidden layer

- One output layer (the outputs of the network)

All neurons from one layer are connected to all neurons in the next layer as shown in Figure 2.21. This forms a whole network with full interconnection, please note also that the weight (and therefore the importance) of each connection is not represented (for practical reason) here but must exist in the reality.
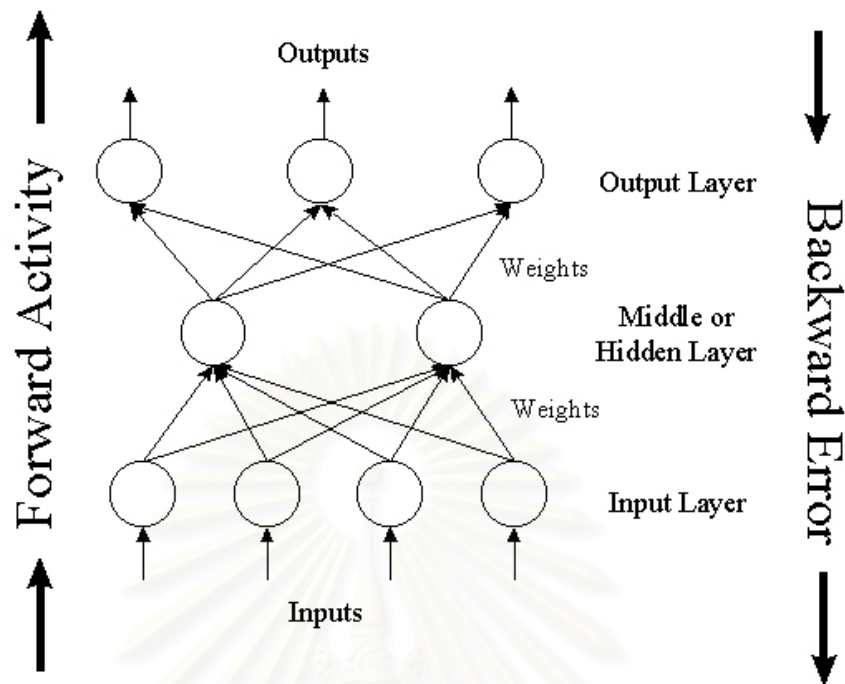
Figure 2.21: Back-propagation Network topology (Caudill and Butler, 1992).

Back-Propagation Neural Network

Back-Propagation Neural Network (BPNN), or propagation of error, is a common method of teaching artificial neural networks how to perform a given task. It is a supervised learning method. It requires a teacher that knows, or can calculate, the desired output for any given input. It is most useful for feed-forward networks (networks that have no feedback, that have no connections with the loop). The methodology of learning process can be summarized as the followings.

Summary of the BPNN learning process:

1. Feed training samples with their desired output or target to the neural network.

2. Compare the network's output to the desired output from that sample. Calculate the error in each output neuron.

3. For each neuron, calculate what the output should have been, and a scaling factor, how much lower or higher the output must be adjusted to match the desired output. This is the local error.

4. Adjust the weights of each neuron to lower the local error.

5. Assign "gradient" for the local error to neurons at the previous level, giving greater responsibility to neurons connected by stronger weights.

6. Repeat the steps above on the neurons at the previous level, using each one's "gradient" as its error. Since we have only moved a small step towards the desired state of a minimized error, the above procedure must be repeated many times until the mean square error (MSE) drops below a specified value. When this happens, the network is performing satisfactorily, and this training session for this particular example has been completed.

As the algorithm's name implies, the errors (and therefore the learning) propagate backwards from the output nodes to the inner nodes. So technically speaking, back-propagation is used to calculate the gradient of the error of the network with respect to the network's modifiable weights. This gradient is almost always then used in a simple stochastic gradient descent algorithm to find weights that minimize the error. Often the term "back-propagation" is used in a more general sense, to refer to the entire procedure encompassing both the calculation of the gradient and its use in stochastic gradient descent. Back-propagation usually allows quick convergence on satisfactory local minima for error in the kind of networks to which it is suited.

It is important to note that back-propagation networks are necessarily multilayer perceptrons (usually with one input, one hidden, and one output layer). In order for the hidden layer to serve any useful function, multilayer networks must have non-linear activation functions for the multiple layers: a multilayer network using only linear activation functions is equivalent to some single layer, linear network. Non-linear activation functions that are commonly used include the logistic function, the Gaussian functions, and other functions. The back-propagation algorithm for calculating a gradient has been rediscovered a number of times, and is a special case of a more general technique called automatic differentiation in the reverse accumulation mode. It is also closely related to the Gauss-Newton algorithm, and is also part of continuing research in neural back-propagation.

Modification of the neuron connection weights

Consider the example in Figure 2.22:
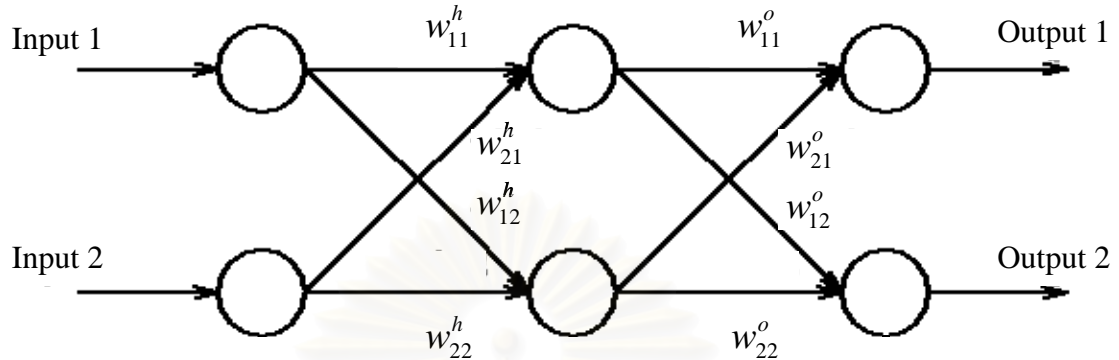
Figure 2.22: Example of (2, 2, 2) BPNN.

This neural network comprises of 2 inputs, 2 hidden nodes, and 2 outputs (usually called (2, 2, 2) back-propagation neural network). Designating (I_1, I_2), (H_1, H_2), and (O_1, O_2) as the inputs, hidden-layer outputs and output-layer outputs respectively, the outputs of hidden node 1 and 2 are given by

$$H_1 = sgm\left(\sum_{i=1}^{2} I_i w_{i1}^h\right) \tag{2.1}$$

and

$$H_2 = sgm\left(\sum_{i=1}^{2} I_i w_{i2}^h\right) \tag{2.2}$$

where w_{ij}^h is a weight parameter between input node i^{th} and hidden node j^{th}, w_{ij}^o is a weight parameter between hidden node i^{th} and output node j^{th}, and sigmoid function sgm(x) is denoted by

$$sgm(x) = \frac{1}{1+e^{-x}} \tag{2.3}$$

The output-layer outputs are given by

$$O_1 = sgm\left(\sum_{j=1}^{2} I_j w_{j1}^o\right) \tag{2.4}$$

and

$$O_2 = sgm\left(\sum_{j=1}^{2} I_j w_{j2}^o\right) \tag{2.5}$$

or, using (2.1) and (2.2),

$$O_1 = sgm\left(\sum_{j=1}^{2} sgm\left(\sum_{i=1}^{2} I_i w_{ij}^h\right) w_{j1}^o\right) \tag{2.6}$$

and

$$O_2 = sgm\left(\sum_{j=1}^{2} sgm\left(\sum_{i=1}^{2} I_i w_{ij}^h\right) w_{j2}^o\right) \tag{2.7}$$

Now we can calculate the output given a particular set of inputs. This allows us to calculate the mean squared error (MSE) between the actual output and the desired output for the given input in this training example. This is simply the average of the squares of the difference between what we want and what we got. Since we are interested in the shape of the error curve rather than the precise MSE function, we don't need to divide by the number of outputs, and the minimisation algorithm will still find the correct minimum. Thus, our error function can be formally written as

$$E = \sum_{k=1}^{2} (D_k - O_k)^2 \tag{2.8}$$

or, using (2.6) and (2.7),

$$E = \sum_{k=1}^{2}\left(D_k - sgm\left(\sum_{j=1}^{2} sgm\left(\sum_{i=1}^{2} I_i w_{ij}^h\right) w_{jk}^o\right)\right)^2 \tag{2.9}$$

where D_k is the kth desired output.

For example in the following example, suppose we have in the output 0.75 and 0.05 and the desired outputs 0.9 and 0.1. The MSE is now $((0.9\text{-}0.75)^2+(0.1\text{-}0.05)^2)/2$, which is equal to 0.0125 (remember in the BPNN algorithm we wouldn't need to divide by N). Clearly, for any given training example, this value is a function only of

the weights of the network. So, to reduce the error, we can try to move to the lowest point on this surface. To find this point, it is necessary to calculate the gradient of the error function with respect to each network weight. One may then move each weight slightly in the opposite direction to the gradient - if the surface is sloping upwards in a particular direction, we adjust the weights so that the point on the error surface moves downwards.

The gradient is fairly straightforward to calculate, due to the convenient fact that the derivative of the sigmoid function can be expressed in terms of the function itself:

$$\frac{d}{dx}\left(\frac{1}{1+e^{-x}}\right) = \frac{e^{-x}}{(1+e^{-x})^2} = (1-sgm(x))sgm(x) \qquad (2.10)$$

The gradient is defined as the vector of partial derivatives of the multivariate function with respect to each of variable. Because the error is a function of the network outputs, calculation of a set of partial derivatives for each output node with respect to each associated connection weight is needed. This turns out to be trivial, since all other variables but the one of interest are held constant when the partial derivative is calculated. Thus, only one linear term is left in the calculation of the partial derivative of the output, and leaving the coefficient which is just the corresponding input. So, we can write

$$\frac{\partial O_k}{\partial w_{jk}^o} = \frac{\partial}{\partial w_{jk}^o}\left(\sum_{m=1}^{2} w_{mk}^o H_m\right) = H_j \qquad (2.11)$$

Now, the gradient of the error function can be calculated (note: $S^o = \sum_{m=1}^{2} w_{jk}^o$):

$$\frac{\partial E}{\partial w_{jk}^o} = \frac{\partial}{\partial w_{jk}^o}\left(\sum_{k=1}^{2}(D_k - O_k)^2\right)$$

$$= -2(D_k - O_k)\frac{\partial}{\partial S^o}\left(sgm(S^o)\frac{\partial S^o}{\partial w_{jk}^o}\right)$$

$$= -2(D_k - O_k)((1 - sgm(S^o))sgm(S^o))H_j \qquad (2.12)$$

The expression $-2(D_k - O_k)((1 - sgm(S^o))sgm(S^o))$ is denoted δ_n^o.

The new values for the network weights are calculated by multiplying the negative gradient with a step size parameter (called the learning rate) and adding the resultant vector to the vector of network weights attached to the current layer. This change does not take place, however, until after the middle-layer weights are updated as well, since this would corrupt the weight-update procedure for the middle layer.

Clearly, the error at the output will be affected by the weights at the middle layer, too. However, the relationship is more complicated. A new gradient is derived, but this time the output weights are treated as constants rather than the hidden-layer weights. Now, the actual output is a function of the weights attached to the middle layer only (and in a generic network there are LM of those, for L input nodes and M middle-layer nodes). Fortunately, it is still a relatively simple expression.

$$\frac{\partial E}{\partial w_{ij}^h} = ((1 - sgm(S^h))sgm(S^h))\sum_{k=1}^{2} \delta_k^o w_{jk}^o I_i \qquad (2.13)$$

The middle weights are updated using the same procedure as for the output layer, and the output layer weights are updated as well. This is a complete training cycle for one piece of training data. It should be noted that the input layer is really only a buffer to hold the input vector. Therefore, it has no weights which need to be modified. However, in a more generic network, one may have more than one hidden layer. Again, the update procedure is quite similar. Once the modifications have been calculated, all weights (hidden and output) may be updated.

Please note: The above description assumes a (2, 2, 2) network. The only difference in the mathematics resulting from a larger network is longer summations. All of the principles are the same. The training process is analogous to the biological process of learning, the strength of individual connections between the neurons increases or decreases as human learn.

2.1.4 Quantitative and Allometric Relationship

Quantitative relation is a relation between magnitudes, and allometry is used to describe the morphological evolution of species, and is based on the relation between an organism's size and the size of any part of the organism.

Allometry is studied during the growth of a single organism; as a comparison between different organisms of the same species; and between organisms in different species. The allometric equation is graphed on an XY axis, with the body size on the x-axis and the part size on the y-axis. The scatter produced by the different measurements being compared can then be analyzed for useful data.

Allometry allows scientists to study biological functions as they increase as a power of body size. For instance, more energy is consumed by an elephant, but a mouse probably consumes more energy when that energy is measured as a function of mouse body weight.

The allometric equation is generally stated as

$$y = mx + b \qquad (2.14)$$

where y = predicted size of body part; x = observed body weight; m = slope acquired; and b = the value of y where it intercepts the vertical axis.

Not all allometric comparisons are linear; the allometric equation is frequently modified to compensate for this. The point is to determine a consistent relationship for the species in question. Another example of allometric equation that compensates for nonlinear functions is:

$$\log(y) = \log(b) + m[\log(x)] \qquad (2.15)$$

Most biological functions increase as some power of body size. For example, more energy is needed to "run" an elephant than to run a mouse; as body size increases, so does the energy needed by the organism. More cognitively, if bodies are operated by brains, then it seems reasonable that the larger the body, the larger the brain needed to operate it (more nerves needed to coordinate more muscles, etc).

However, such size-based relationships are rarely 1:1 (that is, it is rare to have a 1-unit increase in body size produce exactly a 1-unit increase in metabolic rate, or brain size, or whatever).

So, considering in the relationship between body size and brain size; larger animals are expected to have larger brains, but we want to know more about the relationship for two reasons:

- **First**, knowing something about the general relationship might tell us something interesting about brains and cognition and intelligence in general.

- **Second**, if there is a general relationship, then we want to factor it out when talking about brain size in relation to cognition: cows have bigger brains than most monkeys, but that probably has more to do with having really bigger bodies than with unsuspected cow intelligence.

For starters, it makes sense to go out and measure a set of primate's body and brain size samples:
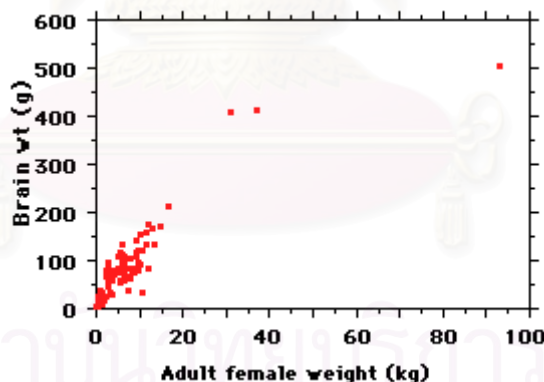
Figure 2.23: A plot of the data for 117 samplings of female body and brain weight.

Figure 2.23 shows a plot of the data for 117 samplings; adult females were used because it simplifies how one deals with sexual dimorphism, and for various theoretical reasons female mammals are thought to be the "ecological sex", with males more a derived form of females (driven by sexual selection). Here is what the data look like; note that body weight is given in kilos (1,000 gm) - so multiply the body weights by 1,000 to get them into the same units as brain weights.

We can see that bigger-bodied species tend to have bigger brains. But how do we express that relationship?

There are several methods for calculating a regression, but the principle is simple: it is a line of best fit between the variables (see Figure 2.24). And the line itself can be described by a simple equation of the form

$$y = mx + b \tag{2.16}$$

where y = predicted brain weight, x = observed body weight, m = slope and b = the value of y where the line intercepts the vertical axis.
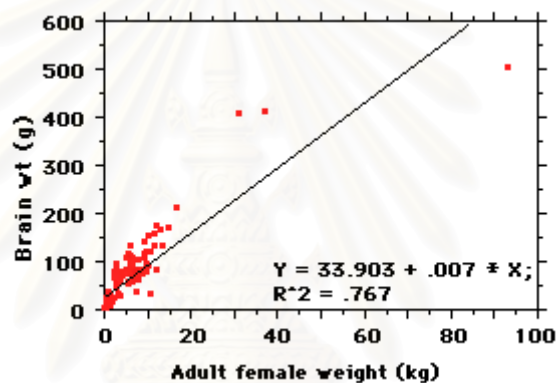
Figure 2.24: Linear regression for describing the relation between body and brain weight of female.

The regression here explains about 77% of the variance (R^2). That means about 77% of variation in y is explained by variation in x. But there are still have some problems, looking at the line, it is clear that while it might be the best average straight line fitting those points, there is a strong tendency for points near the ends to fall below the line and points in the middle to fall above it. Basically, the relationship between body weight and brain weight does not seem to be linear.

Try a nonlinear regression, of course. Figure 2.25 shows a 2nd-order regression, and then the line explains about 89% of the variation.

$$Y = 8.633 + .013 * X - 7.996E\text{-}8 * X\char94 2; R\char94 2 = .889$$
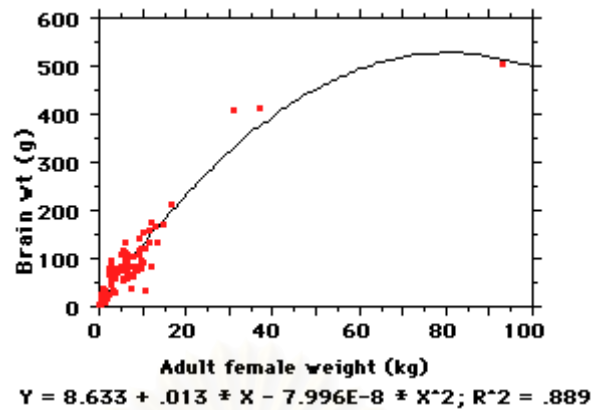
Figure 2.25: The 2nd-order regression for describing the relation between body and brain weight of female.

However, 2nd-order equations are difficult to compare. So we convert the raw data to base-10 logs, as in the Figure 2.26 (note units need to be the same, so body weight is now in grams). When the data are expressed as logs, they fit a nice easy linear equation, the points are spread out, so we can see what is going on, and the R^2 value is essentially unchanged (the slight difference between 0.889 in the untransformed data and the 0.884 here is due to the transformation).

$$Y = -1.197 + .822 * X; R\char94 2 = .884$$
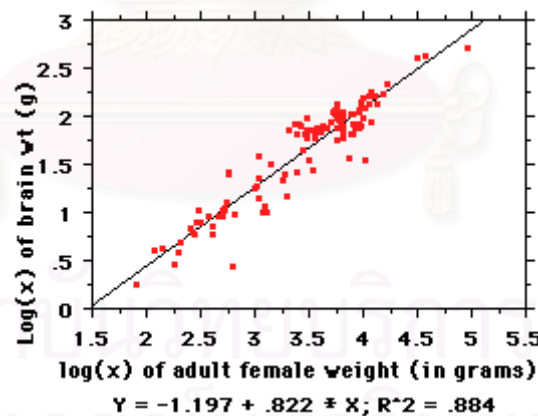
Figure 2.26: The data are converted to base-10 log, then linear regression will be obtained with closely R^2 value to previous method.

Now, the equation for the line here is of the familiar "$y = mx + b$" form, but the "y" and "x" here are actually log(brain weight) and log(body weight).

This is an allometric equation; "allo" comes from Greek: allos is equal to "other", in this case "other than metric" that is, nonlinear (the alternative is a linear or

isometric equation, a 1:1 relationship -- e.g., for every kilo of body weight, add 20gm of brain). To express the same nonlinear relationship directly, that is, with an equation in which x is body weight, not log(body weight), we convert from the above which is really

$$\log(y) = \log(b) + m[\log(x)] \tag{2.17}$$

to the standard form for allometric equations, $y = bx^m$.

2.1.5 L-system

An L-system or Lindenmayer system is a parallel rewriting system, namely a variant of a formal grammar (a set of rules and symbols), most famously used to model the growth processes of plant development, but also able to model the morphology of a variety of organisms [22]. L-systems can also be used to generate self-similar fractals such as iterated function systems. L-systems were introduced and developed in 1968 by the Hungarian theoretical biologist and botanist from the University of Utrecht, Aristid Lindenmayer (1925–1989).

As a biologist, Aristid Lindenmayer worked with yeast and filamentous fungi and studied the growth patterns of various types of algae, such as the blue/green bacteria Anabaena catenula. Originally the L-systems were devised to provide a formal description of the development of such simple multi-cellular organisms, and to illustrate the neighborhood relationships between plant cells. Later on, this system was extended to describe higher plants and complex branching structures.

The recursive nature of the L-system rules leads to self-similarity and thereby fractal-like forms which are easy to describe with an L-system. Plant models and natural-looking organic forms are similarly easy to define, as by increasing the recursion level the form slowly 'grows' and becomes more complex. Lindenmayer systems are also popular in the generation of artificial life.

L-systems are now commonly known as parametric L systems, defined as a tuple

$$G = \{V, S, \omega, P\}, \tag{2.18}$$

where, *V* (the alphabet) is a set of symbols containing elements that can be replaced (variables),

S is a set of symbols containing elements that remain fixed (constants),

ω (start, axiom or initiator) is a string of symbols from V defining the initial state of the system, and

P is a set of production rules or productions defining the way variables can be replaced with combinations of constants and other variables. A production consists of two strings; the predecessor and the successor.

The rules of the L-system grammar are applied iteratively starting from the initial state. As many rules as possible are applied simultaneously, per iteration; this is the distinguishing feature between an L-system and the formal language generated by a grammar. If the production rules were to be applied only one at a time, one would quite simply generate a language, rather than an L-system. Thus, L-systems are strict subsets of languages.

An L-system is context-free if each production rule refers only to an individual symbol and not to its neighbors. Context-free L-systems are thus specified by either a prefix grammar, or a regular grammar. If a rule depends not only on a single symbol but also on its neighbors, it is termed a context-sensitive L-system.

If there is exactly one production for each symbol, then the L-system is said to be deterministic (a deterministic context-free L-system is popularly called a D0L-system). If there are several, and each is chosen with a certain probability during each iteration, then it is a stochastic L-system. Using L-systems for generating graphical images requires that the symbols in the model refer to elements of a drawing on the computer screen.

Examples of L-systems

<u>Example 1</u>: Algae, L-system for modelling the growth of algae.

     variables : A B

     constants : none

     start : A

     rules : $(A \rightarrow AB), (B \rightarrow A)$

which produces:

     $n = 0$: A

     $n = 1$: AB

     $n = 2$: ABA

     $n = 3$: ABAAB

     $n = 4$: ABAABABA

     $n = 5$: ABAABABAABAAB

     $n = 6$: ABAABABAABAABABAABABA

<u>Example 2</u>: Sierpinski triangle, the Sierpinski triangle drawn using an L-system.

     variables : A B

     constants : + −

     start : A

     rules : $(A \rightarrow B-A-B), (B \rightarrow A+B+A)$

     angle : 60°

Here, A and B mean both "draw forward", + means "turn left by angle", and − means "turn right by angle" (see turtle graphics). The angle changes sign at each iteration so that the base of the triangular shapes are always in the bottom (they would be in the top and bottom, alternatively, otherwise).
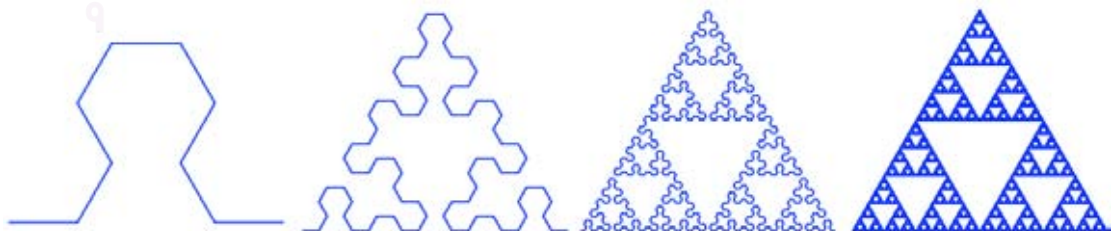
Figure 2.27: Sierpinski triangle draw with evolution for $n = 2$, $n = 4$, $n = 6$, $n = 9$.

Example 3: Fractal plant

      variables : X F

      constants : + −

      start : X

      rules : (X → F-[[X]+X]+F[+FX]-X),(F → FF)

      angle : 25°

which produces the result in figure 2.28.

Figure 2.28: Result of L-system generates the fractal plant (Lindenmayer, 1968).

Here, F means "draw forward", - means "turn left 25º", and + means "turn right 25º". X does not correspond to any drawing action and is used to control the evolution of the curve. The sign "[" corresponds to saving the current values for position and angle, which are restored when the corresponding "]" is executed.

2.1.6 Radiosity Rendering Technique

Radiosity is a global illumination algorithm used in 3D computer graphics rendering. Radiosity methods were first proposed in about 1950 in the engineering field of heat transfer [23]. They were later refined specifically for application to the problem of rendering computer graphics in 1984 by researchers at Cornell University [24]. Radiosity is an application of the finite element method to solving the rendering equation for scenes with purely diffuse surfaces. The surfaces of the scene to be rendered are each divided up smaller surfaces (patches). A form factor is computed for each pair of patches. Form factors are coefficients describing how well the patches can see each other. Patches that are far away from each other, or oriented at oblique angles relative to one another, will have smaller form factors.

The basic radiosity method has its basis in the theory of thermal radiation, since radiosity relies on computing the amount of light energy transferred among surfaces. In order to simplify computations, the method assumes that all scattering is perfectly diffuse. Surfaces are typically discretized into quadrilateral or triangular elements over which piecewise polynomials function is defined (for example see Figure 2.29).
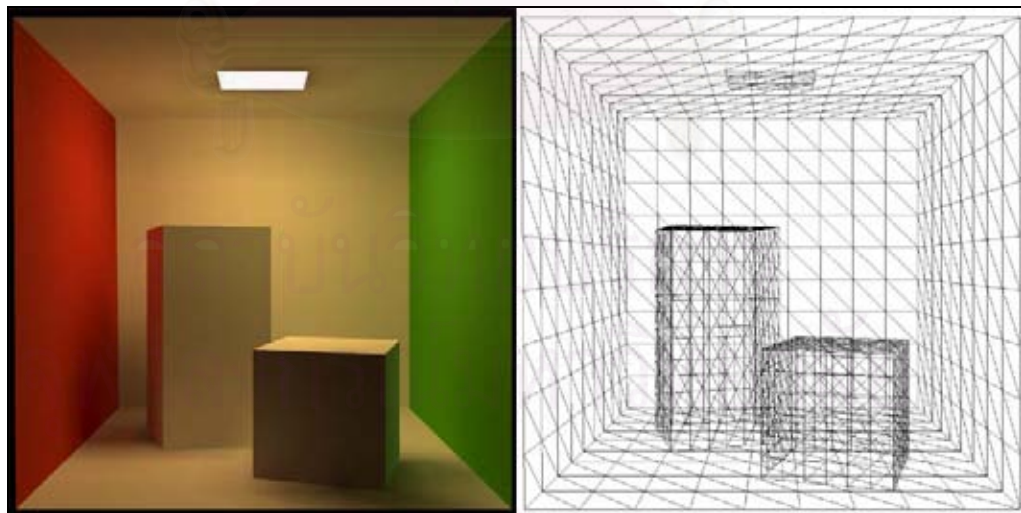
Figure 2.29: Rendered scene with radiosity technique (left), and discretized objects in the same scene (right). (Cornell's box, www.geomerics.com)

After this breakdown, the amount of light energy transfer can be computed by using the known reflectivity of the reflecting patch, combined with the view factor of the two patches. This dimensionless quantity is computed from the geometric orientation of two patches, and can be thought of as the fraction of the total possible emitting area of the first patch which is covered by the second patch.

More correctly, radiosity is the energy leaving the patch surface per discrete time interval and is the combination of emitted and reflected energy:

$$B_i dA_i = E_i dA_i + R_i \int_j B_j F_{ji} dA_j , \qquad (2.19)$$

where:

B_i is the radiosity of patch i.

E_i is emitted energy.

R_i is the reflectivity of the patch, giving reflected energy by multiplying by the incident energy (the energy which arrives from other patches).

All j ($j \neq i$) in the rendered environment are integrated for $B_j F_{ji} dA_j$, to determine the energy leaving each patch j that arrives at patch i.

F_{ij} is the constant-valued view factor for the radiation leaving from patch i and hitting patch j.

Considering

$$A_i F_{ij} = A_j F_{ji} , \qquad (2.20)$$

so the equation 2.19 can be derived to

$$B_i = E_i + R_i \int_j B_j F_{ij} . \qquad (2.21)$$

To ease for use, the integral is replaced and uniform radiosity is assumed over the patch, creating the simpler:

$$B_i = E_i + R_i \sum_{j=1}^{n} B_j F_{ij} \qquad (2.22)$$

This equation can be applied to every patch. The form factor, F_{ji}, can be calculated in a number of ways. Early methods used a *hemicube* (an imaginary cube centered upon the first surface to which the second surface was projected, devised by Cohen and Greenberg in 1985) to approximate the form factor, which also solved the intervening patch problem [50]. This is quite computationally expensive, because ideally form factors must be derived for every possible pair of patches, leading to a quadratic increase in computation with added geometry. New methods include adaptive integration was proposed by G. Walton in 2002 [25]. He described the use of adaptive integration for the calculation of view factors between simple convex polygons with obstructions. The accuracy of the view factor calculation was controlled by a convergence factor. The adaptive integration method was compared with two other common methods implemented in a modern computer program and found to have significant advantages in accuracy and even advantages in computational speed in some cases.
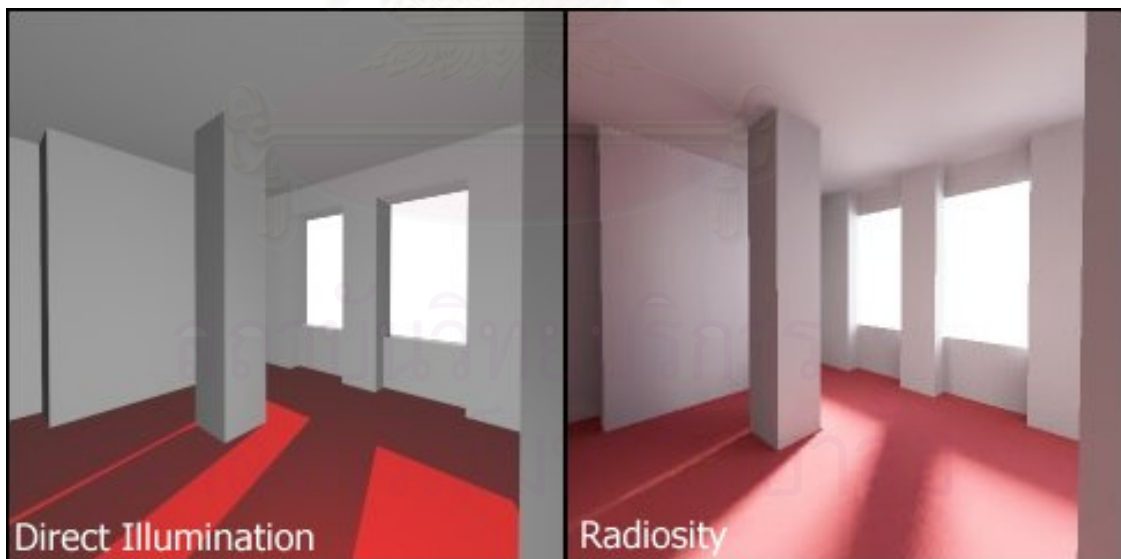
Figure 2.30: Comparison of scenes which are rendered with direct illumination (left) and radioity technique (right), (www.geomerics.com).

Radiosity was perhaps the first rendering algorithm in widespread use which accounted for diffuse indirect lighting. Earlier rendering algorithms, such as Whitted-style ray tracing were capable of computing effects such as reflections, refractions, and shadows, but despite being highly global phenomena these effects were not commonly referred to as "global illumination." As a consequence, the term "global illumination" became confused with "diffuse interreflection," and "Radiosity" became confused with "global illumination" in popular parlance. However, the three are distinct concepts. The scene generated by using direct illumination and global (radiosity) illumination are compared as shown in Figure 2.30.

The radiosity method in the current computer graphics context derives from (and is fundamentally the same as) the radiosity method in heat transfer. Calculation of Radiosity rather than surface temperatures is a key aspect of the radiosity method that permits linear matrix methods to be applied to the problem. However, the Radiosity algorithm is that it is relatively simple to explain and implement. This makes it a useful algorithm for applying to other works related to global illumination algorithms.

2.2 Literature Review

2.2.1 Rice Architectural Model

Since mid-1960's, researchers began to develop computer models for quantitatively studying plant growth [26]. Researches in computer simulations of plant growth, virtual plant research, are widely studied and broad applied in agronomy, forestry, ecology, and other areas. Virtual plant model is based on a description of eco-physiological processes and can be used to simulate synthetic and global variables of plant growth under different environmental conditions such as crop yields, biomass, leaf area index, mass number of organs, and nutrient uptakes. However, these eco-physiological models rarely treated plant morphology in details. In general, eco-physiological models focus on predicting biomass production at a crop level, and they are useful tools for predicting crop production and evaluating land productivity from readily available input data whereas virtual plant models are best suited for the modeling of plant architecture dynamics and processes. Virtual plant models focus on plant architecture and describe plants as individual entities. These models are used to simulate the spatial features of a plant and output the three-dimensional architectural visualized as realistic images.

Physiological models of plants usually contain a simple description of the plant in a few broad compartments (roots, stems, leaves, flowers, fruits). These models aim at predicting the dry matter production as the result of the functioning of the plant (photosynthesis, respiration, biomass partitioning), which regulated by the environmental factors. They usually give accurate predictions of biomass productions and yields, but important aspects of plant architecture are missing. However, plant architectural models have been developed. These morphological models aim at generating 3-dimensional virtual plants that are faithful to botanical knowledge. This approach contains two complementary parts: (1) the mathematical models based on morphological knowledge and experimental measurements and, (2) the computer simulation and graphical representation of plant development based on these mathematical models. A well-known example is L-systems grammar [22], which provides the possibility to formalize the description of plant architecture.

L-studio (http://www.cpsc.ucalgary.ca/Research/bmv/lstudio/) is a software package that uses L-systems grammar in combination with a graphical interface to create a three-dimensional virtual plant. In rice research, Tomonari Watanabe et al. [27] applied the L-systems formalism to create "three-dimensional virtual rice" plants, incorporating models of phonological development and leaf emergence period as a function of temperature and photo period, which were used to determine the timing of tiller emergence. The "three-dimensional virtual rice" model has a possibility to demonstrate the differences in the structure and development between cultivars and under different environmental conditions.

2.2.2 Rice Growth Simulation System

Physiological and architectural plant models have originally been developed for different purposes and therefore have little in common, thus making combined applications difficult [28]. A recent trend is efforts to combine physiological and architectural models, i.e. linking structure and functioning of the plants. Mech and Prusinkiewicz [29] introduced the formalism of open L-systems, allowing exchange of information with the environment. Hence, it becomes possible to make the development of the structure responsive to external and local conditions [30]. One could also think of e.g. calculating assimilate production and organ sink strength (growth potential) using a physiological model, and feed this information into an L-system. The L-system, then, allocates growth to specific buds, shoots and leaves in accordance with their relative growth potentials [31]. The L-system also calculated the numbers and size of organs present in the next cycle (e.g. the next day) and this information is fed into the physiological model. Complete integration of these modeling approaches should combine the strong points of both, resulting in a powerful tool which will bring modeling of ornamental quality a major step forward.

GREENLAB is one of the few plant models that links physiological plant activity with plant architecture. Recently, many papers on the development, simulation results and application of GREENLAB have been published, including colorful pictures of 3-dimensional virtual plants [32]. In GREENLAB plant fresh biomass production is computed from transpiration, assuming transpiration efficiency to be constant and atmospheric demand to be the driving force, under non-limiting

water supply [28]. The fresh biomass is then distributed among expanding organs according to their relative demand (as mentioned above). Demand for organ growth is estimated from allometric relationships (e.g. leaf surface to weight ratios) and kinetics of potential growth rate for each organ type. These are obtained through parameter optimization against empirical, morphological data sets by running the model in inverted mode. The model reproduced accurately the dynamics of plant growth, architecture and geometry of various annual and woody plants, enabling three-dimensional visualization. Although calibrated by optimization to reconstruct observed, prototypic plants, and the model is able to simulate some of the plant's phenotypic plasticity resulting from competition among sinks for resources. GREENLAB is able to simulate the variability of leaf size on the plant as a result of water stress in different phases of plant development and compensatory growth following pruning [28]. This, as well as the dynamic simulation of complex morphogenetic processes using the principle of sub-structures, constitutes important innovations in plant architectural modeling.

2.2.3 Light Interception Model of Plant

Light is usually the most important factor influencing the growth and development of plants while nutrients and water are not limited [9, 10]. To gain more understanding and take advantage from plant, many light interception models were developed and investigated in plant science research. Both 2D and 3D computer graphics was used as a tool for calculating amount of light that can be absorbed by the plant leaves or canopy.

Leaf area estimation for light interception model could be estimated by satellite image. Francisco J. Flores et al. proposed the estimation method of leaf area from the multispectral satellite images [11]. The relationship between leaf area index (LAI) of loblolly pine plantations and broadband simple ratio (SR) vegetation index calculated from Landsat Enhanced Thematic Mapper Plus (ETM+) data was examined. The results suggest that stand LAI of loblolly pine plantations can be accurately estimated from readily available remote sensing data and provide an opportunity to apply the findings from eco-physiological studies in field plots to forest management decisions at an operational scale. R.E.E. Jongschaap proposed the

integrating crop growth simulation and remote sensing to improve resource use efficiency in farming systems [12]. Remote sensing data collected by satellite were used to determined leaf area of plant in farm for predicting wheat production at regional scale.

Also the calculation of light transmission through a plant canopy could be measured by processing the fish-eye hemispherical images. Sinoquet et al. presented a method to measure light interception by vegetation canopies which uses a 3D digitizer and image processing software. Information on light interception is derived from the virtual images by using simple features of image analysis software. The method was applied to cotton, grapevine and young mango plants [13].

Many techniques for estimating light interception on 3D plant canopy were proposed [14-18]. Since 1993, Buwalda et al. proposed a method incorporating interactive computer graphics to simulate spatially variable radiation interception ad canopy photosynthesis [14]. The model was applied to examine spatial variability of photosynthesis within canopies of kiwifruit (*Actinidia deliciosa*) vine growing on two trellis types. R. Manfred et al. developed a three dimensional approach to modeling light interception in heterogeneous canopies in 1999 [15]. They proposed a simulation tool to assess radiation penetration into canopies that (1) give details on light absorption in heterogeneous canopy architectures and (2) comprise simple and easily adaptable routines. In 1999, Maria Luisa Espana et al. presented their 3D model of maize (*Zea mays* L.) canopy structure for accurate reflectance simulation [16]. They focused on fully developed maize plants without paying attention to the reproductive organs. Their 3D model of maize with small number of parameters was presented; they tried to reduce the number of parameter used to describe the 3D maize model. The canopy structure is used to compare the SAIL reflectance model to the reflectance simulated with PARCINOPY which is monte-carlo ray tracing model, but did not compare to the actual plants. B. Pommel et al. calculated the cumulative radiation intercepted by three 3D regular canopies, presenting a regular distribution as three different plant population densities [17]. The ADEL-Maize model which constructed based on L-system formalism, simulated 3D canopies of maize was proposed. The simulation results show that light interception on unchanged leaf size of canopies can be estimated. In 2007, Nathalie Lamanda et al. used 3D architectural

models to assess light availability and root bulkiness in agroforestry systems [18]. Light transmission and the number of coconut roots were assessed in coconut smallholdings from 6 to 60 years old. The modeling of light transmission through coconut stands was based on three-dimensional virtual coconut trees and a numerical light model that computed the shade cast by coconut trees on underlying crops.

More complex model of light calculation was also investigated. Indirect light such as diffuse and penetrated light was considered [9, 19], but did not integrate with the direct light interception model yet. Francisco de Castro and Ned Fetcher proposed their three dimensional model of interception of light by a plant canopy. Their canopy model was divided into small cubic cells, each on characterized by mean leaf angle and the leaf area index. The model can calculate the probability that a beam will penetrate to any given cell without being intercepted by the foliage in the path. The model had been tested against real measurements taken in an artificial plantation, reaching an R^2 of 0.714 between predicted and observed values. Xiping Wang el al. presented their model to simulate the interception of DPAR in plant canopies [19]. Two sub-model were proposed; first is the 3D maize canopy surface which represented as small triangular facets according to 3D digitized data collected from field, and the second sub-model is divided sky for calculating diffused light. The Dividing Sky Hemisphere with Projection (DSHP) model was validated against DPAR measurements made in actual maize (*Zea mays L.*) canopy. However, more accuracy and realistic modeling technique of light calculation still required.

2.2.4 Rice Crop Simulation Model

RICEMOD [5] is a FORTRAN and BASIC based eco-physiological model for irrigated rice production. The models aim to study the relative constraining effects of radiation, leaf blade nitrogen content, respiration rate, and assimilate partitioning on rice plant growth. Useful for predicting future production scenarios, but does not include the influence of CO_2. It includes a number of physical parameters, including accommodation of subroutines dealing with soil and plant chemistry as well as physical processes of the atmospheric environment. The model is very sensitive to soil parameters and has been expanded to consider soil water deficit. Model

components include maximum leaf area index, timings of plant growth initiation and harvest, radiation-use efficiency (RUE), and harvest index (HI).

ORYZA2000 [7, 8] is the successor to a series of rice growth models. The models aim to study the impact of climate change rice yields and explore adaptive management options (fertilizer, cultivar type, irrigation strategy, sowing date, etc.). It is an update and integration of the models ORYZA1 for potential production, ORYZA-W for water-limited production, and ORYZA-N for nitrogen-limited production.

The model combines several modules: aboveground crop growth, evapotranspiration, nitrogen dynamics, soil-water balance, and others. A very simple model (VSM) for yield prediction of rice under different water and nitrogen applications was proposed in latest 2005 [33]. The VSM was developed for simulation of rice grain and biomass yields under different irrigation and nitrogen application management strategies. The model can provide the grain and biomass yields based on maximum leaf area index, harvest index, and light use efficiency. The model assumes a triangular pattern for leaf area changes and proportionately of biomass accumulation to the intercept solar radiation. The accuracy of the model was verified with independent data from other experiments in the study area and in the northern parts of Iran with sub-humid climate.

2.2.5 Application of Neural Network in Agricultural Research

The future challenges confronting this dynamic, architectural plant model [28] will be (1) the need to substitute some of the lumped functions (black boxes) with mechanistic processes, such as energy interception and conversion, and water status dynamics and their physiological feedbacks on plant growth; (2) the formulation of feedbacks of physiological status on architecture, in addition to plant geometry; and (3) the demonstration that the resulting system is useful not only for re-creation of observed structures (representation, explanation), but also for the accurate prediction of the phenotypes in hypothetical environments (extrapolation).

A Neural Network (NN) is an information processing paradigm that is mimic biological nervous systems, such as the brain, process information. The key element

of this paradigm is the novel structure of the information processing system. It is composed of a large number of highly interconnected processing elements (neurons) working in unison to solve specific problems. Neural networks, like people, learn by example. A neural network is configured for a specific application, such as pattern recognition or data classification, through a learning process. Learning in biological systems involves adjustments to the synaptic connections that exist between the neurons. Neural networks are widely used for solving several kinds of problems, including highly complex problems in plant science, ecology, agro-ecology, and agriculture [34, 35, 36, 37].

Neural networks have several advantages over multivariate analysis techniques. They have potential to solve problems where large amount of data exist, but the relationships between system inputs and outputs are not well understood. They can handle noisy data with a higher degree of accuracy, and incomplete data [37]. There are several neural network models that used to describe the relationships between the characteristic of plant organs such as leaf area, or color [38], and their yields. Some models can be used to predict crop yields by considering the environments or climate changes as Uhrig's model [39]. However, there is no integrated model that linking every parts of plant organs together. Especially, virtual rice model, which is performed by sub-network models, will be gained valuable advantages in both scientific and economic study.

CHAPTER III
MATERIALS AND DATA ACQUISITION

3.1 Plant Materials

Experiments were performed on two different model cultivars: Khao Dawk Mali 105 rice (*Oryza sativa* L. cultivar 'KDML105') and Pathumthani 1 rice (*Oryza sativa* L. cultivar 'PTT1'). Both rice cultivars are known as the most famous and very important to Thai export demand.

Khao Dawk Mali 105 rice (*Oryza sativa* L. cultivar 'KDML105')

KDML105 rice is known as "Jasmine rice or Hom Mali rice" in Thailand, which stands for fragrant rice and is Thai specialty. Jasmine rice is smooth, shiny and silky in appearance and is considered the finest grade of rice in Thailand. When cooked, it produces a fragrant aroma and is slightly chewy in texture (see Figure 3.1).

Figure 3.1: Thai Jasmine rice or Hom Mali rice.

Specification:

· Name: Khao Dawk Mali 105

· Characterstic: smooth, shiny and silky, photoperiod sensitive rice, in-season rice field

· Grain: brown color, tapering shape

· Average Height: about 1.50 meters

· Flowering: 20 October

· Texture of the Rice: soft white, tender and naturally fragrant

· Dormancy: 8 weeks

· Productivity: 750-1,047 Kg/Rai

· Cultivation: about 160-180 days (20 November)

Pathumthani 1 (*Oryza sativa* L. cultivar 'PTT1').

Thai Pathumthani Fragrant Rice (Figure 3.2) is a kind of fragrant rice but said to be less fragrant than Jasmine rice. Also it's a year round crop and can be grown in an easier way. It has a natural aroma depending on its age, and when cooked, the rice kernels have a tender texture.

Figure 3.2: Thai Pathumthani Rice

Specification:

- · Name: Pathumthani 1
- · Characteristics: smooth, shiny and silky, photoperiod insensitive rice, double-crop field; off-season paddy field
- · Average Height: 1.04 -1.33 meters
- · Grain: brown color, tapering shape, hairy, long awn
- · Texture of the Rice: soft white, tender and authentic naturally fragrant
- · Dormancy: 3-4 weeks
- · Productivity: 650 - 774 Kg/Rai
- · Cultivation: about 104 - 126 days

3.2 Experimental Site

The field experiment was carried out at the actual rice field in Loei province (17°48′ N, 101°74′ E), Thailand. Experiments for this dissertation were performed in small size (2m. x 3m.). Transplanted rice used in the studies was grown in the chamber (see Figure 3.3). Global weather data were also measured, data logger and its sensor were set on the tripod located in the center of experimental area.
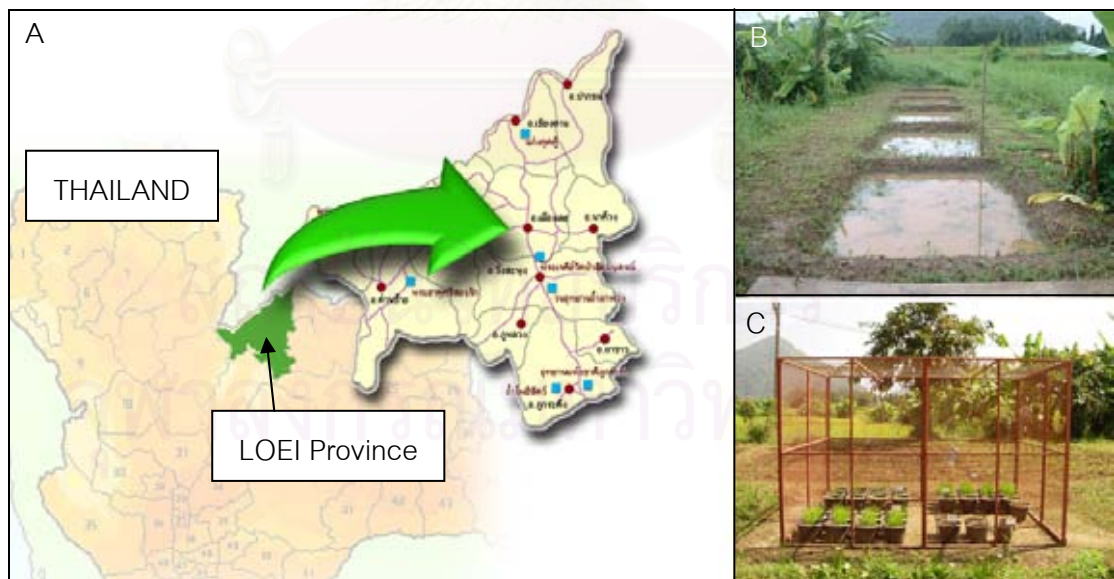
Figure 3.3: A) The experimental site is located in Loei province, north-east of Thailand. B) The 2m. x 3m. plots for seedling plant. C) A chamber set up with nets against bugs.

3.3 Data Acquisition

This dissertation is separated into three main parts of working steps; the first part is modeling and constructing a three-dimension architectural model which was proposed in 2006 [41], the second part is the calculation method of light incidence presented in 2008 [43], and the third part is rice growth system developed by using integrated neural network for describing quantitative and allometric relationship among each rice parts. Thus, we designed three experiments and collected data for those three models separately. And the acquisition of weather data is expressed in the last sub-section.

3.3.1 Measurement of Rice Structure and Rice Growth

The experimental data used for constructing a three dimensional model of rice based on L-system was designed and performed in conditions as followings: Thai Jasmine Rice (*Oryza sativa* L. cultivar 'KDML105') and Pathumthani 1 rice (*Oryza sativa* L. cultivar 'PTT1') were planted on July 9th, 2006 in the actual rice field. Germination behavior of seedlings was observed. After 30 days from emergence, for each cultivar of rice, 10 similarly plants were selected and transplanted into pots. All components and characteristic of rice were observed until harvesting date on December 1st, 2006. Both rice cultivars were 145 days old.

For the measurement of rice growth, number of leaves, leaf width, leaf length, leaf shape, leaf angle, height of internode, and number of tillers were collected weekly. Germination behavior was observed during germination stage. Then a three-dimension structural model of rice was constructed [41].

3.3.2 Measurement of Light Incidence

A three-dimension architectural model of rice which used for modeling the calculation of the amount of light incidence was reconstructed. We observed and collected the characteristic data once again in year 2007. The same rice cultivars were planted on August 1st, 2007 in two blocks of size 2m. x 3m. After 15 days of growth, for each of rice cultivar, 10 similar plants were selected and transplanted into 10 pots each. There were two groups of pots for two types of rice. Details of leaf shape and leaf area were collected carefully.

The intensities of PAR (PPFD, photosynthetic photon flux density) at fifty randomized positions on observed plant were measured. The observation was performed during September 23rd, 2007 and September 30th, 2007. The rice during this time was in the early booting stage and the canopy heights for the KDML105 and PPT1 were 1.25 m and 1.1 m, respectively. There were 8–14 green leaves on every stem in both rice cultivars. Under and above canopy, PAR was measured.

3.3.3 Measurement of Rice Growth Parameters for Constructing Growth System

Two rice cultivars, KDML105 and PTT1 were planted on August 1st, 2007 in the prepared 2m. x 3m. rice plots (Figure 3.3B). Seedlings are placed in a set of pots filled with the same soil. Fertilizer (16-16-16) which composes of Nitrogen (N), Phosphorous (P), and Potassium (K), was applied in the pots (Figure 3.4). The water level of each pot was controlled in equal level. After 15 days of growth, 25 similarly plants (with height, number of leaves, and root density) were selected and were transplanted into 25 pots for each rice cultivar. Plant architecture, rice growth parameters and the intensity of PAR (PPFD, photosynthetic photon flux density) were also measured. The weather station was set up in the middle of the field experiment.

Figure 3.4: Twenty five pots filled with the same soil. Seedlings were transplanted to pots on 15 days after germination.

In this dissertation, we divided rice structure into four main parts as stem, leaves, root, and panicle. Fourteen characteristics of rice parts, considered as the variables of functional model, were defined as shown in Table 3.1.

Table 3.1: Four rice parts and their characteristic variables.

Rice Part	Part Characteristic	Variable name
Stem	Width	W_s
	Length	L_s
	Biomass	M_s
Leaf	Width	W_l
	Length	L_l
	Area	A_l
	Biomass	M_l
Root	Length	L_r
	Number of Root	N_r
	Biomass	M_r
Panicle	Length	L_p
	Number of Panicle Branch	N_p
	Biomass	M_p
	Number of Grain	N_g

Weekly recordings of all rice parts were collected. Fourteen characteristic variables of rice parts are highly concentrated. Width, length, the number of grain, and the number of tillers will be measured from seedling to maturity; alternatively, dry-weight was also collected. We observed the pattern of growth in two steps consistent to the bi-phasic growth of rice [40]. Tiller density is an important indicator of high yields in rice production. Tillering is affected by the rice variety and numerous environmental factors, including temperature, and light. So, the accumulated light was considered as a variable effected to the model. Collected data were used in the analytical method of quantitative model and allometric relationship model.

3.3.4 Weather Data

There are six weather data were collected, five from six were collected by the HOBO data logger (H21-001) with smart sensors (S-LIB-M003, S-LIA-M002, S-THB-M002, and S-WCA-M003, see Figure 3.5 and Appendix). The rain-fall (Rn) data were also retrieved from the meteorology station of Loei province. The experiments were performed during August 15th, 2007 and March 15th, 2008. The weather station was set up in the middle of the field experiment. Lists of five weather parameters which collected automatically are shown as followings:

1. Air Temperature (measured in unit of degree Celsius, $^{\circ}C$), T
2. Relative Humidity (RH, %), H
3. Solar Radiation (Energy flux, MJ/m^2/day), $Solar$
4. Photosynthetically Active Radiation (PAR, Mole quantum /m^2/day), Par
5. Wind Speed (km/day), W_d
6. Rain-fall (mm), R_n

Figure 3.5: The HOBO weather station with smart sensors.

CHAPTER IV

RICE ARCHITECTURAL MODEL, LIGHT INTERCEPTION MODEL, AND INTEGRATED NEURAL NETWORK MODEL

Three models; a three dimension rice architectural model [42], a light interception model [43], and an integrating of neural network model are proposed. This chapter describes the models methodology. Results of these three models led to constructing the rice growth system expresses in the last section of this chapter.

4.1 Three-Dimension Rice Architectural Modeling

A three dimension dynamically model of rice has proposed in 2006 [41], the model was constructed from L-system and the growth model came from a set of weekly observed data under a biologically knowledge. The improvement of the three dimensional model of rice is reconstructed for more accuracy. The leaf shape and leaf area are considered more closely to the real leaf in order to calculate an amount of light incident to leaf area. The leaf shape and leaf curve data have been collected for constructing new model. The L-system of rice is presented in Section 4.1.1. The mechanical of dynamic rice model is shown in Section 4.1.2. The biological motivated conditions are illustrated in Section 4.1.3.

This three-dimension architectural model of rice will be used to calculate the light interception model. Section 4.1.4 shows an analytical method of leaf shape. The leaf curve is expressed in Section 4.1.5. Leaf segmentation method is described in Section 4.1.6, and the calculation of leaf area in the three-dimensional model of rice is presented in Section 4.1.7.

4.1.1 L-system of Rice

The growth stages of rice are considered as three main stages; seedling, vegetative, and reproductive stage. The rice components are denoted by some characters in L-system is indicated in Figure 4.1.

Rice shoot part is important for finding the amount of light incidence in order to develop the rice growth system. During rice growth, apex will be developed to the

set of shoot part: stem, bud, and apex. Steps of rice shoot growth are shown in Figure 4.2.
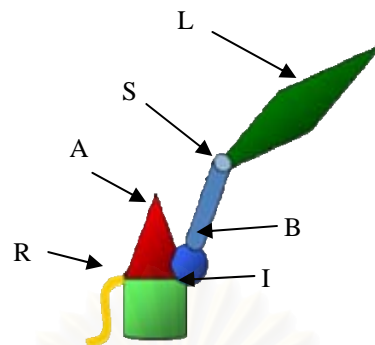
Figure 4.1: Structures of rice which are described by L-system.
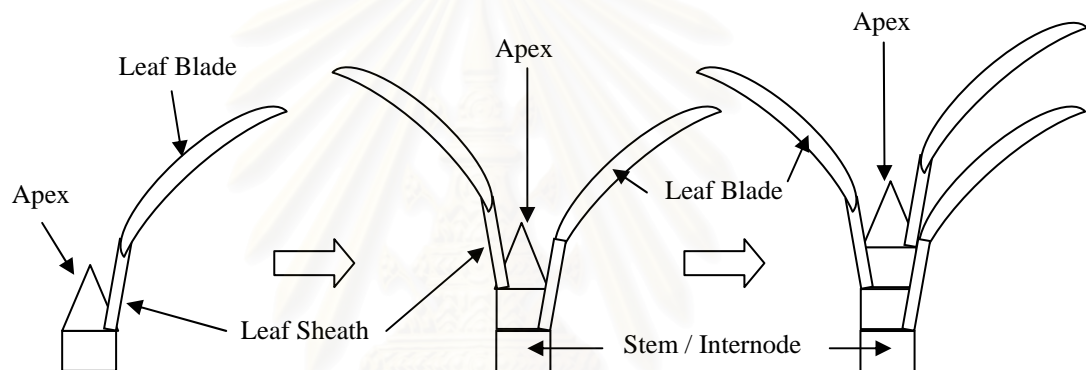
Figure 4.2: Steps of rice shoot growth.

Structure of rice model in each of growth stage can be described by L-system as shown below,

Seedling Stage

Seed → *Seed*[*Coleoptile*][*Radicle*]

Coleoptile → *Mesocotyl* | *Coleoptile* | [*PrimaryLeaf*]A

where *Seed* is the axiom of the model,

Coleoptile is the first appearance component of shoot part,

Radicle is the first appearance component of root part,

Mesocotyl is the second appearance component of shoot part,

PrimaryLeaf is the first leaf of rice, and

A is rice shoot apex.

Vegetative

      A → I[R][F][B][SL]A | [F]A

      B → I[R][F][B][SL]A

      R : {Root path growing by biological motivation}→r[R]

      A : {when DVI=1.0} → iP

where A is rice shoot apex,

      B is the rice bud,

      I is the stem internode,

      F is the second appearance component of shoot part,

      S is a leaf sheath,

      L is a leaf blade,

      P is rice panicle,

      R is rice root part,

      r is root segment,

      i is internode of rice panicle, and

      DVI is a developmental index of rice [42].

Note that, the Developmental Index (DVI) [42] was applied to represent the physiological development of the rice plant. DVI is a continuous variable and defined as 0 at first leaf emergence 1.0 at panicle initiation, 2.0 at heading and 3.0 at maturity.

Reproduction

      P → i[P]PG | iG

where P is the panicle,

      i is internode of rice panicle, and

      G is rice grain.

4.1.2 Dynamic Plant Part

The static three dimension architectural model of rice proposed by T. Watanabe [27] was used to modify the rice movement cause by wind and gravity. Each part of rice is considered as the following:

Stem

Two wind force directions $F_x(t)$ and $F_y(t)$ are considered. Both forces change the angle of each segment of stem. Spring model with the modulus coefficient is also included. Figure 4.3 shows the concept of this part. Angle of stem segment will be change with respect to the direction of x axis. The angle of stem segment (θ_{sx}) is defined as,

$$\theta_{sx} = Sin^{-1}(\frac{\Delta x}{L_s})\qquad(4.1)$$

where L_s is the length of stem.

Distance of stem () which move away from the old direction line is calculated by,

$$\Delta x = -\frac{F_x(t)}{k}\qquad(4.2)$$

where k is the elastic modulus parameter.
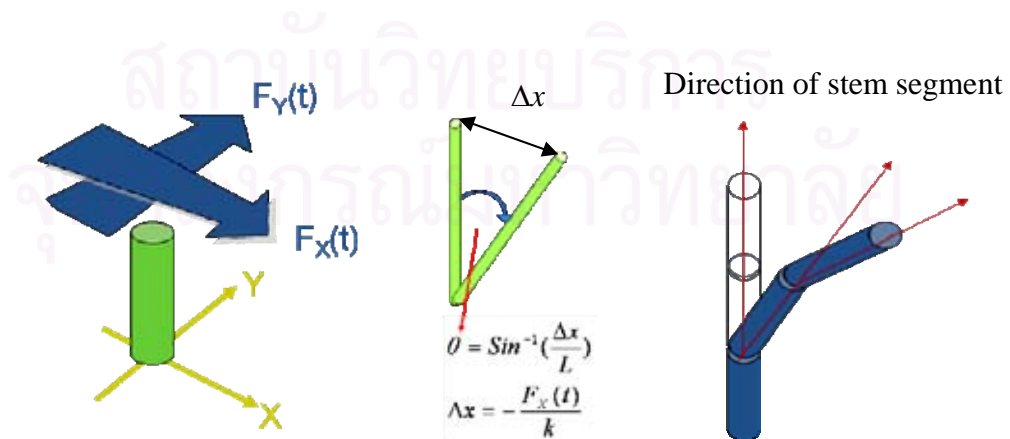
Figure 4.3: Illustration of dynamic model concept.

The angle of stem segment (θ_{sy}) in the direction of y axis is defined as,

$$\theta_{sy} = Sin^{-1}(\frac{\Delta y}{L_s})$$
(4.3)

where L_s is the length of stem.

Distance of stem in direction of y axis (Δy) which move away from the old direction line is calculated by,

$$\Delta y = -\frac{F_y(t)}{k}$$
(4.4)

where k is the modulus parameter.

Leaf

The angle of leaf segment is defined as in the stem part. The gravity is also considered, so the mass of leaf is considered as one parameter in the model. Figure 4.4 shows the details of leaf. Angle of each leaf segment is defined as,

$$\theta_l = Sin^{-1}(\frac{\Delta z}{L_l})$$
(4.5)

where L_l is the length of leaf segment.

Distance of leaf segment move away from the previous direction is calculated by,

$$\Delta z = -\frac{F_z(t) + mg}{k}$$
(4.6)

where k is the elastic modulus parameter depends on plant species.
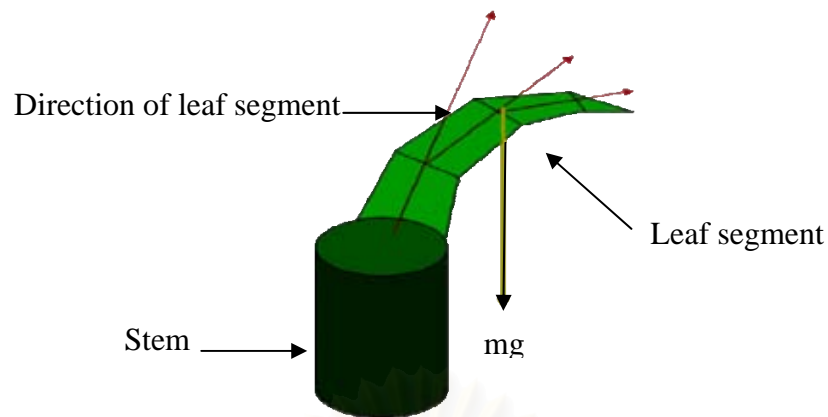
Figure 4.4: Dynamic leaf angle and characteristic.

Root

The calculation of root segment angle (θ_r) is also defined as stem model. The concentration of nutrient solution in soil is onsidered instead of gravity. Figure 4.5 shows the details of root. Angle of each root segment in direction of *x* axis (θ_{rx}) is defined as,

$$\theta_{rx} = Sin^{-1}(\frac{\Delta x}{L_r}) \tag{4.7}$$

where L_r is the length of root segment.

And the angle of each root segment in direction of *y* axis (θ_{ry}) is defined as,

$$\theta_{ry} = Sin^{-1}(\frac{\Delta y}{L_r}) \tag{4.8}$$

where L_r is the length of root segment.

Distance of root segment move away from the previous direction is calculated by the concentration of nutrient in soil defined as biological motivation in Section 4.1.3.
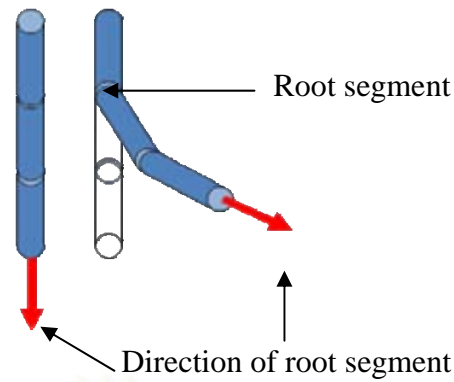
Figure 4.5: Dynamic root angle and its characteristic.

Panicle

The angle of panicle branch segment is also defined as stem model. The gravity is also considered, so mass of panicle is used as a parameter in the model. Figure 4.6 shows the details of panicle branch model. The angle of each panicle segment in the direction of x axis (θ_{px}) is defined as,

$$\theta_{px} = Sin^{-1}(\frac{\Delta x}{L_p})$$
(4.9)

where L_p is the length of panicle branch segment.

Distance of panicle segment move away from the previous direction is calculated by,

$$\Delta x = -\frac{F_x(t) + mg}{k}$$
(4.10)

where k is the elastic modulus parameter depends on plant species.
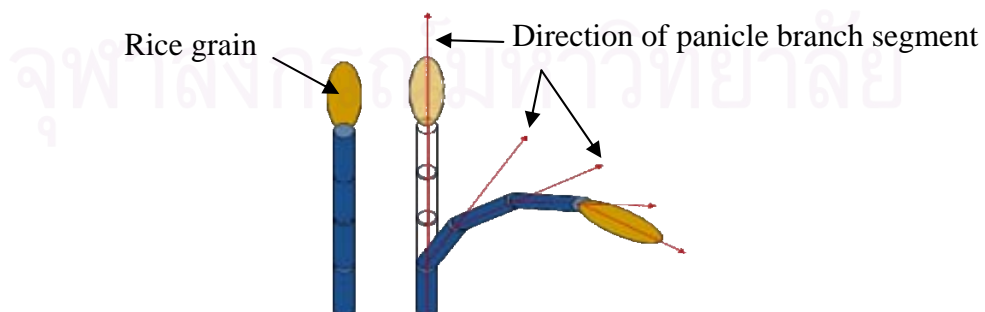
Figure 4.6: Dynamic panicle branch angle and its characteristic.

Also the angle of each panicle segment in the direction of y axis (θ_{py}) is defined as,

$$\theta_{py} = Sin^{-1}(\frac{\Delta y}{L_p}) \tag{4.11}$$

where L_p is the length of panicle branch segment.

Distance of panicle segment move away from the previos direction is calculated by,

$$\Delta y = -\frac{F_y(t) + mg}{k} \tag{4.12}$$

where k is the elastic modulus parameter depends on plant species.

4.1.3 Biologically Motivation

There are four biologically motivated conditions we considered during rice grow. Each condition can be described by mathematical model as shown below.

1. Direction of shoot and root part are defined as shown in Figure 4.7. A new position of new root and shoot segment will be calculated by the equation,

$$newPos = oldPos + \vec{G}f(t)\Delta t, \tag{4.13}$$

where $f(t)$ is a growth rate of shoot or root part, $\vec{G}$ is the direction of shoot or root part which emerge from seed.
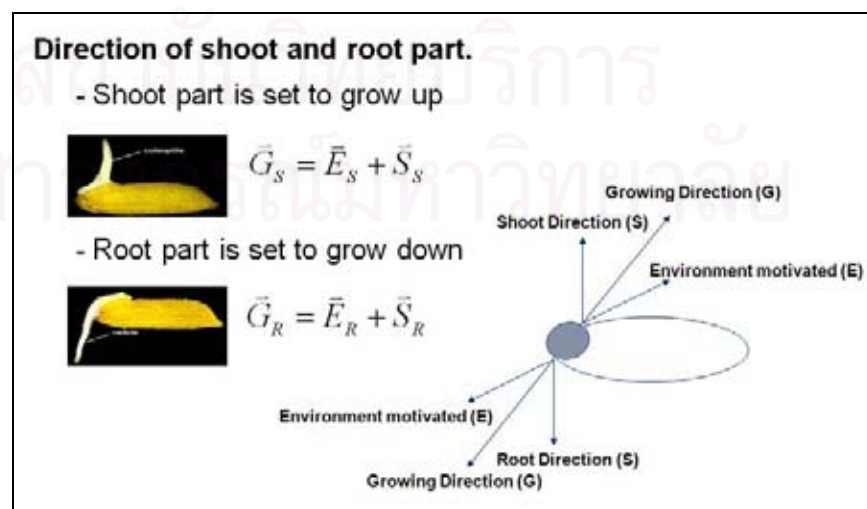
Figure 4.7: Root and shoot direction concept.

2. Mesocotyl emergence is determined by the amount of Oxygen around seed, so L-system can be used to describe this behavior by setting:

    Seed → *Seed*[*Coleoptile*][*Radicle*]

    Coleoptile : {if $O_2 < h$} → *Mesocotyl* [*PrimaryLeaf*]A

    Coleoptile : {if $O_2 > h$} → [*PrimaryLeaf*]A

where *h* is the amount of oxygen threshold obtained by experiment.

The emergence of mesocotyl is shown in Figure 4.8. In case of seed has less Oxygen, Mesocotyl must elongate until Coleoptile grow above soil or water.
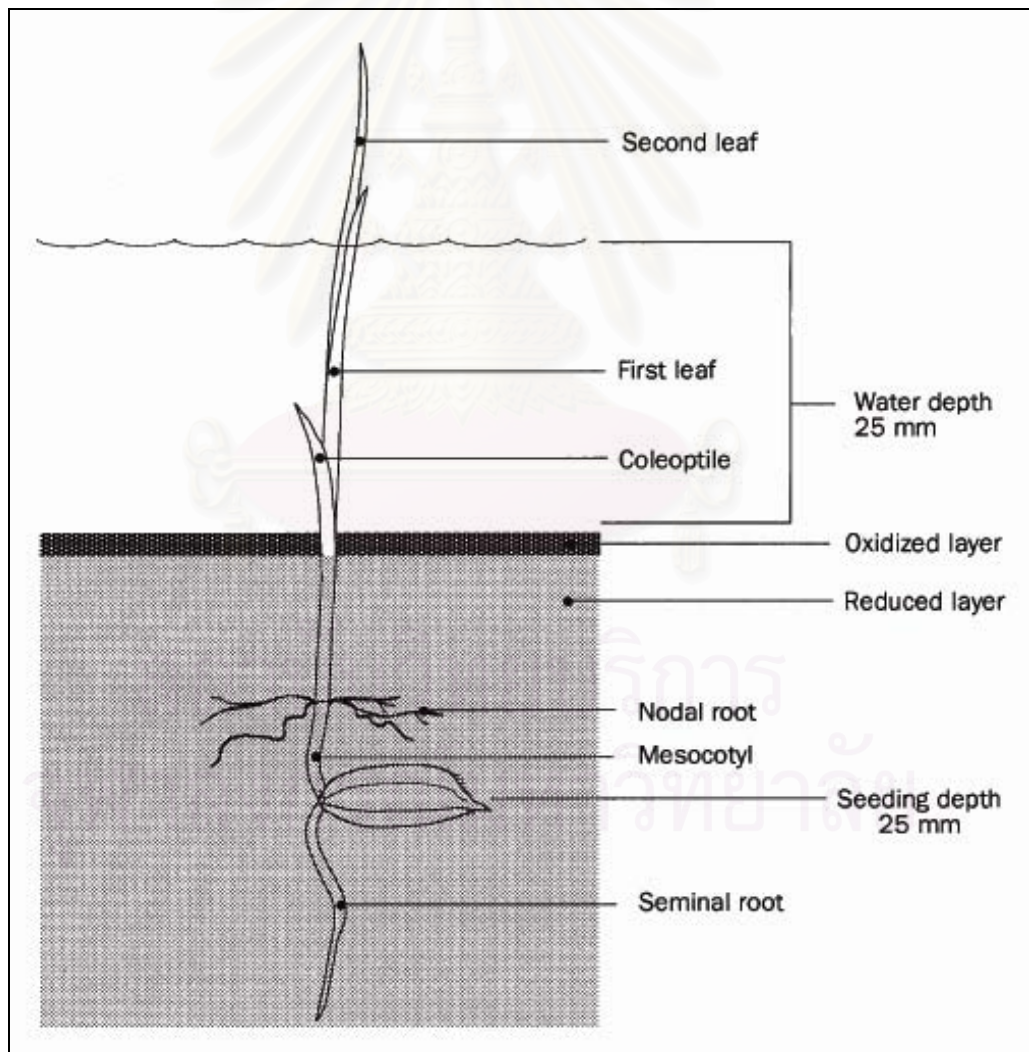
Figure 4.8: Emergence of Coleoptile and Mesocotyl elongation.

3. Sequence of seedling phase is set as followings;

Anaerobic

Seed : {if anaerobic} → 1. Seed [Coleoptile] then

2. Seed [Radicle]

Aerobic

Seed : {if aerobic} → 1. Seed [Radicle] then

2. Seed [Coleoptile].

Root part of rice will be emerged before shoot part when seed breakdown in aerobic environment. In contrast, for anaerobic situation, shoot part will be emerged first.

4. Panicle initialize is determined only in photoperiod sensitive rice. The condition is set as shown below,

A : {n-hours light / day} → iP

For the "Jasmine Rice", the n-hour light per day is eleven. The apex development of Jasmine rice will produce a panicle at this condition. Time and day length depends on a position of plantation site and an annual date as shown in Figure 4.9.
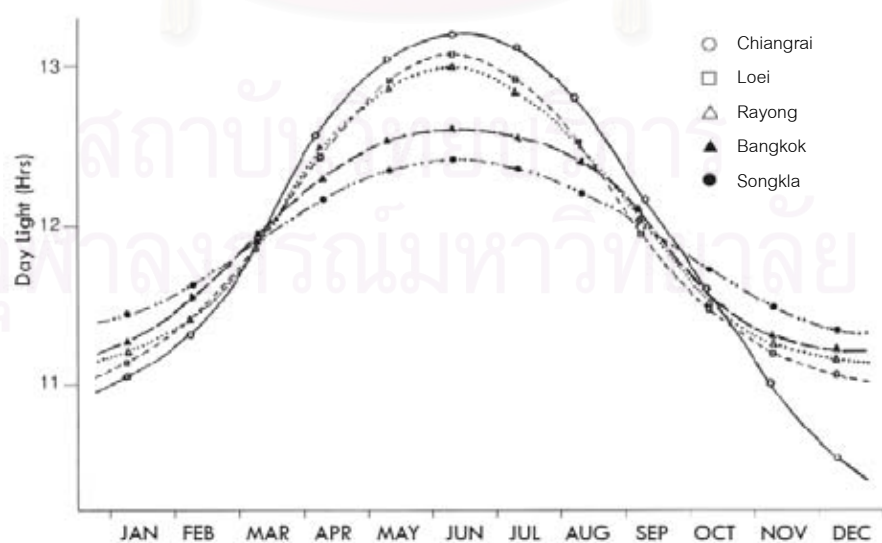
Figure 4.9: Time and day length depends on position of plant and annual date.

4.1.4 Leaf Area and Leaf Shape Analysis

Rice leaves are constructed by using shape and leaf area information collected from field. The shape blade is the same for all leaves, except flag leaves (see Figure 4.10 and 4.11). The shapes of leaf margins are fitted by a polynomial functions constrained by start and end points. A different set of parameter values is used for flag leaves.

Flag leaf

Leaf width (cm.)
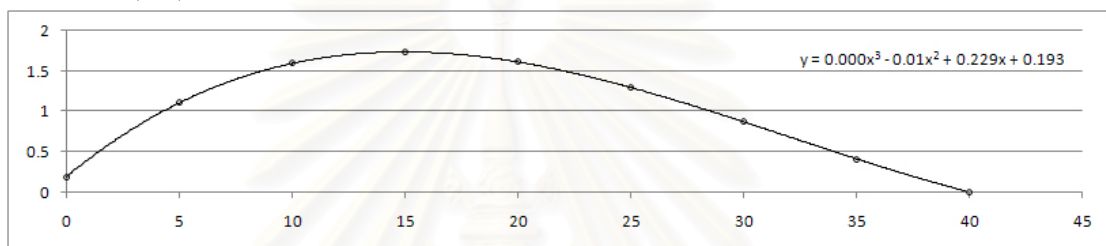
Leaf length (cm.)

Figure 4.10: Shape of rice flag leaf. The polynomial function is used to approximate flag leaf shape. Flag leaf has a different shape from generic leaf.

Generic leaf

Leaf width (cm.)
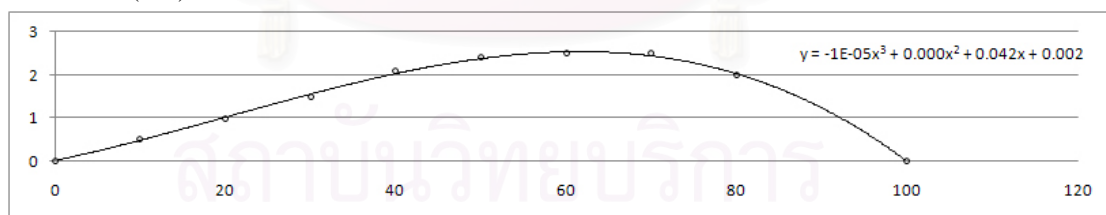
Leaf length (cm.)

Figure 4.11: Shape of generic leaf. The polynomial function is used to approximate generic leaf shape.

4.1.5 Leaf Curves

This work constructs the three-dimensional architectural model using plant images that captured from different rotation positions. The collected images were analyzed, and translated to the coordinates system in three dimension space manually. Figure 4.12 shows the methodology for analyzing a leaf image. The polynomial function was used to determined leaf curve. Leaf curve function will be used to construct the three-dimension architectural model.
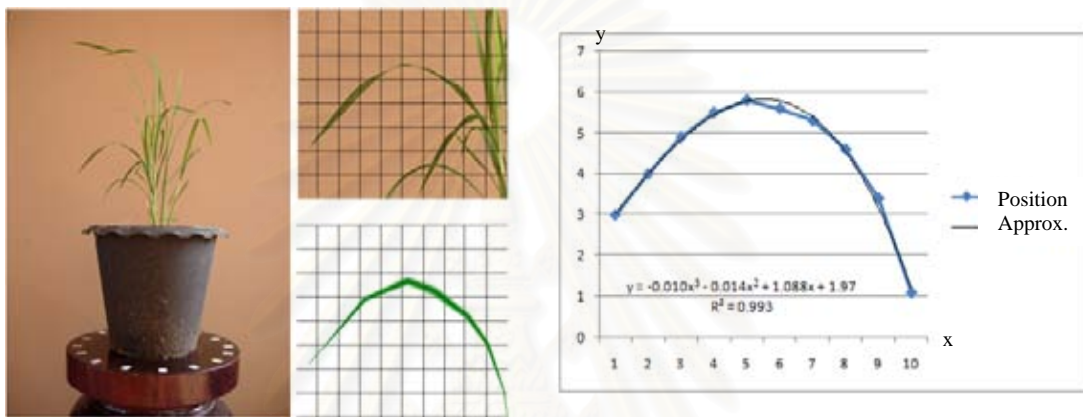
Figure 4.12: Translating the leaf image to polynomial function.

4.1.6 Three-Dimension Representation of Leaf

In this work, leaf is very important for calculating leaf area and the amount of light interception. To obtain the leaf area and the amount of light incident to leaf, each leaf of a three dimensional architectural model is digitized into small quadrilateral segment (polygons) along leaf length (see Figure 4.13). Each segment i[th] on area of leaf patch i[th] with its length ($L_{l,i}$) equal to

$$L_{l,i} = L_l / n \qquad (4.14)$$

where L_l is the leaf length, and n is the number of segment of a leaf.
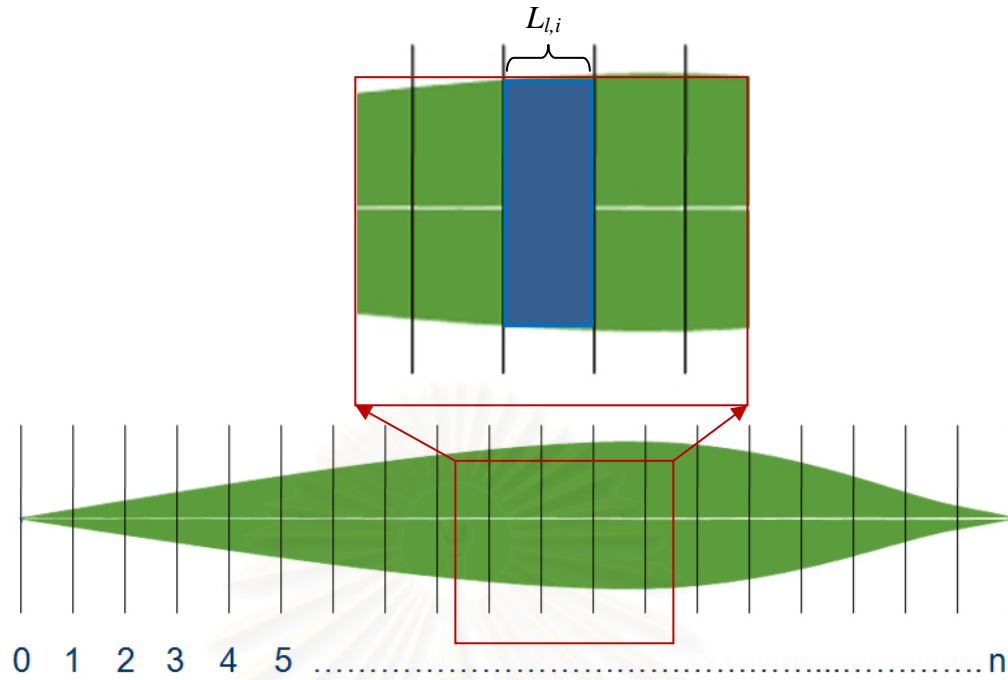
Figure 4.13: Leaf segmentation along the leaf length.

4.1.7 Leaf Area Calculation

From the previous section, a leaf is divided into n segments. The area of the ith segment ($A_{l,i}$) can be calculated as,

$$A_{l,i} = 2 \int_{L_{l,i-1}}^{L_{l,i}} f_l(L_{l,i}) dL_{l,i} \tag{4.15}$$

where f_l is shape function of rice leaf, and $L_{l,i}$ is length of the ith segment.

Therefore, area of a leaf (A_l) is obtained by sum all segment together as following,

$$A_l = \sum_{i=1}^{n} A_{l,i} \tag{4.16}$$

where n is the number of leaf segments.

4.2 Light Incidence Model

A 3D architectural model of rice was reconstructed based on the experimental data. Details of virtual rice are illustrated in later section. Radiosity method is applied and modified appropriately for calculating amount of light in which impact to all position on plant leaves.

4.2.1   Position of the Sun
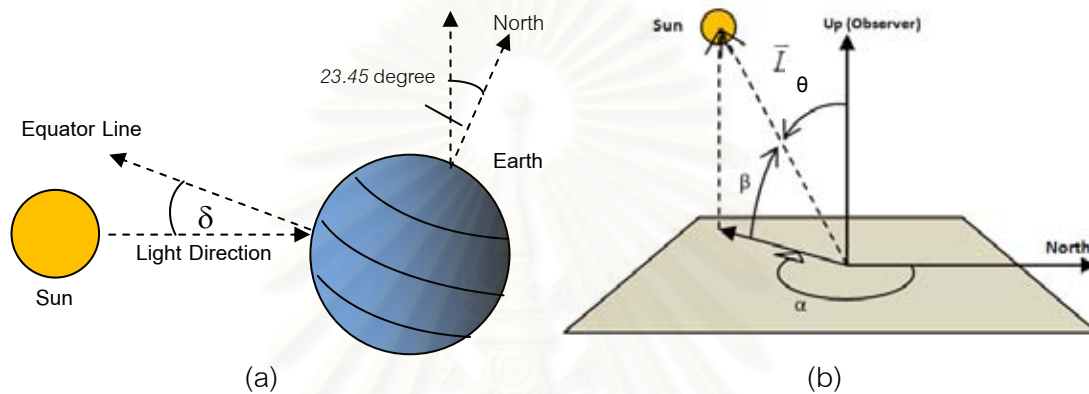
Figure 4.14: a) The earth orbit causes the declination angle (δ) with respect to Julian day. b) Show the elevation angle (β) measured up from horizontal, azimuth angle (α) measured clockwise from north, and zenith angle (θ) measured from vertical.

Since our model is developed in three dimensions, the geometrical relationships between the foliage element and the incident radiation are of primary importance. The model calculates the position of the sun at the latitude, longitude, date and hour of the simulation. The declination angle δ (in radians) of the sun depends on the date, is calculated by the formula:

$$\delta = -0.4093 \times Cos\left(\frac{2\pi(D_y + 10)}{365} \right)$$

(4.17)

where D_y is day of year: January 1st is set to 1 and December 31st is set to 365,

the value -0.4093 is the degree of 23.45 in radian unit [44].

The elevation angle β and azimuth angle α (angle in the horizontal plane measured from north eastward) of the sun (Figure 4.14) with respect to observer [9] are calculated by

$$Sin\ \beta = Sin\ \phi\ Sin\ \delta + Cos\ \phi\ Cos\ \delta\ Cos\ h \qquad (4.18)$$

$$Sin\ \alpha = -\frac{Cos\ \delta\ Sin\ h}{Cos\ \beta} \qquad (4.19)$$

where ϕ is the latitude, and h is the "hour angle" (the angle between the meridian of the observer and the sun) of the sun at the position of rice plant.

4.2.2 Direct Intercepted Light (DiPAR)

The amount of direct intercepted light depends on the position of the sun in the sky and leaf patch angle. Position of the sun can be obtained as described in previous section. Normal vector, $\vec{N}$, perpendicular to a surface of the ith leaf patch represents a direction of maximum light interception capability (Figure 4.15).
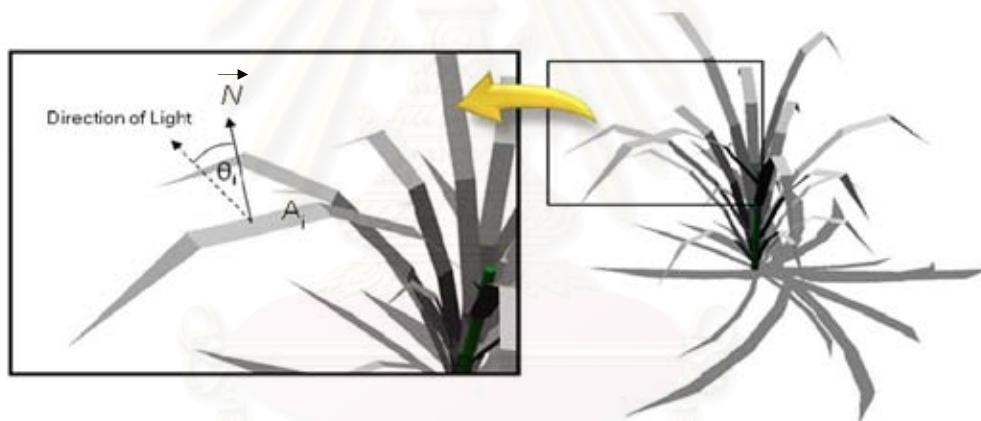
Figure 4.15: Light incident to leaf element.

Thus, direct light from sun (E_i) with respect to position of sun and leaf angle is

$$E_i = \vec{L} \cdot \vec{N_i} \times A_i, \qquad (4.20)$$

where $\vec{L}$ is the sun direct light beam, and A_i is the area of patch i[th].

4.2.3   Diffuse Intercepted Radiation (DfPAR)

Diffuse light come to leaf from every direction, in this work, the DSHP model [19], which is simulated a hemisphere over the object as a light source is applied to calculate the sky diffuse PAR (DfPAR) of each patch on 3D rice model. The sky diffuse PAR (DfPAR) is the ratio of the light calculate using Long's method [45]. The diffuse ratio is depended on amount of light in observed day with respect to the amount of light on clearly sky day (the maximum value of PAR in a year). DfPAR value is depended on the amount of cloud and other environments. The hemisphere was divided by horizontal line and vertical line as shown in Figure 4.16. The light of each element of divided hemisphere is proportion to their area. Total diffuse light is calculated by summing light of all hemisphere elements.

Diffuse light from every elements of hemisphere to leaf patch are considered as a link from light source to target, but only light which can be lined to a leaf patch is considered. The sum of DfPAR, D_i, on each 3D model patch is

$$D_i = \sum_j (D_f \times H_j),$$ (4.21)

where H_j is the area of the jth element of sky hemisphere, D_f is the sky diffuse light, $D_f = \rho L$, and ρ is the diffuse ratio.

(a)   (b)
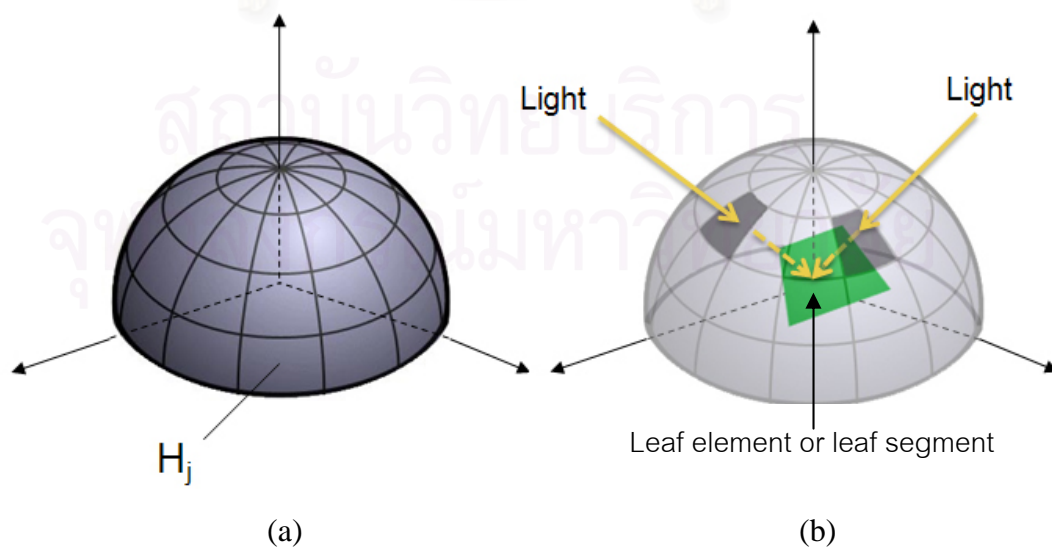
Figure 4.16: a) Sky hemisphere and b) diffuse light (DfPAR) calculation.

4.2.4   Light Penetration Through a Leaf (DpPAR)

The light penetration though rice leaf is considered as a ratio of the amount of light (PAR) measured at the position above and under a leaf (see Figure 4.17). Twenty five sample data from the experiment with rice leaves and the transmission ratio (y) which is used to find DpPAR (P_i) are shown in Figure 4.18. The estimated light penetration ratio is in polynomial form, and the amount of light transmission through rice leaf and impact to leaf segment ith is illustrated as follow:

$$P_i = y \cdot E_i , \qquad (4.22)$$

where y is the transmission ratio obtained from experiment, E_i is direct light incident to patch ith.
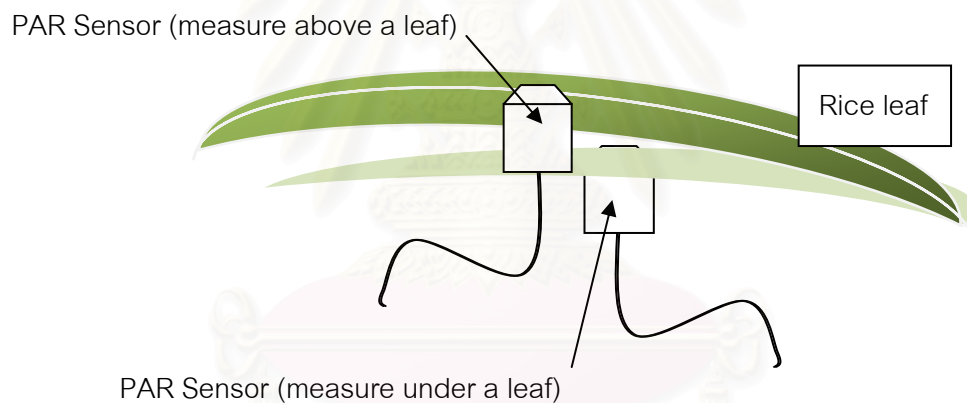
Figure 4.17: Measurement of the amount of light at position above and under a leaf.
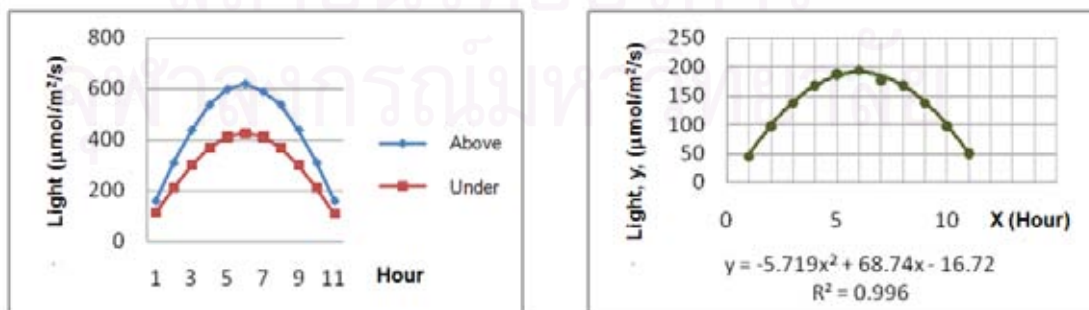
Figure 4.18: Light intensity at the position above and under a rice leaf collected from the field experiment (left). Penetration ratio over a day (right).

4.2.5 Total Intercepted Radiation of Each Element

The basic radiosity method has its basis in the theory of thermal radiation, since radiosity relies on computing the amount of light energy transferred among surfaces. In order to simplify computations, the method assumes that all scattering is perfectly diffuse. Surfaces are typically discretized into quadrilateral elements. The total intercepted light, λ, on each element i^{th} can be calculated by considering three light compositions; direct light (E_i), diffuse light (D_i), and penetration light through other leaf impact to the ith element (P_i).

The amount of light energy transfer can be computed by using the known reflectivity of the reflecting patch, combined with the form factor of the two patches. This dimensionless quantity is computed from the geometric orientation of two patches, and can be thought of as the fraction of the total possible emitting area of the first patch which is covered by the second patch. More correctly, radiosity is the energy leaving the patch surface per discrete time interval and is the combination of emitted and reflected energy. So, we formulate the light calculation as following,

$$\lambda_i dA_i = E_i dA_i + D_i dA_i + P_i dA_i + R_i \int_j \lambda_j F_{ji} dA_j \, , \qquad (4.23)$$

where λ_i is the radiosity (amount of light interception) of patch i. E_i is direct light. R_i is the reflectivity of the patch, giving reflected light by multiplying by the incident light (the light which arrives from other patches). All j ($j \neq i$) in the rendered environment are integrated for $\lambda_j F_{ji} dA_j$, to determine the light. F_{ji} is the constant-valued form factor for the light leaving j and hitting patch i. In this work, all area is discretized, so the integral is replaced by summation and uniform radiosity is assumed over the patch, creating the simpler:

$$\lambda_i = E_i + D_i + P_i + R_i \sum_{j=1}^{n} \lambda_j F_{ji} \qquad (4.24)$$

where R_i is the reflectivity of the patch (defined by 20% of light incident to patch), F_{ji} is the constant-valued form factor for the light leaving patch i^{th} and hitting patch j^{th}.

This equation can then be applied to each patch. The equation is monochromatic, so shading value on the three-dimensional model to represents the amount of light absorbed by each of leaf patch.

4.3 Setting Number of Segment (*n*)

The number of segment (*n*) which can be set by user is very important to indicate the accuracy of both leaf area and light interception calculation. Higher number of leaf segments (patches) will give the integral leaf area (calculated using equation 4.15 and 4.16) closely the actual leaf area.

Same as the calculation of light interception, higher accuracy of the calculation means that the relative error is a small number. Relative error of light interception calculation using radiosity method of two rice cultivars: Jasmine rice (KDML105) and Pathumthani 1 (PTT1) were analyzed. Figure 4.19 shows that the relation between the number of leaf segments and relative error of light interception calculation on Jasmine rice is

$$y = 31.60x^{-0.45} \tag{4.25}$$

where y is the relative error, and x is the number of leaf segments.
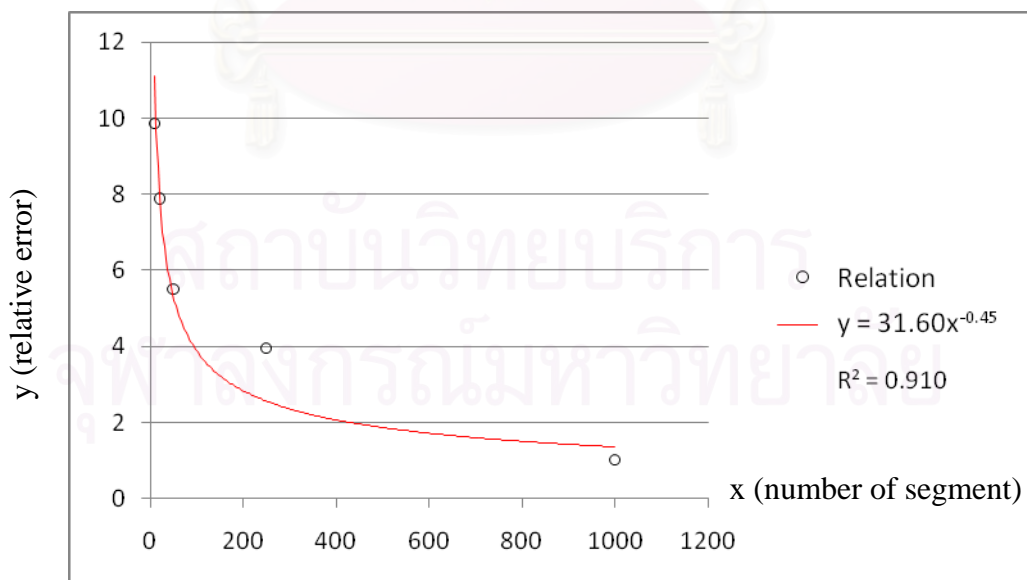
Figure 4.19: The relation between the number of leaf segments (patches) and the relative error of light interception calculation of the Jasmine rice (KDML105).

As in Pathumhani rice (PTT1), Figure 4.20 shows that the relation between the number of leaf segments and relative error of light interception calculation on Pathumthani rice is

$$y = 22.22x^{-0.56} \qquad (4.26)$$

where y is the relative error, and x is the number of leaf segments.
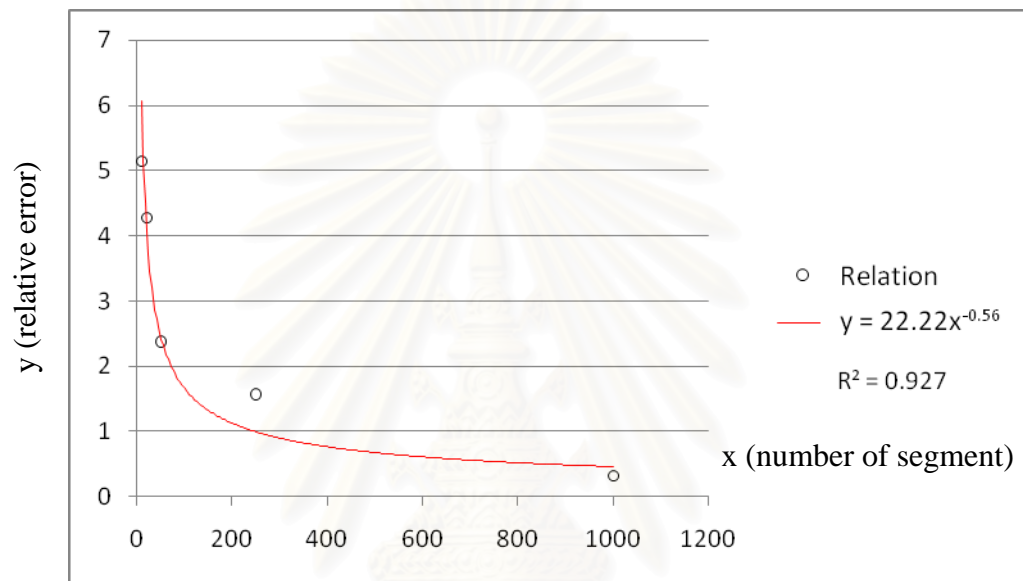
Figure 4.20: The relation between the number of leaf segments (patches) and the relative error of light interception calculation of the Pathumthani rice (PTT1).

4.4 Allometric Relationship of Characteristics and Rice Growth System

Allometric relationship models are widely used in agriculture and related fields. The models have potential to describe the relation between at least two of quantitative variables, these are relationship model for seed plant annual reproductive biomass based on standing leaf, stem and root biomass [46], root/shoot weight ratio, specific leaf area (SLA), specific root length (SRL), and leaf blade/sheath length ratio in rice [47], or other growth rate of an organism's parts in relation to the whole [48]. In this work, relationships between characteristics of rice and its biomass are needed. A new allometric relationship model namely "Neuro-Allometric Relationship model" is proposed to solve this problem.

In this study, a backpropagation (BP) algorithm was employed to train our multilayer feed-forward neural network. Levenberg-Marquardt (LM), a second-order nonlinear optimization technique, was chosen from the various BP training algorithms available for use in this study. The LM algorithm is widely applied to many different domains and is faster and produces better results than other training methods [51, 52]. To update weights, the LM algorithm uses an approximation to the Hessian matrix.

We developed a neuro-allometric relationship model of each rice part, which are divided into 4 main parts as shown in Table 3.1. Development of a neural network requires extensive patterns or pairs of inputs and outputs (Figure 4.21).
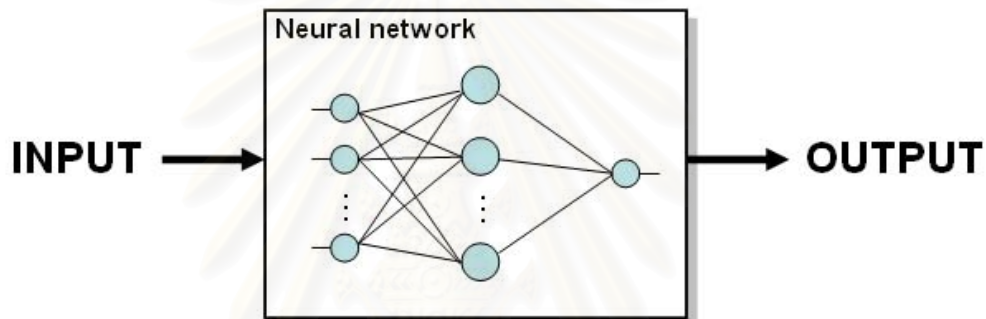
Figure 4.21: Schematic diagram of a neural network.

The model of individual parts is linked together with respect to the actual plant structure. Neuro-allometric models are also fed into an integrated model as a time series consideration. The proposed structure of integrated model is shown in Figure 4.22. A final model will potentially mimic the growth of rice plant.

To obtain the complete neural network model which can be used for rice biomass prediction as dry weight, neuro-allometric relationship models must be incorporated.

Dry weight or biomass of rice will be obtained as output of the neuro-allometric relationship model of leaf part. Eight characteristic parameters and six weather parameters including the amount of light calculated from light interception model are also considered. The neural network predicts each rice part's biomass, so, the biomass of whole rice plant is the summation of the biomass of every rice parts.
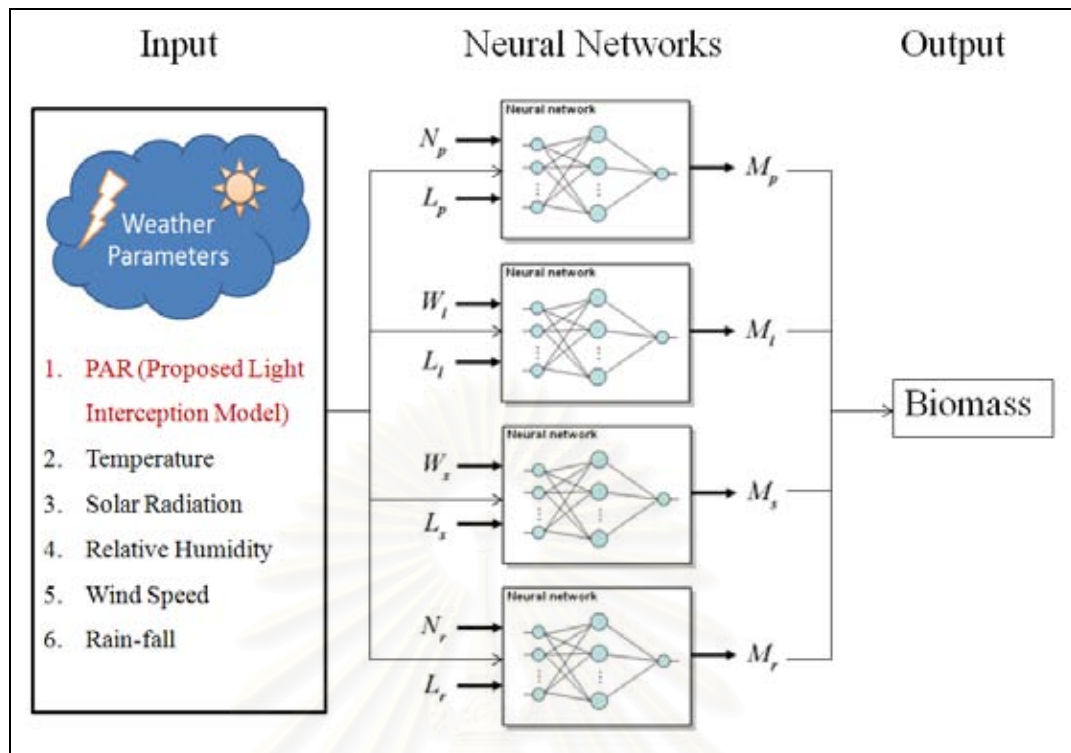
Figure 4.22: Diagram of rice growth system with integrated neural network.

Six weather parameters which collected from the experiment (as shown in Table 4.1) are also considered and fed into every rice parts as input values. So, considering as time series model, outputs (dry weight or mass) of each rice part are considered as the input values for feeding to connected part in the next time step.

Table 4.1: Weather parameters which are fed into the rice growth system.

Weather Parameters	Unit	Variable Name
Air Temperature	$^\circ C$	T
Relative Humidity	%	H
Solar Radiation	MJ/m^2/day	$Solar$
Photosynthetically Active Radiation	mole-q /m^2/day	Par
Wind Speed	km/day	W_d
Rain-fall	mm.	R_n

We can write the relation of all parameters in rice growth system as followings,

$$M_s^{t+1} = f(M_s^t, M_r^t, M_l^t, T, H, Solar, Par, W_d, R_n, t) \qquad (4.27)$$

$$M_r^{t+1} = f(M_r^t, M_s^t, T, H, Solar, Par, W_d, R_n, t) \qquad (4.28)$$

$$M_l^{t+1} = f(M_l^t, M_s^t, T, H, Solar, Par, W_d, R_n, t) \qquad (4.29)$$

$$M_p^{t+1} = f(M_p^t, M_s^t, T, H, Solar, Par, W_d, R_n, t) \qquad (4.30)$$

where t denotes time, and f denotes the neuro-allometric relationship of each part.

The results of the three-dimension rice architectural model, the light interception model, the integrating of neural network model and the constructing of the rice growth system will be shown in the next chapter.

CHAPTER V
RESULTS

5.1 Three-Dimension Rice Architectural Modeling

A three dimension architectural model of rice was constructed based on the L-system [41]. Characters in L-system described the structure of a plant. The growth of each structure can be controlled by the growth function. The model is capable animate its scene by changing physical parameters such as wind force and gravity. The visualization result of three dimension rice model and its growth simulation is shown in Figure 5.1. The growth of root and emergence of mesocotyl simulation is shown in Figure 5.2.
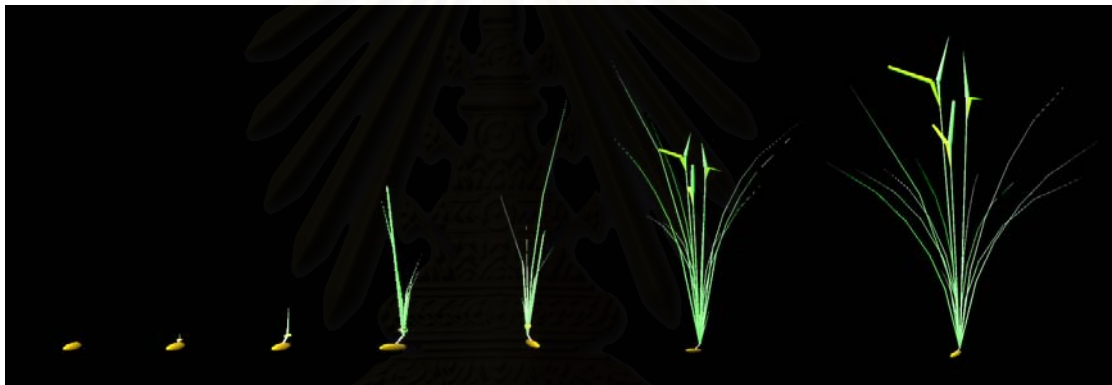
Figure 5.1: Growth of rice along the time since seedling to maturity.

Figure 5.2: Growth of root and mesocotyl in anaerobic condition (left), and the mature rice plant on 130 days after emergence (right).

5.2 Evaluation of Light Incidence Model

To obtain the light interception model, a three-dimension architectural model of rice was reconstructed, leaf shape and leaf curve are investigated in details. Leaf blade is discretized into small patch for calculating the light interception model. Leaf area of simulated 3D rice and classical leaf area measurement are compared at different number of digitized patch (Table 5.1).

Table 5.1: Comparison of simulated leaf area calculation based on classical method and our model. Both types of Thai rice with 85 days old was measured and observed. More number of polygons per a leaf gave more accuracy.

No. of Patch / Leaf	Actual Leaf Area (m^2)		Classical Method (m^2)		Our 3D Model (m^2)	
	KDML105	PTT1	KDML105	PTT1	KDML105	PTT1
10	0.1470	0.1845	0.1250	0.1620	0.1325	0.1750
20	0.1470	0.1845	0.1250	0.1620	0.1354	0.1766
50	0.1470	0.1845	0.1250	0.1620	0.1389	0.1801
250	0.1470	0.1845	0.1250	0.1620	0.1412	0.1816
1000	0.1470	0.1845	0.1250	0.1620	0.1455	0.1839

Selected ten leaves of each rice variety were used for calculating their area. The actual leaf area of the rice type: Khao Dawk Mali 105 (KDML105) is about 0.1470 m^2, and the actual leaf area of ten leaves of Pathumthani 1 (PTT1) is about 0.1845 m^2. We calculated leaf area by using the classical calculation method which is the fraction of leaf width multiply leaf length ($W \times L$) obtain by the observation. The average leaf area of ten leaves of KDML105 is 0.1250 m^2, and leaf area of PTT1 is 0.1620 m^2, respectively.

In the three-dimension architectural model, the accuracy of leaf area calculation can be specified by user. The results in Table 5.1 show that increasing of the number of polygon will give closer calculation to the actual area.

Each organ is being modeled in the 3D [x, y, z] feature space. However, due to the complexity of the resulting model, it is not easy to display images and compute the radiative transfer in the canopy. We will thus approximate the 3D structure by a set of simple elementary patches allowing the rendering of leaf and stem surfaces and the computation of the photon fluxes within the canopy (see Figure 5.3).
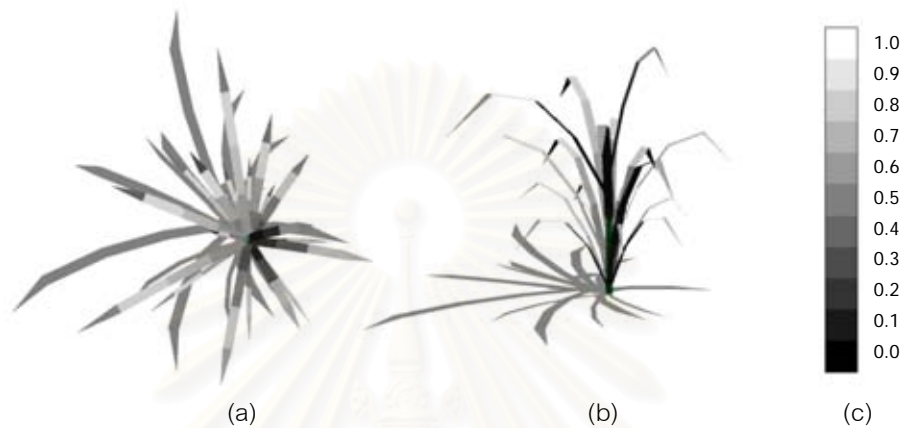
Figure 5.3: 3D architectural model of rice. a) Top view of the model, b) side view of the same rice plant, and c) represents amount of light intercepted on each leaf element as shading color, black color (0) means no light intercepted and white color (1) shows the maximum light assessment on leaf element.

The amount of light is observed and measure using two methods in both canopy level and leaf part level; light calculation with classic leaf area measurement, and our radiosity approach. The calculation using classic leaf area measurement will calculate the amount of light by ignoring leaf angle, diffuse light, and leaf shadow.

Figure 5.4 shows five sample positions of light measurement on actual rice leaf. Each measured value is used for model evaluation by compare with the result of light calculation at the same position on leaf of architectural model. In this dissertation, fifty randomized position on rice leaf were selected, then amount of light were measured and collected. Also in the same fifty randomized position as on actual plant, amount of light on the architectural model is calculated. Results of light interception simulation comparing to observed data are shown in the Figure 5.5. Simulated amount of light approach to the actual value measured at the same positions.
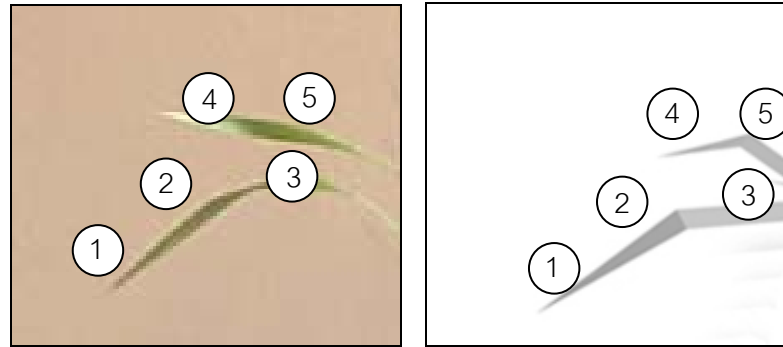
Figure 5.4: Five sample positions of light measurement on the actual rice leaf (left) and the three-dimension architectural model (right).
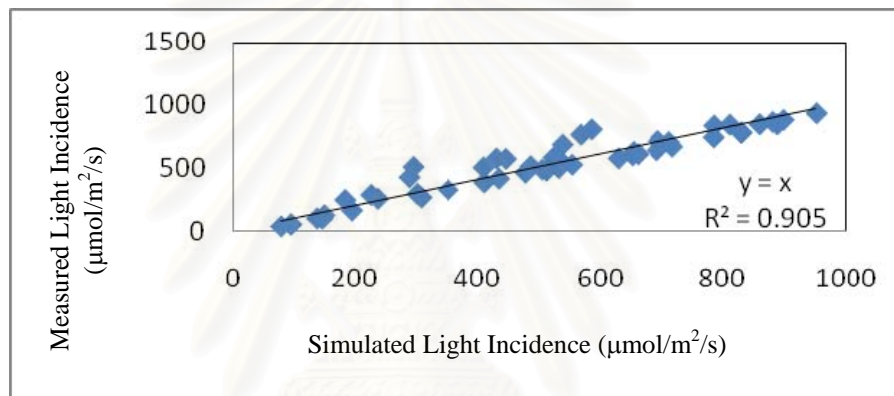
Figure 5.5: Comparison of light interception between observed and actual data.

The results of two types of rice cultivars are compared in Table 5.2. High resolution of three-dimension architectural model supposes to give more accuracy than lower resolution in both types of rice.

Table 5.2: Comparison of simulated light interception calculation using classical method and our method.

No. of Polygon	Classical Method ($\mu mol/m^2/day$)		Proposed Light Model ($\mu mol/m^2/day$)	
per Leaf	KDML105	PTT1	KDML105	PTT1
10	5.3875	6.9822	5.7064	7.5727
100	5.3875	6.9822	6.1245	7.7666
1000	5.3875	6.9822	6.2711	7.9045

Figure 5.6 shows the graphical representation of each light measurement method. The amount of light calculated by classic method at several leaf positions were performed and represented as shaded color compare to our method (see Figure 5.4). Our approach gave more realistic light shading than the classical method.

(a)   (b)
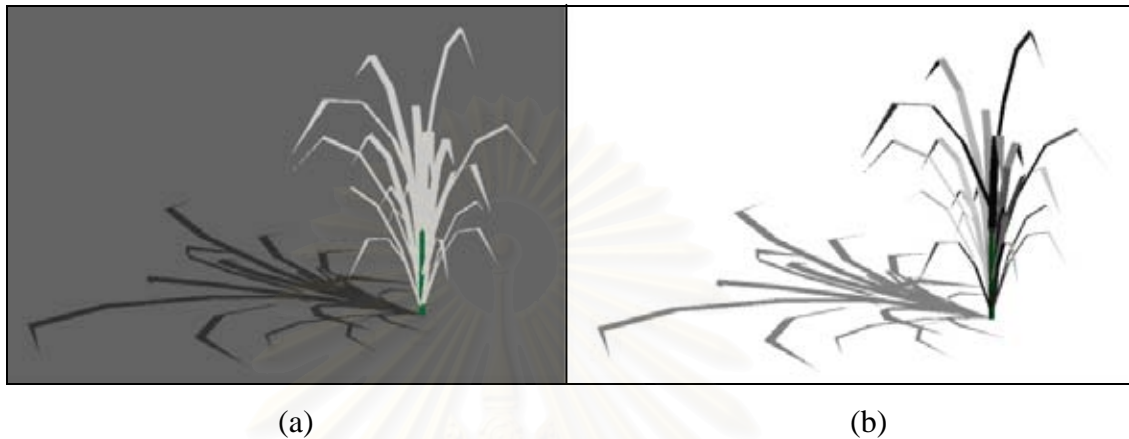
Figure 5.6: Comparison of graphical representation of two light measurement methods. a) Classical light calculation, b) Our approach, which considered the interception angle and amount of diffuse light.

5.3 Rice Growth Simulation

Ten plants were selected, their measured data, which collected weekly, were prepared as input pattern of neural network. Eight parameters of plant data with six weather data and time were fed into the network. Each plant was 20 weeks old accounted from emergence, so 300 patterns of growth data were prepared.

After the neural network was trained, validation of the result of rice growth prediction by using data of the testing data set (other ten plants) was also tested. Measured data from plant emergence to 63 days old (9 weeks old) were fed the rice growth system, then the growth of rice since 64 days after emergence (week tenth) until it grow as mature were predicted. The accuracy of prediction measured by the relative error is less than 10%. Figure 5.11, 5.12, 5.13, and 5.14 show the results of predicted growth data comparing to actual growth data.
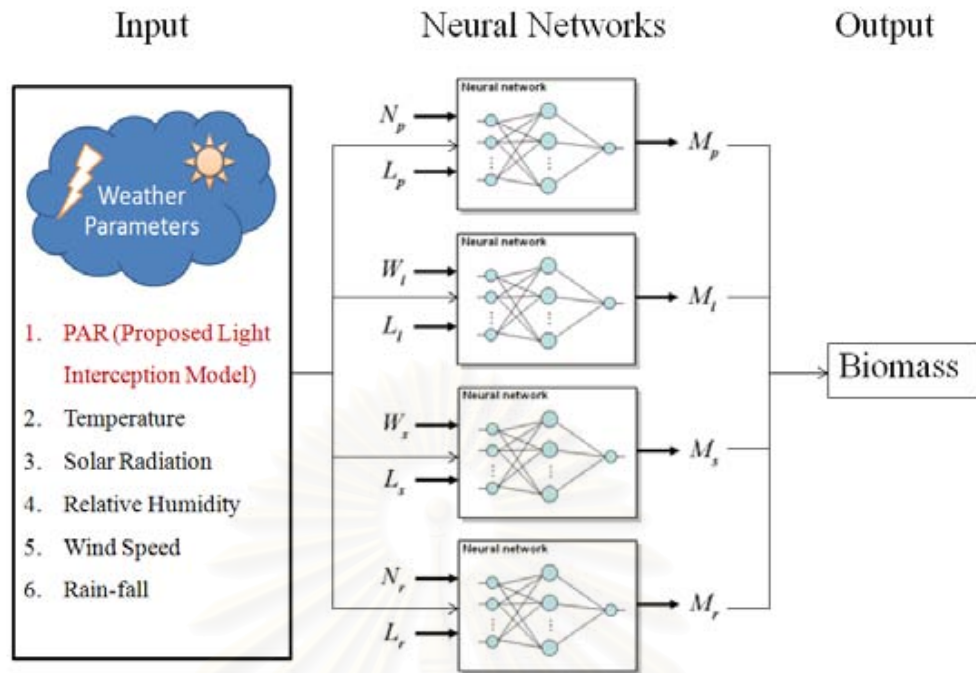
Figure 5.7: Schematic diagram of four neuro-allometric relationship models which are combined together. Weather data are also considered as input parameters in the rice growth system.
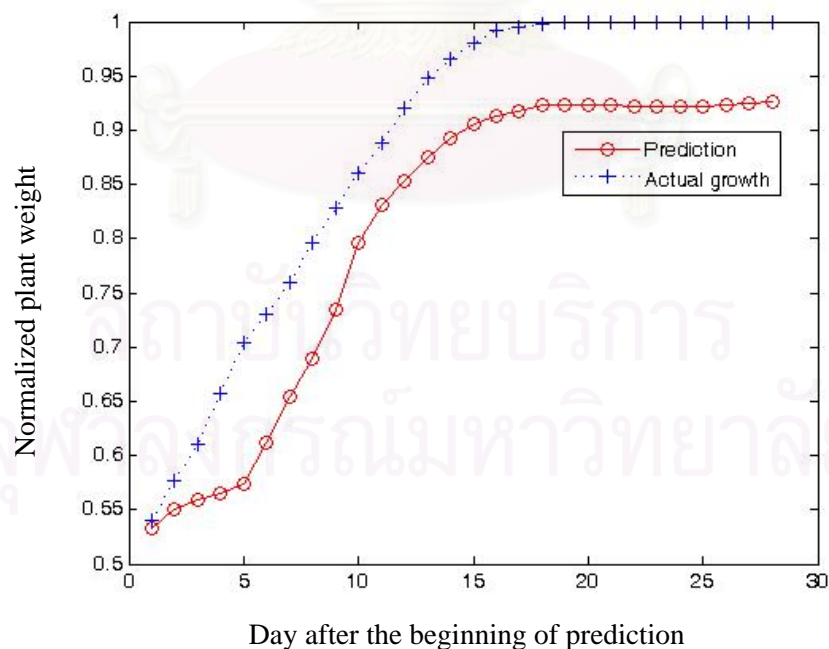
Figure 5.8: Comparison of rice growth prediction using proposed rice growth system and observed data. The number of hidden nodes is set to 21. Relative error of the prediction is equal to 9.7%.
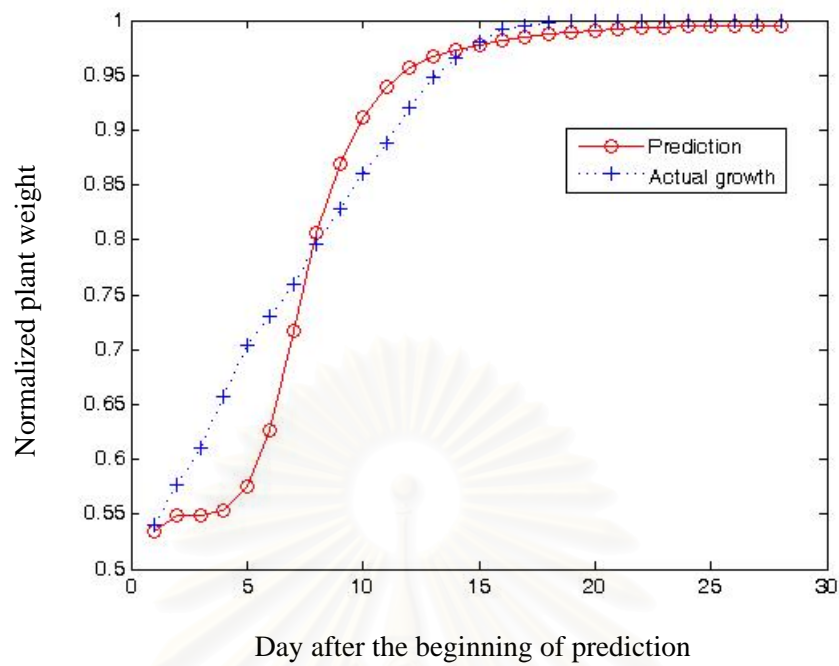
Figure 5.9: Comparison of rice growth prediction using proposed rice growth system and observed data. The number of hidden nodes is set to 26. Relative error of the prediction is equal to 7.4%.
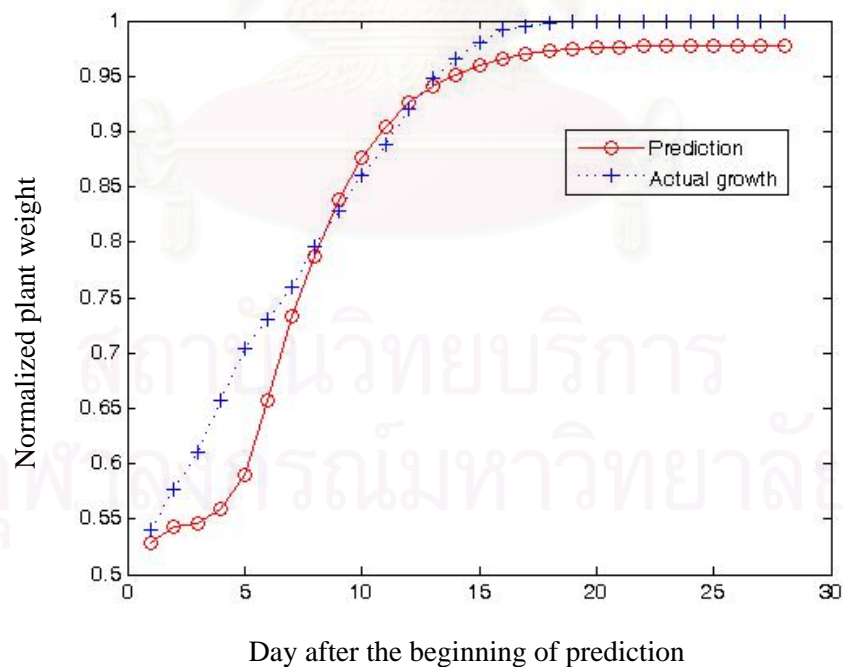
Figure 5.10: Comparison of rice growth prediction using proposed rice growth system and observed data. The number of hidden nodes is set to 29. Relative error of the prediction is equal to 4.6%.
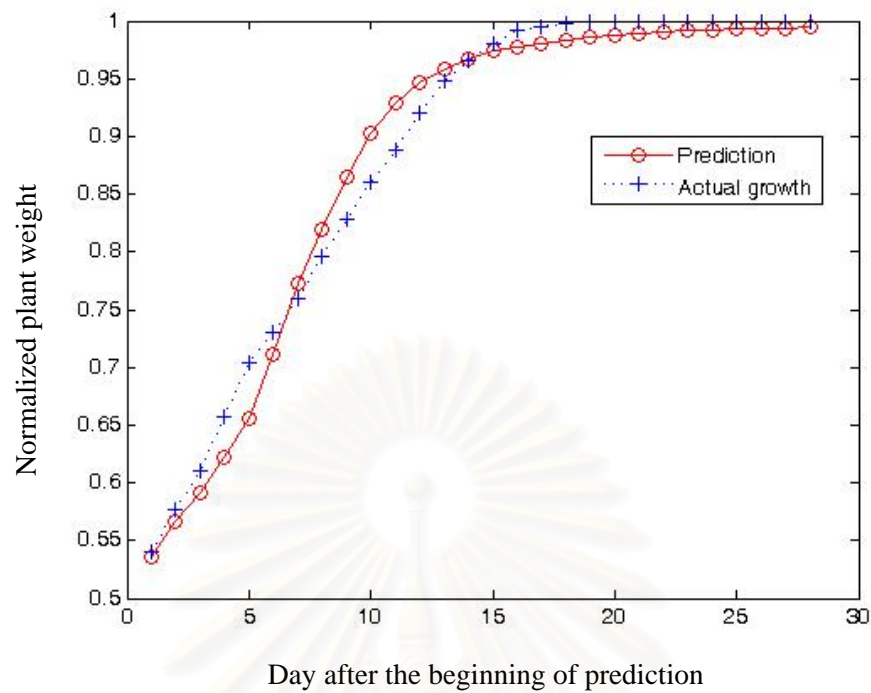
Figure 5.11: Comparison of rice growth prediction using proposed rice growth system and observed data. The number of hidden nodes is set to 30. Relative error of the prediction is equal to 2.4%.

CHAPTER VI
CONCLUSIONS AND FUTURE WORKS

6.1 Conclusions

This dissertation proposes an algorithm and an application using artificial neural network (ANN) for creating the quantitative relation and allometric relation among individual parts of rice: stems, roots, leaf, and panicles. The neural networks can be used for estimating the quantitative and allometric relation between rice parts, and simulated the growth of rice during vegetative stage. The novel methodology for calculating the amount of light incident to leaves is also proposed. The amount of light which is calculated by radiosity technique can be considered as the input light parameter in rice growth system.

Firstly, a three-dimension structural model of rice, (*Oryza sativa* L.), which is developed based on botanical knowledge and observed data in the field was proposed in 2006 [41]. The developed model is based on the rice growth stages proposed by IRRI (International Rice Research Institute). Each part of the model was considered as a unit of the growth characteristics, and combined each unit together using the physical linked model. Growth data were collected from two types of experiment. The Pathumthani1 rice (PTT1, 90071-93-8-1-1) was grown in pots under outdoor conditions, and the Jasmine rice (KDML105) was cultivated in rice field during paddy rice season in Loei province, northeast of Thailand.

A novel approach for calculating light interception was proposed in early April, 2008 [43]. The most realistic computer graphic technique, radiosity, is applied to the model, it makes more precise of light assessment on plant leaf. The three-dimension architectural model was reconstructed using the same concept. More accuracy light calculation has more advantage in further researches. The proposed model has capable to be applied to the other kinds of plant.

Neural networks were used to approximate the growth of rice with many number of input parameters (growth conditions and environments), and applied the model to the three-dimension architectural model of rice during life cycle for the reality appearance. The integrated neural network model was linked to the three-

dimension architectural model by linking neuro-allometric of rice parts together. The results of rice growth simulation using the proposed method led to conclude that the proposed rice growth model has capable to simulate rice growth system which can be used for predicting rice biomass.

6.2 Future Works

This descriptive model may also serve as a stepping stone for constructing the mechanistic model. The model will provide a framework into which mechanistic components can easily be embedded. Neuro-allometric relationship model are obtained from analytical observed data, whereas functions are directly related to the characterized key attributes of each organ as the neuro-quantitative model. Then, an integrated model will be used for easier simulating of rice development in physiological, ecological, farming processes, and crop yields management. In addition, the linked three-dimension architectural model, which is dramatically enhanced the realistic rendering can be used as a visual model for software, movies, and games. Moreover, light interception model has capable to used in the further architectural research.

Other possibilities can be investigated:

- Automatic reconstruction of rice and other plant modeling.

- Graphic adjustment for creating more realistic scene.

- Studying of moreover environments should be investigated.

- Reducing computational time of both light interception model and neural network model.

- The amount of light which is calculated by radiosity technique will be considered as the input light parameter in rice growth system. It should be used to calculate the productivity of rice in reproductive stage.

REFERENCES

[1]   Prusinkiewicz, P. Modeling Plant Growth and Development. *Current Opinion in Plant Biology* 7(1): 79-83.

[2]   International Rice Research Institute (IRRI), www.irri.org.

[3]   Lisson, S., and Robertson, M. 2003. APSIM Rice: A growth and development model for rice. *Proceedings of the 11th Australian Agronomy Conference*.

[4]   Guowei, W. 1998. A Physiologically-based Rice Population Simulation Model (RICEPSM). *AgroEcoSystems Research Group*.

[5]   McMennary, J. and O'Toole, J.C. 1985. RICEMOD: A Physiologically-Based Rice Growth Model. *IRRI research paper series* 87

[6]   International Rice Research Institute (IRRI). Increase Rice Plant Yield by Getting More Sunlight to Leaves. www.irri.org, 2005.

[7]   Bouman, B.A.M., Kropff, M.J., Tuong, T.P., Wopereis, M.C.S., ten Berge, H.F.M., and van Laar, H.H. *ORYZA2000: Modeling Lowland Rice*. International Rice Research Institute (IRRI), Philippines and Wageningen University and Research Centre, Wageningen, Netherlands, 2001.

[8]   Matthew, R.B., Bachelet, D., and van Laar, H.H. 1995. Modeling the Impact of Climate Change on Rice Production in Asia. *CAB International*.

[9]   Castro, F., and Fetcher, N. 1998. Three Dimensional Model of the Interception of Light by a Canopy. *Agricultural and Forest Meteorology* 90: 215-233.

[10]   Decoteau, D. 1998. Plant Physiology: Environmental Factors and Photosynthesis. *Greenhouse Glazing & Solar Radiation Transmission Workshop*.

[11]   Flores, F.J., Allen, H.L., Cheshire, H.M., Davis, J.M., Fuentes, M., and Kelting, D. 2006. Using multispectral satellite imagery to estimate leaf area and response to silvicultural treatments in loblolly pine stands. *Canadian Journal of Forest Research* 36: 1587–1596.

[12]   Jongschaap, R.E.E. 2006. Integrating crop growth simulation and remote sensing to improve resource use efficiency in farming systems. *Ph.D. Thesis*, Wageningen, the Netherlands: Wageningen University: 130 pp.

[13] Sinoquet, H., Thanisawanyangkura, S., Mabrouk, H., and Kasemsap, P. 1998. Characterization of the Light Enironment in Canopies Using 3D Digitising and Image Processing. *Annals of Botany* 82: 203-212.

[14] Buwalda, J.G., Curtis, J.P., and Smith, G.S. 1993. Use of Interactive Computer Graphics for Simulation of Radiation Interception and Photosynthesis for Canopies of Kiwifruit Vines with Heterogeneous Surface Shape and Leaf Area Distribution. *Annals of Botany* 72: 17-26.

[15] Rohrig, M., Stutzel, H., and Christoph, A. 1999. A Three-Dimensional Approach to Modeling Light Interception in Heterogeneous Canopies. *Journal of Agronomy* 91.

[16] Espana, M.L., Baret, F., Aries, F., Chelle, M., Andrieu, B., and Prevot, L. 1999. Modeling Maize Canopy 3D Architecture Application to Reflectance Simulation. *Ecological Modelling* 122: 25-43.

[17] Pommel, B., Sohbi, Y., and Andrieu, B. 2001. Use of Virtual 3D Maize Canopies to Assess the Effect of Plot Heterogeneity on Radiation Interception. *Agricultural and Forest Meteorology* 110: 55-67.

[18] Lamanda, N., Dauzat, J., Jourdan, C., Martin, P., and Malezieux, E. 2007. Using 3D Architectural Models to Assess Light Availability and Root Bulkiness in Coconut Agroforestry Systems. *Journal of Agroforestry Systems*.

[19] Xiping, W., Yan, G., Baoguo, L., Ziyong, W., and Yuntao, M. 2006. Evaluating a Three Dimensional Model of Diffuse Photosynthetically Active Radiation in Maize Canopies. *International Journal of Biometeorol*: 349-357.

[20] ProdSTAT. FAOSTAT. (Retrieved on December 26th, 2006).

[21] Smith, B.D. *The Emergence of Agriculture*. New York: Scientific American Library, A Division of HPHLP, 1998.

[22] Prusinkiewicz, P. and Lindenmayer, A. *The Algorithmic Beauty of Plants*, Berlin: Springer Verlag, 1990, 228 pp.

[23] Incropera, F.P., and Dewitt, D.P. *Fundamentals of Heat and Mass Transfer*, John Wiley&Sons, Inc., 2006.

[24] Goral, C.M., Torrance, K.E., Greenberg, D.P., and Battaile, B. 1984. Modelling the interaction of light between diffuse surfaces. *Computer Graphics* 18: 213-222.

[25] Walton, G. Calculation of Obstructed View Factors by Adaptive Integration. *NIST Report NISTIR-6925*.

[26] GUO, Y., and Baoguo, L. 2001. New advances in virtual plant research. *Chinese Science Bulletin* 46.

[27] Watanabe, T., Hanan, J.S., Room, P.M., Hasegawa, T., Nakagawa, H., and Takahashi, W. 2005. Rice Morphogenesis and Plant Architecture: Measurement, Specification and the Reconstruction of Structural Development by 3-dimensional Architectural Modelling. *Annals of Botany* 95: 1131-1143.

[28] Yan, H.P., Kang, M.Z., De Reffye, P., and Dingkuhn, M. 2004. A Dynamic, Architectural Plant Model Simulating Resource Dependent Growth. *Annals of Botany* 93: 1-12.

[29] Mech, R., and Prusinkiewicz, P. 1996. Visual Model of Plants Interacting with Their Environment. *Proceedings of SIGGRAPH'96 (New Orleans, Louisiana, August 4th-9th, 1996), In Computer Graphics Proceedings, Annual Conference Series, ACM SIGGRAPH*: 397-410.

[30] Prusinkiewicz, P. 1999. A Look at the Visual Modeling of Plants using L-systems. *Agronomie* 19: 211-224.

[31] Hanan, J.S., and Hearn, A.B. 2003. Linking Physiological and Architectural Models of Cotton. *Agricultural Systems* 75: 47-77.

[32] Hu, B.G., and Jaeger, M. (eds). *Plant Growth Modeling and Applications*. Beijing, China: Tsinghua University Press and Springer, 435 pp.

[33] Pirmoradian, N. and Sepaskhah, A.R. 2005. A Very Simple Model for Yield Prediction of Rice under Different Water and Nitrogen Applications. *Biosystems Engineering*.

[34] Lek, S., and Guegan, J.F. 1999. Artificial neural networks as a tool in Ecological Model. *An Introduction to Ecological Model*. 120 (6573).

[35] Schultz, A., and Wieland, R. 1997. The use of neural networks in agroecological modeling. *Computer and Electronic in Engineering* 18 (7390).

[36] Schultz, A., Wieland, R., and Lutze, G. 2000. Neural networks in agroecological modelling-stylish application or helpful tool? *Computer and Electronic in Engineering* 29 (7397).

[37] Peart, R.M., and Curry, R.B. *Agricultural Systems Modeling and Simulation.* New York: Marcel Dekker, inc., 1998.

[38] Thai, C.N., and Shewfelt R.L. 1990. Modeling Sensory Color Quality: Neural Networks vs. Statistical Regression. *ASAE Paper* 90 (6038), St. Joseph, MI: ASAE.

[39] Uhrig, J.W., Engel, B.A., and Baker, W.L. 1992. An Application of Neural Networks: Predicting Corn Yields. *Proceedings of 4th International Conference on Computers in Agricultural Extension Programs.*

[40] Sheehy, J.E., Mitchell, P.L., and Ferrer, A.B. 2004. Bi-Phasic Growth Patterns in Rice. *Annals of Botany* 94: 811-817.

[41] Bamrungrajhirun, M., Lursinsap, C., and Siripant, S. A Dynamic 3D Structural Model of Rice Based on Morphogenesis Development. *International Conference on High Performance Scientific Computing*, Hanoi, Vietnam, March 6th -10th, 2006.

[42] Nakagawa, H., and Horie, T. 1995. Modelling and prediction of developmental process in rice II, A model for simulating panicle development based on daily photoperiod and temperature. *Japanese Journal of Crop Science* 64: 33–42.

[43] Bamrungrajhirun, M., Lursinsap, C., and Siripant, S. A Three-Dimensional Approach to Calculating Light Interception in Rice Canopy Based on Photosynthetically Active Radiation Data and Radiosity Rendering Technique. *Proceedings of the 1st Symposium on Simulation Models for a Better Decision*. Kasetsart University, April 1st - 2nd, 2008.

[44] Christopher T. *Introduction to Mathematical Modeling of Crop Growth, How the Equations are Derived and Assembled into a Computer Program.* BrownWalker Press, 2006, 276 pp.

[45] Long, C.N., George, A.T., Mace, G.G., and Ackerman, T.P. A Simple Formula for Determining Globally Clear Skies. *Proceedings of the 5th Atmospheric*

Radiation Measurement (ARM) Science Team Meeting. San Diego, California, March, 1995.

[46] Niklas, K.J., and Enquist, B.J. 2003. An allometric model for seed. plant reproduction. *Evolutionary Ecology Research* 5: 79-88.

[47] Luquet, D., Zhang, B.G., Dingkuhn, M., and Dexet, A. Phenotypic plasticity of rice seedlings: case of p deficiency. *Proceedings of the 4th International Crop Science Congress.* Brisbane, Australia, 2004.

[48] Niklas, K.J. *Plant Allometry: The Scaling of Form and Process.* Chicago: University Of Chicago Press, October 17th, 1994.

[49] Christ, M.M. 2005. Temporal and Spatial Patterns of Growth and Photosynthesis in Leaves of Dicotyledonous Plant Under Long-Term CO_2 - and O_3 –Exposure. *Reihe Umwelt / Environment Band* 5.

[50] Cohen M.F., and Greenberg D.P. 1985. The hemi-cube: A radiosity solution for complex environments. *Proceedings of ACM SIGGRAPH'85.*

[51] Hagan, M.T., and Menhaj, M.B. 1994. Training feedforward networks with the Marquardt algorithm. *IEEE Transactions on Neural Networks* 5: 989-993.

[52] Tan, Y., and van Cauwenberghe, 1999. A. Neural-network-based d-step-ahead predictors for nonlinear systems with time delay. *Engineering Applications of Artificial Intelligence* 12: 21-35.

APPENDIX

APPENDIX A

WEATHER STATION AND SENSORS

A1. Data Logger (H21-001 Weather Station)

Overview

The award-winning HOBO Weather Station offers easy configuration and dependable research-grade measurements at a reasonable cost. The HOBO Weather Station records up to 15 channels of measurements, and a broad range of plug-and-play smart sensors are available for monitoring all kinds of environmental conditions from temperature and humidity to soil moisture, wind speed/direction, rainfall, leaf wetness, solar radiation, and barometric pressure. Input adapters for 4-20mA, DC voltage, and pulses increase the range of possible measurements.

Technical Specifications

· Operating Range: -20° to 50°C (-4° to 122°F) with alkaline batteries,

· -40° to 70°C (-40° to 158°F) with lithium batteries

· Sensor Inputs: 10, expandable to 15 with optional adapters

· Data Channels: Maximum of 15 (some sensors use more than one data channel

· Communication: 3.5 mm serial port or weatherproof external connector

· Dimensions: 23 cm H x 10 cm D x 18 cm W (9 x 4 x 7 inches)

· Weight: 0.9 kg (2 lbs)

· Memory: 512K nonvolatile flash data storage

· Memory Modes: Stop when full, wrap around when full

· Operational Indicators: Seven status lights provide logging and sensor network status

· Logging Interval: 1 second to 18 hours, user-specified interval

· Battery Life: 1 year typical use (up to 10 sensors with 10 minutes or longer logging interval)

· Battery Type: Four standard AA alkaline batteries included (for operating conditions -20° to 50°C [-4° to 122°F]); optional AA lithium batteries available for operating conditions of -40° to 70°C (-40° to 158°F)

- Time Accuracy: 0 to 2 seconds for the first data point and ±5 seconds per week at 25°C (77°F)
- Data Type: Supports measurement averaging based on availability of supporting data from sensor
- Logger Start Modes: Immediate, push-button, or delayed start options
- Data Communication: Current reading while logging, offload while logging, or offload when stopped
- Environmental Rating: Weatherproof
- Mounting Mast: (3.8 cm [1.5 inches] maximum diameter) or wall mount
- Enclosure Access: Hinged door secured by four screws
- Sensor Network Cable Length: 100 m (328 ft) maximum

Figure A1: HOBO Weather station (Data Logger).

This product meets CE specification EN61326 criterion C for ESD, criterion C for Radiated Immunity, criterion C for Fast Transient, criterion B for Conducted Immunity, and criterion A for Power Frequency Magnetic Fields. To minimize measurement errors due to ambient RF, use the shortest possible probe cable length and keep the probe cable as far as possible from other cables.

A2. Silicon Pyranometer Smart Sensor (S-LIB-M003)

Overview

The Solar Radiation Smart Sensor is a light sensor (silicon pyanometer) with a measurement range of 0 to 1280 W/m^2 over a spectral range of 300 to 1100 nm. This sensor reports the average light intensity over a user-set set logging interval from a minumum of 1 second. Although the azimuth error is only ±2% error at 45° from vertical, a light sensor bracket and light sensor level are recommended.

Figure A2: Solar radiation sensor.

Technical Specifications

· Measurement parameters: average over logging interval, user-defined sampling interval from 1 second

· Measurement range: 0 to 1280 W/m^2

· Operating Temperature Range: -40° to 75°C (-40° to 167°F)

· Accuracy: ±10 W/m^2 or ±5%, whichever is greater in sunlight. Additional temperature induced error ±0.38 W/m^2 /°C from 25°C (0.21 W/m^2/°F from 77°F)

· Resolution: 1.25 W/m^2

· Drift: <±2% per year

· Spectral Range: 300 to 1100 nm

· Cosine Response Error: ±5%, 0° to 70°; ±10%, 70° to 80° from vertical

· Azimuth Error: ±2% error at 45° from vertical, 360° rotation

- · Calibration: Factory recalibration available

- · Housing: anodized aluminum housing with acrylic diffuser and o-ring seal

- · Dimensions: 4.1 cm high x 3.2 cm diameter (1 5/8 in. x 1 1/4 in.)

- · Approximate Weight: 120 g (4 oz)

- · Cable Length: 3 m (9.8 ft)

Note: Light sensor bracket (M-LBA) and light sensor level (M-LLA) are also recommended.

Operation

The Silicon Pyranometer smart sensor supports measurement averaging. When measurement averaging is enabled, data is sampled more frequently than it is logged. The multiple samples are then averaged together and the average value is stored as the data for the interval. For example, is the logging interval is set at 10 minutes and the sampling interval is set at 1 minute, each record data point will be the average of 10 measurements. Measurement averaging is useful for reducing noise in the data. It is recommended that you use measurement averaging whenever the Silicon Pyranometer smart sensor is placed in an area where the light level can vary quickly with respect to the logging interval (for example, during partly cloudy conditions).

Spectral Characteristics

This sensor uses a silicon photodiode to measure solar power per unit area (watts per square meter). Silicon photodiodes are not ideal for use as solar radiation sensors and the photodiode in this Silicon Pyranometer is no exception (see Figure B3). An ideal pyranometer has equal spectral response from 280 to 2800 nm. However, when calibrated properly and used correctly, the Silicon Pyranometer smart sensor should perform well in most situations.

The sensor is calibrated for use in sunlight. Accordingly, if the sensor is used under natural sunlight, the measurement errors will be small. Note that significant errors may result from using the sensor under artificial light, within plant canopies, in greenhouses, or any other conditions where the spectral content differs from sunlight.

Sun's Relative Intensity and the Typical Relative Response of

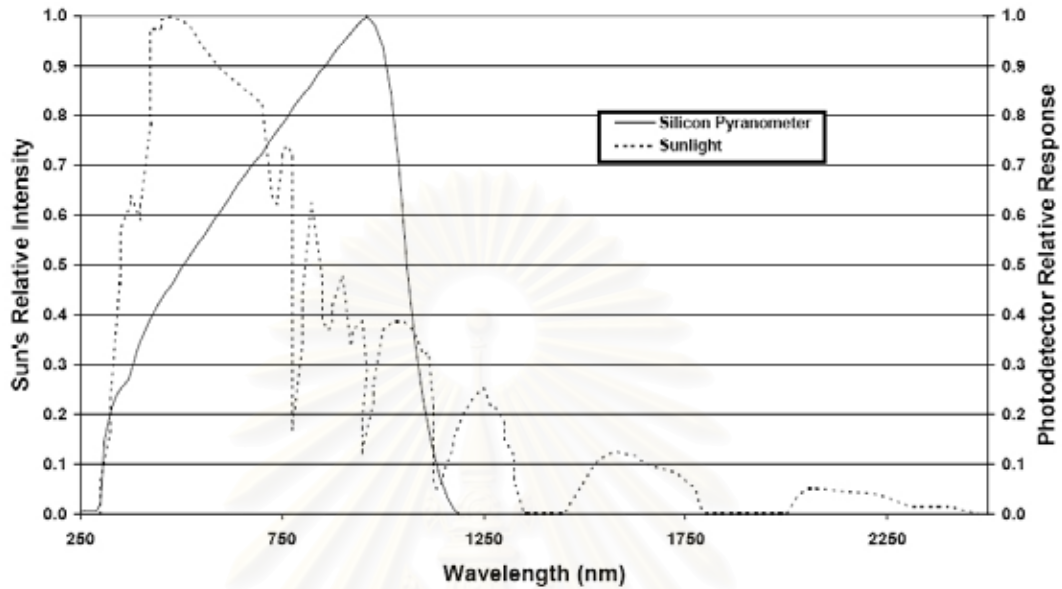**the Silicon Pyranometer versus Wavelength**

Figure A3: S-LIB-M003 Silicon Pyranometer Response Curve.

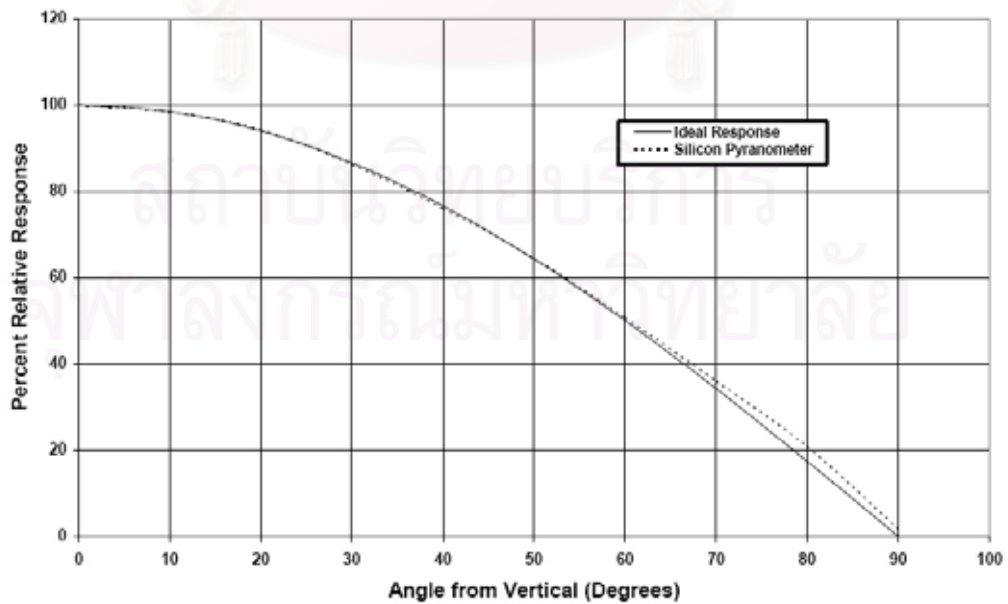**Typical Cosine Response of Silicon Pyranometer**

Figure A4: S-LIB-M003 Typical Cosine Response Curve.

Cosine Correction

The Silicon Pyranometer smart sensor housing is designed to give an accurate cosine response. Figure B4 shows a plot of relative intensity versus angle of incidence for a typical sensor and for the theoretical ideal response. Deviation from ideal response is less than 5% from 0 to 70 degrees and less than 10% from 70 to 80 degrees. Note that as the angle approaches 90 degrees, the ideal cosine response approaches zero. As a result, small errors in measured intensity will result in very large percentage errors compared to the ideal response from 80-90 degrees.

A3. PAR Smart Sensor (S-LIA-M002)

Overview

The Photosynthetic Light (PAR) Smart Sensor is intended to measure light intensity for the frequencies relevant for photosynthesis. This sensor has a measurement range of 0 to 2500 $\mu mol/m^2/sec$ over wavelengths from 400 to 700 nm. Enclosed in the anodized aluminum housing with acrylic diffuser and o-ring seal, this model has a 3m cable; a light sensor bracket and light sensor level are recommended.

Technical Specifications
- Measurement parameters: average over logging interval, user-defined sampling interval from 1 second
- Measurement range: 0 to 2500 $\mu mol/m^2/sec$, wavelengths of 400 to 700 nm
- Operating Temperature Range: -40° to 75°C (-40° to 167°F)
- Accuracy: ±5 $\mu mol/m^2/sec$ or ± 5%, whichever is greater in sunlight; additional temperature-induced error ±0.75 $\mu mol/m^2/sec/degree$ C from 25°C. Cosine corrected 0 - 80 degrees, 360 degree rotation.
- Resolution: 2.5 $\mu mol/m^2/sec$
- Drift: <±2% per year
- Housing: anodized aluminum housing with acrylic diffuser and o-ring seal
- Dimensions: 4.1 cm. height x 3.2.4 cm. diameter
- Approximate Weight: 120 g (4 oz)
- Cable Length: 3 meter (10')

Figure A5: Photosynthetically Active Radiation (PAR) sensor.

The PAR smart sensor is designed to detect photons between 400-700 nm. in wavelength. Ideally the sensor would count photons with equal efficiency between 400-700 nm. and no photons would be counted outside this range. However, in reality, this sensor undercounts photons between 400-550 nm. and between 670-700 nm., and t over counts photons between 550-670 nm. In most applications (where the sensor is used in natural sunlight) the error is not significant (see Figure B6).
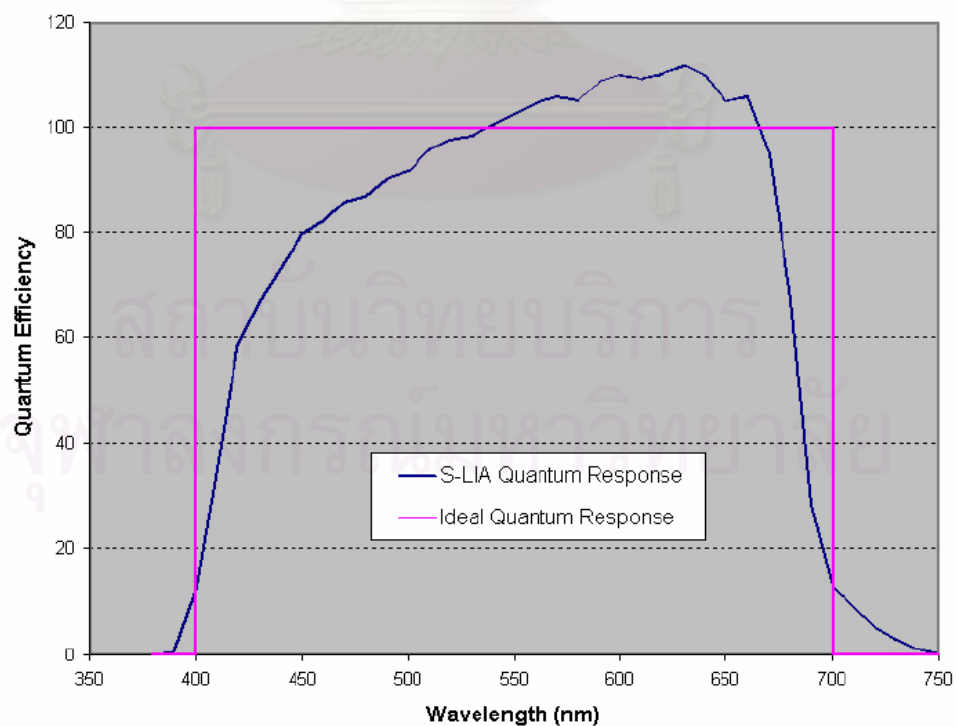

Figure A6: PAR Smart Sensor Typical Quantum Response.

A4. Temperature and Relative Humidity Smart Sensor (S-THB-M002)

Overview

The 12-bit Temperature/RH Smart Sensor is designed to work with all Onset data loggers that accept Smart Sensors. All sensor parameters are stored inside the Smart Sensor, which automatically communicates configuration data information to the logger without any programming, calibration, or extensive user setup.

Technical Specifications

- Measurement range: -40° to +75°C (-40° to +167°F), 0 to 100 %RH at -40° to +75°C (-40° to +167°F)
- Operating Range: Exposure to conditions below -20°C (-4°F) or above 95 %RH may temporarily increase the maximum RH sensor error by an additional 1%
- Temperature range: -40°C to +75 °C (-40 °F to +167 °F)
- Accuracy: ±0.2°C over 0 to 50 °C (±.36°F over +32 to 122 °F); ±2.5 %RH from 10 to 90 %RH
- Resolution: 0.02°C @ +25°C (0.04°F at +77°F); 0.1% RH @ +25°C (+77°F)
- Drift: Temp: <0.1° C (0.18°F) per year; RH: <1% RH per year; hysteresis 1%
- Response time: Temp: 5 minutes in air moving 1 m/sec, RH: 10 minutes in air moving 1 m/sec with protective cap
- Housing: PVC cable jacket with ASA styrene polymer RH sensor cap modified hydrophobic polysulfide membrane
- Dimensions (sensor): .9 cm x 3.5 cm (.35 in x 1.39 in)
- Approximate Weight: weight varies with cable length
- Cable Length: 2 meter

Figure A7: Temp/RH smart sensor, Onset product.

Note: Sensor requires protection from rain or direct splashing; Radiation shield (RS3) strongly recommended for use in sunlight; sensors can be used in intermittent condensing environments up to +30°C and non-condensing above +30°C.

A5. Wind Speed and Direction Smart Sensor (S-WCA-M003)

Overview

The combination Wind Speed and Direction Smart Sensor provides average wind speed, highest three second wind gust and average wind direction in the measurement interval. Designed with a large wind vane area for high sensitivity, the Wind Speed/Direction Smart Sensor offers high accuracy at an affordable price. This model measures average wind speed, highest three second wind gust and average wind direction (unit vector average) and utilizes anodized aluminum and stainless steel construction for durability in adverse conditions. Wind speed sensor has fiberglass reinforced thermoplastic cups and shielded stainless steel ball bearings for fast response. Wind vane has metal bushings.

Technical Specifications
- Measurement parameters: average wind speed, highest three second wind gust, average wind direction (unit vector average)
- Operating Temperature Range: -40° to 75°C (-40° to 167°F)

- · Housing: Anodized aluminum and stainless steel construction for durability in adverse conditions. Wind speed sensor has fiberglass reinforced thermoplastic cups and shielded stainless steel ball bearings for fast response. Wind vane has metal bushings.
- · Dimensions: Sensor: 317 mm (12.5 in.) Height x 419 mm (16.5 in.) Width
- · Mounting Pole: 355 mm (14 in.) L x 12.7 mm (0.5 in.) diameter
- · Approximate Weight: 700 g (1.5 lbs) (Sensor + cable + PC board in housing)
- · Cable Length: 3.0 m (9.8 ft)
- · Number of Data Channels: 3
- · Length of Smart Sensor Network Cable: 3.0 m (9.8 ft)

Figure A8: Wind speed and direction smart sensor.

Note: Cross Arm is recommended please see the Half Cross Arm (M-CAB) or the Full Cross Arm (M-CAA) at vender's website (www.onsetcomp.com).

BIOGRAPHY

Name: Mr.Maytee Bamrungrajhirun

Date of Birth: April 2nd, 1975.

Place of Birth: Loei Province, Thailand.

Educations:

- Ph.D., Program in Computer Science, Department of Mathematics, Chulalongkorn University, Thailand.

- M.Sc. Program in Computational Science, Department of Mathematics, Faculty of Science, Chulalongkorn University, Thailand. (June 1999 – May 2003)

- B.Sc. Program in Computer Science, Department of Mathematics, Faculty of Science, Chulalongkorn University, Thailand. (June 1993 – April 1997)

Publications, National and International Conferences:

- M. Bamrungrajhirun, S. Siripant, and F. Lin, "Models for the Thai Currency Exchange Rate", *Shanghai International Symposium on Nonlinear Science and Applications*, Shanghai, China, November 9-13, 2003.

- M. Bamrungrajhirun, S. Siripant, and F. Lin, "Models for the Thai Currency Exchange Rate", *Shanghai International Symposium on Nonlinear Science and Applications*, Shanghai, China, June 3-7, 2005.

- M. Bamrungrajhirun, C. Lursinsap, and S. Siripant, "Dynamic 3-Dimensional Structural Model of Rice Based on Morphogenesis Development", *International Conference on High Performance Scientific Computing (HPSC2006)*, March 6-10, 2006, Hanoi, Vietnam.

- M. Bamrungrajhirun, C. Lursinsap, and S. Siripant, "A Three-Dimensional Approach to Calculating Light Interception in Rice Canopy Based on Photosynthetically Active Radiation Data and Radiosity Rendering Technique", *the Symposium on Simulation Models for a Better Decision 2008*, Modeling and Simulation Society of Thailand, Kasetsart University, April 1-2, 2008.

Scholarship and Research Fund:

- The National Electronics and Computer Technology Center (NECTEC), Thailand.

- National Science and Technology Development Agency (NSTDA), Thailand.

- The 90th Anniversary of Chulalongkorn University Fund (Ratchadaphiseksomphot Endowment Fund).